Defining the Role of Mesenchymal Stromal Cells in Treatment Resistance in Acute Lymphoblastic Leukaemia

Richard James Burt

Thesis submitted for the degree of Doctor of Philosophy

University College London

2019

Declaration

I, Richard James Burt, confirm that the work presented in this thesis is my own. Where information has been derived from other sources, I confirm that this has been indicated in the thesis.

Signed:

Date:

Acknowledgements

Firstly, I would like to thank Professor Adele Fielding for her exceptional supervision and mentorship throughout my PhD. I will be forever grateful for the time, thought and effort she has put into both this project and my development as a clinician and scientist. I feel exceedingly fortunate to have worked in her lab and am looking forward to collaborating closely with her in the future. Put more simply she has taught me a lot!

I'd also like to thank all members of the Fielding lab for their continued support and help throughout my PhD. I'm especially grateful to Dr Aditi Dey who has been incredibly helpful with various technical aspects of the project and put up with my continuous mumblings about CAFs and mitochondria. She has become a good friend.

Thanks to my parents for their continued support and encouragement. I'm so grateful for all the time and energy they've invested in me. It is a large part due to them that I have the self-belief and confidence to complete this thesis.

Finally, and most importantly, thanks to my wife and best friend Barbara and my two wonderful girls – Olivia and Georgia. No matter how badly wrong the experiment went on Friday afternoon you three always managed to put a smile on my face and put things into perspective. I'm so grateful for all the support from you guys and am looking forward to more free time with you all once this thesis is submitted!

Abstract

The bone marrow microenvironment is crucial in treatment resistance in B-cell acute lymphoblastic leukaemia (B-ALL). Recent murine models suggest that treatment resistant cells are intrinsically no different to the treatment sensitive 'bulk population' but instead depend on a protective niche for survival.

In this thesis I set out to investigate and model the mesenchymal stromal cell (MSC) niche in B-ALL. I initially showed, that MSC directly isolated from the primary bone marrow specimens of patients with B-ALL frequently adopted an activated or cancer associated fibroblast (CAF)-like phenotype. This was characterised by morphological changes, up-regulation of CAF relevant genes and enhanced cytokine/chemokine secretion.

I uncovered a sub-set of B-ALL cell lines and primary B-ALL cells are capable of inducing the CAF-like phenotype in MSC cell lines and healthy donor MSC in vitro. These changes occur relative to the intrinsic reactive oxygen species (ROS) level and genetic sub-type of the B-ALL cell. Next, I showed that normal primary human MSC and the MSC cell line HS27a became activated de novo, when exposed to the reactive oxygen species (ROS)-inducing chemotherapy agents' cytarabine (AraC) and daunorubicin (DNR). This phenomenon did not occur with non-ROS inducing chemotherapy - vincristine (VCR) and was blocked by NAC or the corticosteroid, dexamethasone.

Finally, I demonstrated that activated MSC protected B-ALL cells from ROS-inducing chemotherapy via mitochondrial transfer through tunnelling nanotubes (TNT). Inhibition of mitochondrial transfer by selective mitochondrial depletion of MSC or interference with TNT formation by microtubule inhibitors such as VCR -prevented the 'rescue' function of the activated MSC.

In summary, my thesis proposes a model in which the eradication of residual ALL cells by conventional chemotherapy is ineffective, at least in part due to MSC-mediated transfer of mitochondria to B-ALL cells to overcome chemotherapy induced oxidative stress at the MSC niche. My work proposes the clinically testable hypothesis that ROS-inducing chemotherapies should always be combined with corticosteroids and/or microtubule inhibitors to overcome MSC mediated protection of B-ALL cells.

Impact Statement

Acute Lymphoblastic Leukaemia (ALL) is a highly chemotherapy sensitive malignancy with almost all patients achieving remission after chemotherapy. However, the majority of adults fail to achieve long-term survival due to a combination of relapse and toxicity from treatment. Recent studies suggest the few leukaemic cells that survive post chemotherapy and lead to relapse are intrinsically no different from cells that are killed by chemotherapy. The few leukaemia cells that survive are believed to be protected by 'normal' healthy cells in the bone marrow called mesenchymal stromal cells (MSC).

In this thesis I have shown that leukaemia cells 'corrupt' MSC for their own survival benefit both before but especially after chemotherapy used in ALL treatment. This protective effect is achieved through physical connections and transfer of mitochondria between 'activated' MSC and ALL cells. I have shown that the connections and transfer of mitochondria can be inhibited by both commonly used chemotherapy drugs (vincristine, dexamethasone) and non-chemotherapy drugs. Importantly by inhibiting the interaction between the MSC and leukaemia cells I was able to overcome resistance to chemotherapy. This provides a strong scientific rationale for combining drugs that inhibit the interaction between MSC and ALL cells and those which effectively kill ALL cells.

My thesis has furthered our understanding of the leukaemic microenvironment or 'protective bone marrow niche' and in particular its response to different chemotherapeutics. It has improved our understanding of how a small number of

leukaemic cells survive after chemotherapy despite intrinsically appearing no different to the chemotherapy sensitive population. My thesis suggests the treatment resistant population survive due to rescue from oxidative stress by mitochondrial transfer from the stroma. This finding opens up a number of avenues to explore to overcome this protective effect including targeting the mechanisms of transfer (tunnelling nanotubes) and altering the metabolic state of the B-ALL cell to overcome this protective effect.

Intriguingly, vincristine and dexamethasone inhibit this protective mechanism and have been used successfully for forty years in patients as part of maintenance chemotherapy to eradicate the few remaining cells without a clear scientific rational. However, toxicity with these agents remains an issue and an improved understanding of microenvironment mediated protection of B-ALL cells offers the tantalising opportunity for a more targeted therapy with less toxicity.

However in the interim, following on my findings, we will be able to extend and optimise the potential of conventional chemotherapy. Through a continued connection and collaboration with the UK National Cancer Research Institute Adult ALL subgroup, there are plans in place to use this knowledge to re-schedule chemotherapy regimens for future large clinical trials for adults with ALL in the UK. The proposed UKALL15 trial will directly test my findings, comparing the current, standard-of-care regimen with a regimen wherein drugs inhibiting the interaction between MSC and ALL cells are always given together with chemotherapy which effectively kills ALL cells. Furthermore,

appropriate, longitudinal specimens will collected as part of the clinical trial to assess the relationship between MSC activation and outcome in clinical specimens.

Publications and abstracts

Publications and abstracts arising from the work described in this thesis at the time of submission:

1. Burt R, Dey A, Aref S, Aguiar M, Akarca A, Bailey K, Day W, Hooper S, Kirkwood A, Kirschner K, Lee S-W, Lo Celso C, Manji J, Mansour M, Marafioti T, Mitchell R, Muirhead R, Ng K, Pospori C, Puccio I, Zuborne-Alapi K, Sahai E and Fielding AK **Activated Stromal Cells Transfer Mitochondria to Rescue Acute Lymphoblastic Leukaemia Cells from Oxidative Stress.** *Blood. Accepted for publication 26th August 2019.*

2. *European School of Haematology International Conference on Acute Lymphoblastic Leukaemia, May 17-19, 2019, Berlin, Germany*. Burt R, Dey A, Ng K, Sahai E, Fielding A **Commonly Used Chemotherapy Drugs Differentially Determine Microenvironment-Mediated Protection, Via Mitochondrial Transfer, to B-Precursor Acute Lymphoblastic Leukaemia Cells.** ORAL PRESENTATION.

3. *European School of Haematology 3rd Scientific Workshop -The Haematological Tumour Microenvironment and its Therapeutic Targeting, February 24-26, 2019, London, United Kingdom.* Burt R, Dey A, Ng K, Sahai E, Fielding A **Commonly Used Chemotherapy Drugs Differentially Determine Microenvironment-Mediated Protection, Via Mitochondrial Transfer, to B-Precursor Acute Lymphoblastic Leukaemia Cells.** POSTER PRESENTATION.

4. *American Society of Haematology (ASH) 60th Annual Meeting and Exposition, December 1-4, 2018, SAN Diego, California, USA*. Burt R, Dey A, Ng K, Sahai E, Fielding AK. **Commonly Used Chemotherapy Drugs Differentially Determine Microenvironment-Mediated Protection, Via Mitochondrial Transfer, to B-Precursor Acute Lymphoblastic Leukaemia Cells.** POSTER PRESENTATION.

5. *European Haematology Association (EHA) Meeting, June 14-17, 2018, Stockholm, Sweden.* Burt R, Dey A, Ng K, Pospori C, Hooper S, Lo Celso C, Sahai E, Fielding A. **Mesenchymal Stromal Cells Protect Acute Lymphoblastic Leukaemia Cells from Cytarabine induced Apoptosis by Transfer of Mitochondria via Tunnelling Nanotubes in a Treatment Resistant Niche Model.** ORAL PRESENTATION.

6. *British Society Haematology Annual Scientific Meeting, April 16-18, Liverpool, United Kingdom.* Burt R, Dey A, Ng K, Liu B, Marafioti T, Sahai E, Fielding AK. **The differential effects of chemotherapy on the Acute Lymphoblastic Leukaemia microenvironment suggests a possible mechanism for maintenance chemotherapy.** ORAL PRESENTATION.

7. *European Haematology Association-Scientific Working Group (EHA-SWG) Scientific Meeting on New Molecular Insights and Innovative Management Approaches for Acute Lymphoblastic Leukaemia, April 12-14, 2018, Barcelona, Spain.* Burt R, Dey A, Ng K, Liu B, Marafioti T, Sahai E, Fielding AK **The differential effects of chemotherapy on the Acute Lymphoblastic Leukaemia microenvironment suggests a possible mechanism for maintenance chemotherapy.** ORAL PRESENTATION.

8. *American Society of Haematology (ASH) 59th Annual Meeting and Exposition, December 9-12, 2017, Atlanta, Georgia, USA.* Burt RJ, Dey A, Cheuk K, Ng Y, Liu B, Marafioti T, Sahai E, Fielding AK. **Acute Lymphoblastic Leukaemia (ALL) Cells and Commonly-Used Chemotherapy Drugs Can Induce Bone Marrow-Derived Mesenchymal Stromal Cells to Become Cancer Associated Fibroblasts (CAF), Leading to Enhanced ALL Proliferation and Treatment Resistance.** POSTER PRESENTATION.

Statement of work undertaken

Aditi Dey assisted with the RQ-PCR of the CAF defining genes and PCR gels. Ayse Akarca performed the immunohistochemistry staining on the murine femur. All other work was carried out by the author.

Table of contents

List of Figures

List of Tables

List of Abbreviations

αSMA	Alpha-smooth muscle actin
ABL	Abelson
Akt	Protein kinase B
ALL	Acute Lymphoblastic Leukaemia
AlloHSCT	Allogeneic haematopoietic stem cell transplant
AML	Acute Myeloid Leukaemia
APC	Allophycocyanin
AraC	Cytarabine
ASNS	Asparagine synthetase
AT-TNT	Actin containing tunnelling nanotubes
B-ALL	B-cell Acute Lymphoblastic Leukaemia
BCR	Break point cluster region
bFGF	Basic fibroblast growth factor
BFP	Blue fluorescent protein
BM-MSC	Bone marrow derived mesenchymal stromal cells
BSA	Bovine Serum Albumin
BV	Brilliant violet
c-ALL	Common B-cell Acute Lymphoblastic Leukaemia
CAF	Cancer Associated Fibroblasts
Cav-1	Caveolin-1
CCL	Chemokine ligand

cDNA	Complementary DNA
CLL	Chronic Lymphocytic Leukaemia
CML	Chronic myeloid leukaemia
CNS	Central nervous system
COL	Colchicine
CR	Complete remission
CRUK	Cancer Research United Kingdom
CXCL	C-X-C motif chemokine
CXCR	C-X-C chemokine receptor
DAPI	4', 6-diamidino-2-2phenylindole
DEX	Dexamethasone
DNA	Deoxyribonucleic acid
DNR	Daunorubicin
DMSO	Dimethyl sulfoxide
EGF	Epidermal growth factor
ERK	Extracellular signal-related kinases
EVC	Extracellular vesicle
FACS	Fluorescence-activated cell sorting
FBS	Foetal bovine serum
FC	Flow cytometry
FISH	Fluorescent in situ hybridization
FMO	Flow minus one
FSC	Forward scatter

G-CSF	Granulocyte colony-stimulating factor
GDF-15	Pro-survival growth/differentiation factor 15
GM-CSF	Granulocyte-macrophage colony-stimulating factor
H_2O_2	Hydrogen Peroxide
HD	Healthy donor
hERG1	Human ether a-go-go related gene 1
HGF	Hepatocyte growth factor
HIF	Hypoxia-inducible factor
HSC	Haematopoietic stem cell
iAMP21	Intrachromosomal amplification of chromosome 21
ICC	Immunocytochemistry
IgH	Immunoglobulin heavy chain
Ig/TCR	Immunoglobulin heavy chain/T-cell receptor rearrangements
IL	Interleukin
IMP	Investigational medicinal products
IP	Intraperitoneal
ISCT	International Society Cell and Gene Therapy
IT	Intrathecal
JNK	c-Jun N-terminal kinase
AP1	Activator protein 1
KMT2A	Histone-Lysine N-Methyltransferase 2A
MEM	Minimum Essential Media
MGG	May-Grünwald-Giemsa

MMP	Matrix metalloproteinase
MNC	Mononuclear cells
MRD	Minimal residual disease
mRNA	Messenger ribonucleic acid
MSC	Mesenchymal stromal cell
MT-TNT	Microtubule containing tunnelling nanotube
NAC	N-acetyl cysteine
NAD+	Oxidised nicotinamide adenine dinucleotide
NADH	Reduced nicotinamide adenine dinucleotide
NADPH	Nicotinamide adenine dinucleotide phosphate
NF-κB	Nuclear factor kappa-light-chain-enhancer of activated B cells
NK	Natural Killer
NOC	Nocodazole
NOX2	NADPH Oxidase 2
NSG	NOD scid gamma
OXPHOS	Oxidative phosphorylation
PBS	Phosphate buffered saline
PCR	Polymerase chain reaction
PE	Phycoerthyrin
PGC1α	Peroxisome proliferator-activated receptor-gamma coactivator 1 alpha
Ph	Philadelphia chromosome
PI3K	Phosphoinositide-3-kinase

Pre-B ALL	Precursor B-cell Acute Lymphoblastic Leukaemia
Pro-B ALL	Pro B-cell Acute Lymphoblastic Leukaemia
RNA	Ribonucleic acid
ROS	Reactive oxygen species
RQ-PCR	Real-time polymerase chain reaction
SSC	Side scatter
T-ALL	T-cell Acute Lymphoblastic Leukaemia
TAM	Tumour associated macrophages
TCR	T-cell receptor
TdT	Terminal deoxynucleotidyl transferase
TGF-β1	Transforming growth factor beta 1
TNT	Tunnelling nanotubes
TKI	Tyrosine kinase inhibitors
UK	United Kingdom
UV	Ultraviolet
VCAM1	Vascular cell adhesion molecule 1
VEGF	Vascular endothelial growth factor
VCR	Vincristine
VLA-1	Very Late Antigen-4

Chapter 1: Introduction

1.1 Acute Lymphoblastic Leukaemia Overview

1.1.1 General Introduction

Acute Lymphoblastic Leukaemia (ALL) is the most common malignancy in childhood with a second peak in incidence in older adults[1]. It is predominantly a bone marrow-based malignancy although peripheral blood, liver, spleen, testis and the central nervous system can also be involved. ALL is a highly aggressive, rapidly progressive malignancy and prior to the use of multi-agent chemotherapy regimens in the 1950s it was universally fatal with death usually occurring within weeks after the diagnosis.

The advent of multi-agent chemotherapy regimens and refinement of chemotherapy protocols, including in large scale clinical trials over the past 50 years, coupled with improved supportive care and the advent of allogeneic stem cell transplants has led to a marked improvement in patient outcomes[2-4]. This is most notable in childhood ALL, where long-term survival now approximates 90%[3,4]. Long-term survival in adults with ALL is considerably lower at 40 - 50%, with outcomes worsening with increasing age[5,6]. This is largely due to an increased rate of relapse in adults and increased toxicity from treatment as compared to children[5,6].

However, the biology of the increased risk of relapse in adults as compared to children is to date largely unexplained. A greater incidence of high-risk genetic abnormalities in adult as compared to childhood ALL is believed to partly account for the difference[7]. However, the mechanism behind the differing responses to chemotherapy across different genetic sub-types remains unclear. The different genetic sub-types of relevance to this thesis will be discussed further below.

Importantly, despite the relatively poor long-term survival rates, the vast majority of adults with ALL (approximately 90%) achieve complete remission (CR) with conventional chemotherapy regimens[2]. However, a significant number of those in CR have so-called minimal residual disease (MRD) which is associated with a high risk of relapse[8]. The nature of the cells which comprise MRD and how they differ from the bulk population of cells is a subject of both academic debate and considerable clinical relevance. Unlike in acute myeloid leukaemia (AML), no leukaemic stem cell has been definitively identified[9,10]. Instead, relapse is thought to arise from residual disease (MRD) which may remain after initial therapy, typically quantified by PCR-amplification of patient-specific immunoglobulin heavy chain/T-cell receptor (Ig/TCR) gene rearrangements.

MRD monitoring studies in both B and T ALL show that relapsed ALL usually has the same Ig/TCR re-arrangements found at diagnosis[11]. Murine models also suggest that relapse of ALL does not necessarily arise from intrinsic chemo-

resistance by genetically distinct cells, but more likely occurs due to protection of a subset of cells whose behaviour can also be modified within a specific niche[12,13].

In this thesis I will explore the role of the protective bone marrow niche in ALL, specifically focussing on the role of mesenchymal stromal cells within the niche and how niche formation is modified both by the genetic sub-type of ALL cells and different chemotherapy drugs commonly used in ALL.

1.1.2 Acute Lymphoblastic Leukaemia Symptoms and Demographics

ALL is an aggressive malignancy of T or B lymphocytes with the primary site of disease in the bone marrow. The onset of ALL is usually rapid with patients presenting with signs and symptoms of bone marrow failure. Patients with ALL typically present with a combination of symptoms of bone marrow failure including symptoms due to anaemia, thrombocytopenia and/or infections due to neutropenia. Ten percent of patients at diagnosis have evidence of disease outside the bone marrow with splenomegaly, liver impairment, lymphadenopathy, testicular swelling or central nervous system involvement[14].

ALL is primarily a childhood disease with approximately 75% cases occurring in children under the age of 6 years at diagnosis[1]. However, although ALL is rare in adults, incidence increases after the age of 40 years[15]. The aetiology of ALL remains unknown[16].

1.1.3 Acute Lymphoblastic Leukaemia Definition

The World Health Organisation (WHO) defines ALL in subgroups by the cell of origin, either B cell or T cell[17]. This is determined by the surface antigen expression of the ALL cells by immunophenotyping, detailed below. B cell ALL is also further sub classified based on recurrent cytogenetic abnormalities known to have prognostic value clinically, also discussed below.

(i) B-lineage ALL definition and subgroups

B ALL accounts for approximately 75% of adult cases of ALL. The vast majority of cases of B ALL express HLA-DR, terminal deoxynucleotidyltransferase (TdT) and CD19, while the expression of CD79a, CD22 and CD34 is frequently positive but can be variable or negative[18]. B ALL is subdivided by immunophenotyping into the following groups:

Pro-B ALL represents approximately 10% of adult ALL. CD10 is negative as is cytoplasmic immunoglobulin.

Common ALL (c-ALL) is the major immunological subtype in adult ALL comprising more than 50% of all cases. c-ALL is characterized by the presence of CD10 and absence of cytoplasmic immunoglobulin.

Pre-B ALL is characterized by the expression of cytoplasmic immunoglobulin, which is absent in c-ALL, but is identical to c-ALL with respect to the expression of all other cell markers.

(ii) T-lineage ALL definition and subgroups

T cell ALL accounts for approximately 25% of adult ALL. Cells are TdT+ in addition to cytoplasmic Cd3+ and CD34+. All cases express the T-cell antigen gp40 (CD7) and they may, according to their degree of T-cell differentiation, express other T-cell antigens, for example the E rosette receptor (CD2) or the cortical thymocyte antigen T6 (CD1)[18]. In most cases of T-cell ALL, one or more of the T-cell receptor (TCR) genes are rearranged. These properties make it possible to classify T-cell ALL according to their stage of differentiation.

Early T-precursor ALL accounts for 6% of adult ALL. It shows characteristic T-cell markers (cyCD3 and CD7) but no further differentiation markers.

Thymic (cortical) T-ALL is the most frequent subtype of T-ALL (10%). It is characterized particularly by the expression of CD1a. Surface CD3 may be present. Since this subtype is associated with a better prognosis, its identification is of particular importance.

Mature T-ALL has a frequency of 6%. The blast cells do not express CD1a but they are positive for surface CD3.

1.1.4 Acute Lymphoblastic Genetic Abnormalities Overview

Both B- and T ALL are characterised by primary, driver genetic abnormalities which frequently occur with secondary abnormalities in key genes– insertions, deletions, single nucleotide variants and copy number abnormalities[15,19,20]. In clinical practice, karyotyping and fluorescent in situ hybridisation (FISH) is most commonly used to identify reoccurring abnormalities which include translocations or gain and loss of gross chromosome material[7]. These include *BCR-ABL1* (t9;22), *ETV6-RUNX1* (t12;21),

TCF3-PBX1 (t1;19) and *KMT2A – AFF1* (t4;11) which are discussed in more detail below due to their relevance to my thesis.

Studies report detection of clonal chromosomal abnormalities in up to 85% of cases of adult ALL[21]. Other techniques including DNA microarray analyses, genomic sequencing and next generation sequencing have been used to identify additional genetic abnormalities[20]. This has resulted in the identification of new subtypes of ALL: for example, Ph-like (also known as *BCR–ABL1*-like) B cell precursor ALL (B-ALL)[22], B-ALL with intrachromosomal amplification of chromosome 21 (iAMP21)[23] and *ZNF384*-rearranged B-ALL[24]. The pie-chart on the following page (***Figure 1-1***) demonstrates the range of genetic abnormalities in paediatric ALL[20].

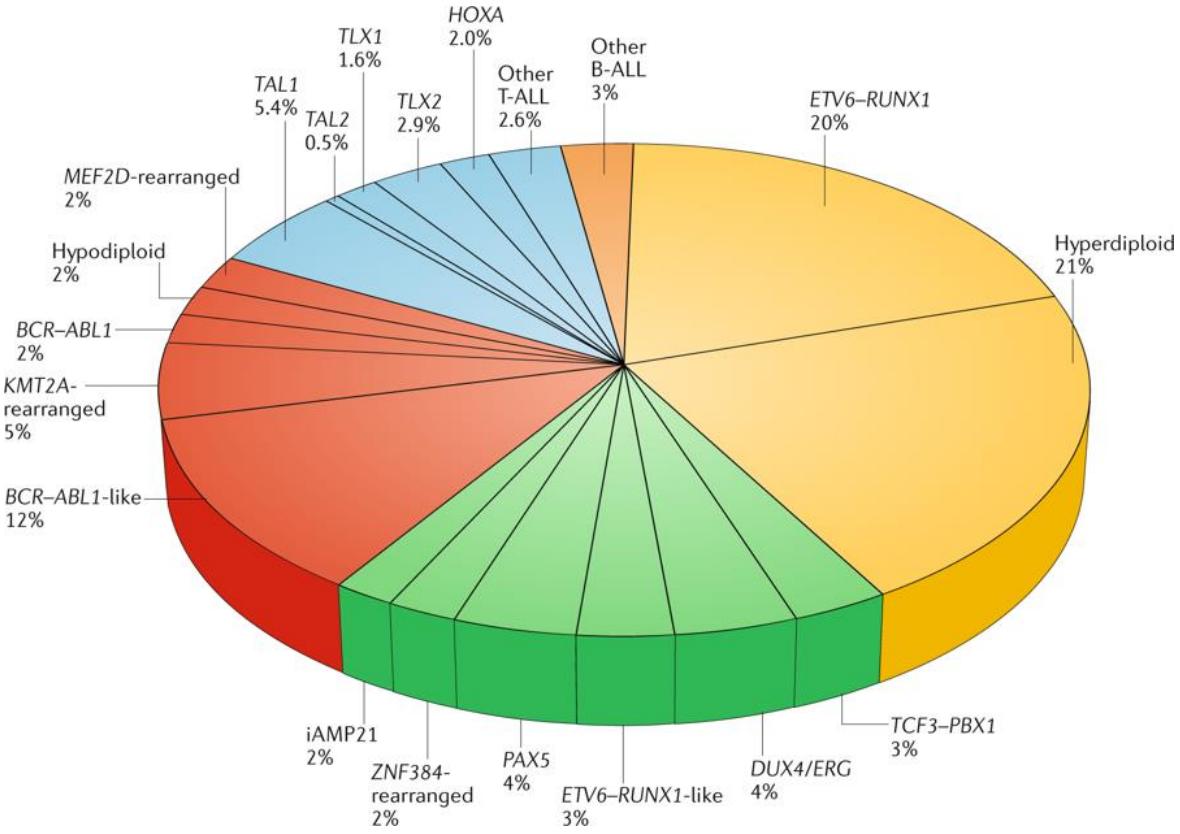

Figure 1-1: Genetic sub-types of childhood ALL – The pie chart demonstrates estimated frequencies of different genetic sub-types of childhood ALL in St Jude Total Therapy Study XV[20].

Many of these genetic changes have important prognostic significance and predict response to chemotherapy[25], although the reasons for the differential responses to chemotherapy are largely unknown. Notably, 70% of children between 1 and 10 years presenting with ALL will have good risk cytogenetics with the presence of either hyperdiploidy (between 51 and 65 chromosomes) or the translocation t(12;21)(p12;q22) resulting in the fusion product *TEL-AML1*[7,20]. The presence of good risk cytogenetic abnormalities are rare in adult leukaemia due to a falling incidence with increasing age as demonstrated in the subsequent bar chart (***Figure 1-2***)[7].

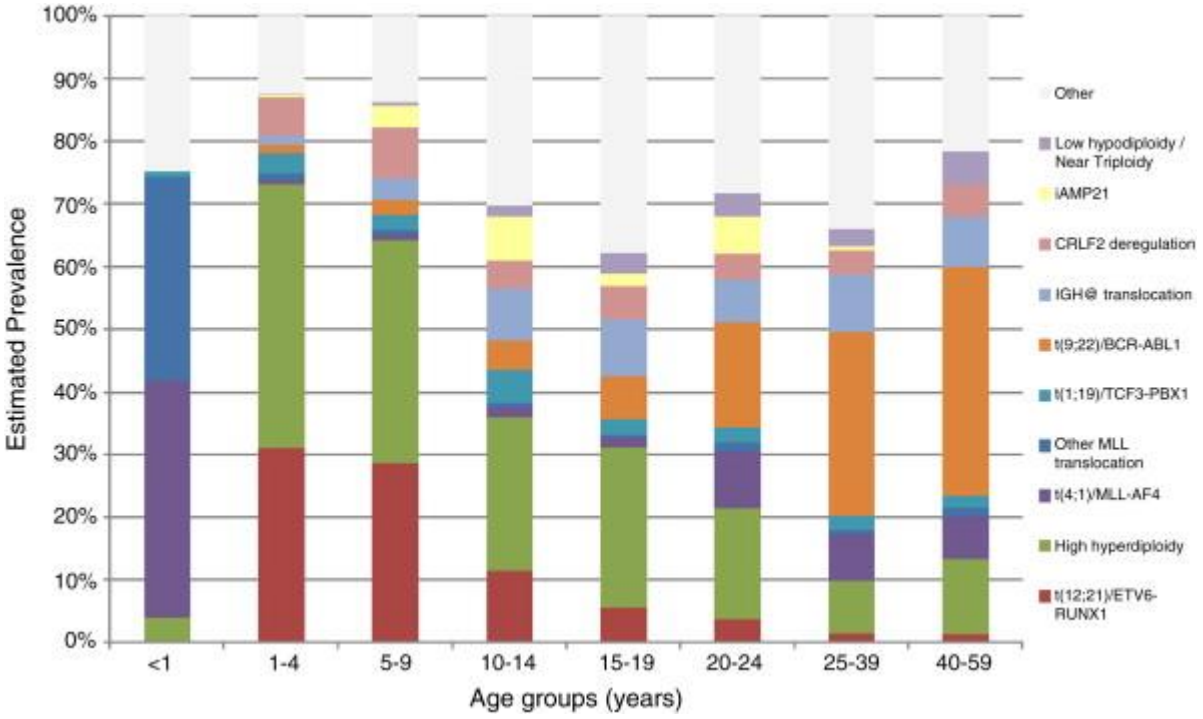

Figure 1-2: Genetic sub-types ALL by age – Estimated age-specific frequency of selected chromosomal abnormalities in ALL[7].

However, when good risk aberrations are detected at diagnosis in adults they carry the same prognostic value as they do in children[7]. The incidence of poor risk cytogenetics such as hypodiploidy and *BCR-ABL1* ALL rises with age. In an analysis of data from 1522 adult patients participating in the UKALLXII/ECOG2993 study, the following four groups of patients with distinct karyotypes were shown to have markedly inferior rates of event free survival and overall survival when compared to the whole cohort; t(9;22), t(4;11), complex karyotype (defined as 5 or more chromosomal abnormalities) and low

hypodiploidy/near triploidy[25]. This was the first demonstration that cytogenetic subgroups other than *BCR-ABL1* positive ALL (t9;22) can be used for risk-stratification of adults with ALL.

Below I provide further detail on the genetic subtypes of particular relevance to this thesis which include the most common genetic rearrangements in infants (*KMT2A-AFF1/MLL-AF4*), children (*ETV6-RUNX1*) and adults (*BCR-ABL1*).

1.1.5 Acute Lymphoblastic Leukaemia Specific Genetic Abnormalities

(i) *BCR-ABL1*

BCR-ABL1 or Philadelphia chromosome positive ALL is due to a fusion between the Abelson (ABL) tyrosine kinase gene on chromosome 9 and the break point cluster region (BCR) gene on chromosome 22, which results in a BCR-ABL fusion protein, a constitutively active tyrosine kinase. The altered chromosome 22 is termed the Philadelphia chromosome. The BCR-ABL translocation is characteristic of chronic myeloid leukaemia (CML), but also occurs in approximately 25-30% of adult B-ALL patients[7]. It is rare in childhood B-ALL occurring in 2-4% of cases[20]. There are two common variants of the fusion gene BCR-ABL1, which are named p190 or p210 according to the break point on chromosome 22. The p210 isoform of BCR-ABL1 occurs in almost all cases of CML whereas the p190 isoform predominates in B-ALL[26].

Historically, *BCR-ABL1* conferred a very poor prognosis and response to conventional intensive combination chemotherapy, with an allogeneic stem cell transplant being necessary to achieve long term disease free survival[25]. However, the biological explanation for the relative resistance to chemotherapy of *BCR-ABL1* positive ALL as compared to other genetic sub-types of ALL has remained unexplained to date.

The treatment of *BCR-ABL1* ALL has been revolutionized by the addition of selective inhibitors of the action of the fusion protein - tyrosine kinase inhibitors, (TKI) - to treatment[27,28]. These non-chemotherapy agents, examples of which include imatinib and dasatinib bind to the kinase domain of *ABL* and disrupt the ATP binding site. Although there have been no randomized controlled trials comparing chemotherapy with chemotherapy plus imatinib in *BCR-ABL1* ALL, there is little doubt that the overall outcome of therapy is superior[27,28]. However, in contrast to CML, treatment with single agent TKIs in *BCR-ABL1* positive ALL does not lead to sustained remissions[29]. Despite the improvements in outcome in *BCR-ABL1* positive ALL, eradicating the disease and achieving long term remission remains a challenge, especially in older patients.

Interestingly and important for this thesis, is the recent finding that when a TKI is included with induction treatment, less intensive chemotherapy achieves similar outcomes to more conventional intensive chemotherapy regimens[30]. In the GRAAPH 2005 trial[30], in patients treated with the less intensive induction chemotherapy of vincristine and dexamethasone, the early CR rate was 98.5% as compared to 91% in

the more intensive chemotherapy arm, with the difference being due to treatment related mortality. Therefore the balance of evidence suggests that at least during induction, TKI combined with steroid and vincristine can result in *BCR-ABL1* ALL patients achieving complete remission with minimal toxicity.

(ii) KMT2A – AFF1/MLL-AF4

The *KMT2A* or *MLL* gene on chromosome 11, which is required for normal haematopoiesis, is a promiscuous gene which is known to undergo fusion with several different partner genes in ALL and acute myeloid leukaemia (AML). The most common fusion partner gene in ALL is AFF1 on chromosome 4. It is widely believed that it is the 5' portion of the *MLL* gene fusing to the 3' portion of the partner gene on the derivative chromosome 11 which generates the leukaemogenic effect[7]. Interestingly, a recent whole-genome mutational landscape of KMT2A B-ALLs revealed that infant KMT2A B-ALL has one of the lowest frequencies of somatic mutations of any sequenced cancer, with the predominant leukemic clone carrying only 1.3 non-silent mutations[31].

The age-specific incidence of *KMT2A-AFF1* in ALL is highly skewed with approximately 50% of infants having the translocation, whereas the incidence is low in childhood ALL and increases with age among adults[7]. Its overall incidence in adult ALL is estimated at approximately 5%.

It is known to be a highly aggressive, rapidly proliferative form of B-ALL and typically presents with a very high number of leukaemic cells in the peripheral blood both in infants and adults. It is associated with a poor prognosis across all age groups and high rates of relapse in the bone marrow despite initial responses to therapy[32,33]. However, cells harbouring the MLL-AF4 translocation are known to be unusually sensitive to AraC[34]. The reason for the cells enhanced sensitivity to AraC *in vitro*, remains largely unexplained although some authors have suggested it could be due to enhanced transport of AraC across the cell membrane[35]. Despite this, AraC containing regimens often fail to achieve sustained remission with the biological basis for the differences between the *in vitro* and *in vivo* responses remaining unclear. The work in this thesis provides a possible explanation for the observed discrepancy in the *in vitro* versus *in vivo* sensitivity to AraC.

(iii) ETV6-RUNX1

This genetic subtype of ALL is characterised by a chromosomal translocation between chromosomes 12 and 21 creating the chimeric fusion product *ETV6-RUNX1*. Unlike many chromosomal translocations, it is cytogenetically cryptic and was discovered by FISH in the mid-1990s[7]. Interestingly, in *ETV6-RUNX1* ALL there is clear evidence of a long latency between the development of the initial genetic lesion (*ETV6-RUNX1*) and clinically overt disease[36,37]. Monozygotic twin studies with concordant ALL and 'backtracking' studies using archived neonatal blood spots established that *ETV6-RUNX1* is an initiating event arising prenatally in a committed B-cell progenitor.

However, the fusion gene *ETV6-RUNX1* is not sufficient alone to cause overt ALL and additional mutations are essential for the development of ALL[38].

It is the most common translocation in childhood ALL, found in approximately 25% of cases but is very rare in adults (0-3%)[7]. It predicts a very good prognosis and response to treatment in children with very low rates of relapse. Children with ETV6-RUNX1 ALL typically have a rapid response to standard chemotherapy regimens achieving molecular remission quicker than almost all other genetic sub-types of ALL[39].

(iv) TCF3-PBX1

This is characterised by a translocation between chromosome 1 and 19, creating the fusion gene *TCF3-PBX1*. The translocation is unusual because it can present either as a balanced translocation, t(1;19), or unbalanced where just the der(19)t(1;19) is present. The ratio of balanced to unbalanced is approximately 50:50[7]. It is one of the few genetic abnormalities in ALL whose frequency does not vary significantly with age; being present in approximately 3–5% of cases at all ages, except infant ALL as demonstrated in the bar-chart earlier.

TCF3-PBX1 historically predicted a poor outcome in childhood ALL but with newer therapy regimens is associated with a good or even excellent prognosis in children[40]. This marked improvement in prognosis has not been observed to the same degree in

other genetic subtypes of childhood ALL. The reasons for the improved outcomes remain unclear, although is possibly due to early more intensive remission induction regimens in newer therapy protocols[40]. In fact, recent evidence with current treatment protocols, suggests TCF3-PBX1 ALL patients achieve molecular remission more rapidly than any other genetic sub-type of paediatric ALL[39]. The prognostic impact of *TCF3-PBX1* in adult ALL is less clear although recent evidence in small case series of patients, suggests it may not predict a poor prognosis as was previously thought[41].

1.2 Acute Lymphoblastic Leukaemia Treatment

1.2.1 Overview of Acute Lymphoblastic Leukaemia Treatment

ALL was universally fatal prior to the development of effective chemotherapeutics in the 1940s onwards. ALL represents the first cancer where the potential of chemotherapy was demonstrated by Farber and colleagues in the 1940s initially with a folic acid antagonist[42]. The way the disease evolves after treatment has taught us much about the biology of the disease. Although initial treatment with single agent chemotherapy induced remission in some patients, this was short-lived prior to inevitable relapse.

Therefore, combination chemotherapy regimens were developed which improved both the remission rate and duration of response[43]. Drugs included in the early

combination regimens to achieve remission included corticosteroids, vincristine, anti-folate agents and mercaptopurine and later, central nervous system directed therapy. All these drugs continue to remain important parts of B-ALL treatment.

The observed occurrence of late relapses led to the recognition of the need for prolonged chemotherapy to achieve durable remission. This included the development of maintenance chemotherapy, low dose continuous chemotherapy over several years, which includes corticosteroid and vincristine and remains an essential part of treatment. It remains one of the very few examples in cancer to date where maintenance chemotherapy has been demonstrated to have clear benefit[44]. However, the mechanism by which maintenance chemotherapy clears the few remaining ALL cells where high dose combination chemotherapy fails is unclear. In this thesis I offer a potential explanation for the success of maintenance chemotherapy through the discovery of novel mechanism of action of vincristine and dexamethasone, a corticosteroid.

In the United Kingdom, improvements in outcomes can clearly be demonstrated in the UK wide National Cancer Research Institute ALL trials in both children and adults[2,27]. This continued progress in improving treatment outcomes in ALL has largely been achieved through optimization of multi-drug chemotherapy regimens and improvement in supportive care especially management of neutropenic infections, most notably in children and adolescents. More recently the addition of novel agents

including the previously discussed TKIs for *BCR-ABL1* B-ALL[28,30] and the CD20 targeted monoclonal antibody Rituximab[45,46] has led to improved outcomes in sub-groups of patients with B-ALL.

However, treatment resistance, relapsed disease and toxicity from treatment remain significant issues[5]. There therefore remains an unmet need for a better understanding of the mechanisms behind treatment resistance and relapse in ALL so treatment can be better designed to overcome resistance while also being more targeted with the intention of reducing unacceptable toxicity.

1.2.2 Rationale and Stages of Acute Lymphoblastic Leukaemia treatment

The current treatment of B-ALL initially involves multiple cycles of multi-agent chemotherapy with the aim of inducing remission with high-dose intensive combination chemotherapy followed by prolonged low-dose chemotherapy with the intention of eradicating the residual sub-microscopic leukaemia known as minimal residual disease (MRD). Bone marrow or stem cell transplants in select sub-groups of patients have also been shown to be beneficial post induction of remission. The treatment of ALL is prolonged and typically takes 2-3 years to complete.

Treatment is divided into 3 phases called Induction, Consolidation or Intensification and Maintenance, as represented in the image ***Figure 1-3*** and discussed below. Induction is often preceded by a corticosteroid pre-phase with the intention of

reducing the burden of disease and improving the tolerance of subsequent intensive chemotherapy.

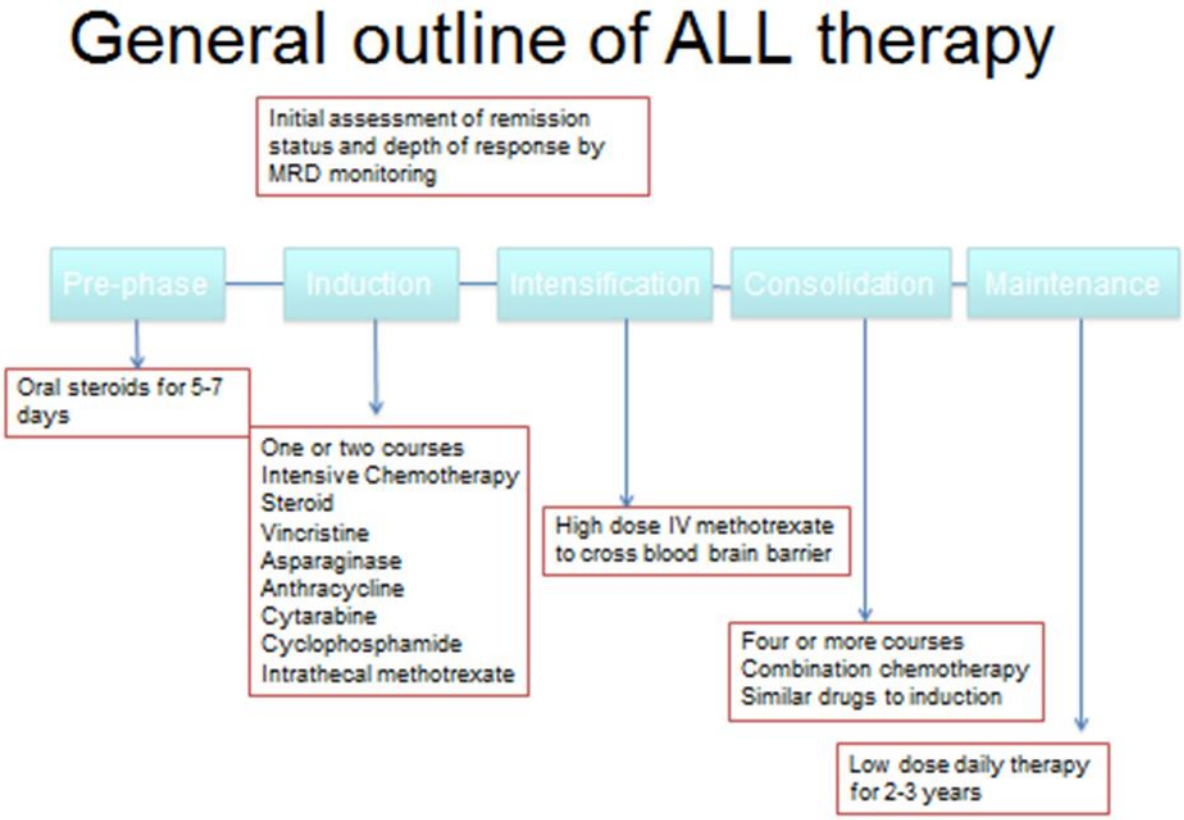

Figure 1-3 General Outline of ALL therapy – The diagram gives a general outline of ALL therapy with the names of courses in the cyan coloured boxes and the individual drugs or combination of drugs listed in the lower red boxes. The top red box describes monitoring of response to treatment.

(i) Induction Chemotherapy

The aim of induction chemotherapy is to achieve a complete remission, which is currently defined on a morphological basis of less than 5% blasts in the bone marrow in the presence of overall haematological recovery. Induction chemotherapy usually involves 1-2 cycles of multi-agent intensive chemotherapy with the intention of

inducing remission which equates to disease undetectable at the microscopic level. This typically induces remission in upwards of 90% of patients.

(ii) Consolidation/Intensification Chemotherapy

The aim of consolidation therapy is to eliminate residual leukaemia cells and to prevent the re-emergence of drug resistant disease. It involves different combinations of chemotherapy drugs used in induction and is usually 3-4 cycles of multi-agent chemotherapy. It also involves central nervous system directed therapy in the form of either intrathecal chemotherapy or high dose intravenous methotrexate. In selected patients, including adults with a suitable sibling donor and patients deemed to have high-risk disease, a bone marrow transplant or stem cell transplant may be used in place of consolidation or intensification chemotherapy.

(iii) Maintenance Chemotherapy

Treatment is completed with maintenance chemotherapy which typically includes daily 6-mercaptopurine and weekly methotrexate with pulses of vincristine and steroids for a period of approximately 2 years post consolidation. However individual protocols vary. Maintenance chemotherapy has been demonstrated to be crucial in eradication of residual sub-microscopic leukaemia and reducing the risk of relapse[44]. As discussed above and demonstrated in experiments below, a possible novel mechanism by which maintenance chemotherapy (Vincristine, Dexamethasone) may work is proposed.

(iv) Prophylaxis against the development of CNS leukaemia

The presence of lymphoid blasts within the central nervous system (CNS) occurs in 5-10% of adults with newly diagnosed ALL[47,48]. Patients at increased risk of CNS disease include those with T-ALL, a high white cell count, extramedullary disease and with high risk cytogenetic abnormalities such as *BCR-ABL1* and *KMT2A-AFF1*[47,48].

It is therefore important to prophylactically target treatment to prevent development of progression of ALL in the CNS. Cranial irradiation, intrathecal (IT) chemotherapy and components of systemic therapy which cross the blood-brain barrier have all been widely and successfully used to prevent the development of CNS-ALL. In adults several trials have reported CNS recurrence rates of less than 10% when a combination of high dose methotrexate (which crosses the blood brain barrier) and intrathecal chemotherapy is used[48,49].

(v) Allogeneic Stem cell transplantation

An allogeneic haematopoietic stem cell transplantation (alloHSCT) can be used effectively in place of consolidation and maintenance chemotherapy in treatment of ALL. It involves the use of conditioning chemotherapy, which is used both to eradicate residual leukaemic cells and adequately immunosuppress the recipient to allow them to receive the donated peripheral blood or bone marrow derived haematopoietic stem cells from an HLA-matched sibling or unrelated donor. The effectiveness of an alloHSCT relies both on the use of high dose intensive chemotherapy and in selected patients

total body irradiation to eradicate remaining ALL cells but also on a 'graft-versus-ALL' effect, which is the donor's T cells effectively attacking and killing the remaining ALL cells[50].

AlloHSCT is undoubtedly one of the most effective anti-ALL therapies available with one of the biggest ever studies of adult ALL (UKALL12/E2993) demonstrating a survival advantage for sibling alloHSCT over chemotherapy in a "donor versus no donor", intention-to-treat analysis[51]. Unfortunately, it is also the most toxic approach within the therapeutic scope, with significant associated morbidity and mortality directly related to the transplant. Thus necessitating a careful and selective approach about which patient's with ALL should be transplanted and those that should receive consolidation and maintenance chemotherapy instead.

The approach to selection of patients suitable for an alloHSCT varies across different countries. However factors typically favouring the use of alloHSCT include patients predicted to be at high risk of relapse at diagnosis with predictive factors including a high white count, advancing age or poor risk cytogenetics. Furthermore patients who have an inadequate response to induction chemotherapy determined by the presence of minimal residual disease (MRD) are also deemed to be high risk of relapse thus favouring the use of alloHSCT[52], which is discussed further below. Finally the availability of a matched donor either sibling or unrelated, age and fitness of the patient are also important determinants of the treatment approach selected.

1.2.3 Acute Lymphoblastic Leukaemia Monitoring Response to Treatment

The response to treatment in ALL was historically measured by morphological assessment of bone marrow blasts and cytogenetics following induction chemotherapy. Morphological detection of remission post treatment has very limited sensitivity of 1-5% and a patient in a morphological complete remission may still bear a considerable disease burden.

The advent of MRD monitoring via real-time quantitative polymerase chain reaction (RT-qPCR) of patient specific immunoglobulin heavy chain (IgH) and t-cell receptor (TCR) rearrangements or flow cytometry of a leukaemia associated immunophenotype has led to much improved sensitivity of disease monitoring post treatment[8,52]. It is now possible to quantitate treatment response very accurately and reproducibly, [53535353]in a patient specific-assay with a sensitivity of 10^{-5} (1 in 100,000 cells)[53].

Studies in both childhood and adult ALL have shown a significant correlation between MRD levels and subsequent relapse risk[8,52]. The presence of MRD positivity following two cycles of induction chemotherapy has been demonstrated to be a powerful predictor of subsequent relapse on our current treatment protocol [52], hence MRD assessment has become standard practice in monitoring ALL post treatment and in aiding treatment decisions including bone marrow transplant [52].

MRD assessment is important to this project as the bone marrow samples used for expansion of MSCs post treatment are used for assessment of MRD in patients. The possible relevance of residual leukaemia cells and the associated effects on mesenchymal stromal cells will be discussed below.

1.2.4 Acute Lymphoblastic Leukaemia Clinical Trial – UKALL14

UKALL14 is a clinical trial (NCT01085617) for adult ALL ongoing in the UK. A brief overview is relevant since the primary patient samples I have used are taken from the trial.

UKALL14 is a Cancer Research United Kingdom (CRUK)-funded, phase III randomised controlled trial. It opened in December 2010 to patients with de novo ALL between the ages of 25 – 65 years or 19 – 65 years in patients with the Philadelphia chromosome (t9;22). The B-ALL arm of the trial closed in 2018. The trial to date has recruited in excess of 900 patients.

The treatment protocol includes the standard 'backbone' of ALL treatment including a steroid pre-phase, induction, consolidation and maintenance chemotherapy along with the addition of novel drugs to examine their benefit in the treatment of ALL. These include rituximab, a CD20 monoclonal antibody for patients with B-ALL and nelarabine, an anti-metabolite for patients with T-ALL. The trial includes the newer formulation of

PEGylated asparaginase in place of the standard asparaginase drug and will also aim to further delineate which patient sub-groups with ALL benefit from an AlloHSCT.

The monitoring of response to treatment on the trial includes assessment of response by conventional means including morphological assessment of the bone marrow post treatment to determine complete remission but also by the newer technique of MRD monitoring by real time quantitative PCR in my host laboratory as discussed above. The schema is shown in ***Figure 1-4*** below.

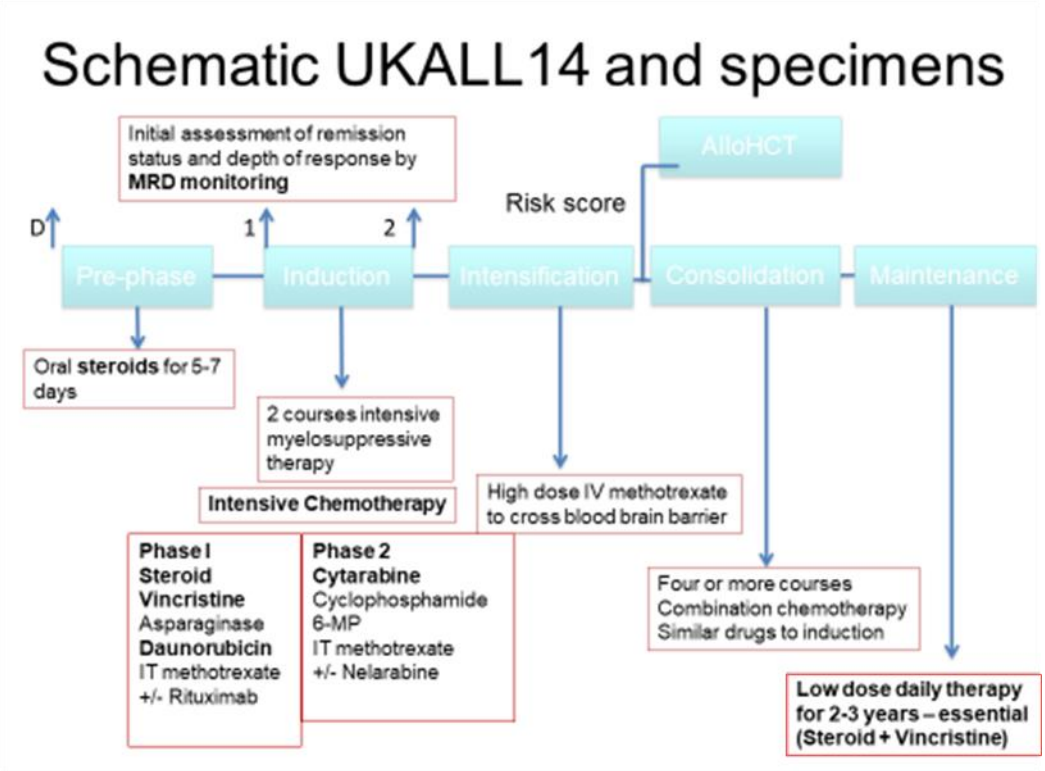

Figure 1-4 Schematic of UKALL14 trial – The diagram gives an overview of the UKALL14 trial with the courses labelled in the cyan boxes, chemotherapy listed in the lower red boxes and response to treatment monitoring in the top red box.

1.3 Bone Marrow Microenvironment

1.3.1 Healthy Bone Marrow Microenvironment

Haematopoiesis defines the process of development, self-renewal and differentiation of haematopoietic stem cells (HSCs), a crucial tightly-regulated process in the development of all haematopoietic cells. The bone marrow microenvironment provides a location for HSCs to reside, be maintained and differentiate into multiple blood lineages.

The stem cell niche first described by Schofield[54] describes the specific microenvironment in which HSCs are located and is composed of cytokines, stromal cells and extracellular matrix as regulatory elements that control the fate of HSCs.

Bone marrow stromal cells include mesenchymal stromal cells (MSCs), fibroblasts, adipocytes, endothelial cells, osteoblasts and macrophages. Stromal cells play a crucial role in the haematopoietic stem cell niche via secretion of growth factors, cytokines and extracellular matrix and cell to cell interactions between HSCs and stromal cells is critical in regulation of homeostasis in vitro[55].

Bone marrow adipocytes comprise the largest population of cells in the bone marrow cavity, accounting for 70% of adult bone marrow volume[56]. Although they were previously thought to be 'inert space fillers' in the bone marrow[57], more recently their

important role in energy storage[58], endocrine function[59], bone metabolism[60] and regulation of growth of tumours, including leukaemia, within the bone marrow has been recognised[61]. Bone marrow adipocytes are derived from bone marrow mesenchymal stromal cells.

1.3.2 Mesenchymal Stromal Cells

Mesenchymal Stromal Cells were first discovered by Friendstein in the 1970s when isolated from bone marrow[62]. They are a heterogeneous group of progenitor cells that aside from bone marrow have also been isolated from adipose tissue, placenta, skin and umbilical cord amongst other sources[63]. They have the capacity to self-renew and can also differentiate into several cell types including adipocytes, osteoblasts and chondrocytes.

Aside from their vital role in supporting maintenance and proliferation of HSCs discussed above, they also play an important role in tissue regeneration and increasingly are recognized for their ability to modulate the immune response in either an immune-stimulatory or immunosuppressive direction depending on the stimulation[64].

Due to problems with definition and difficulties comparing studies due to the fact MSCs lack a specific marker, ISCT proposed criteria for their definition listed on the following page in ***Table 1-1***, which focused on their ability to adhere to plastic in vitro,

surface markers and differentiation ability[65]. The criteria are considered by some to be unduly constraining and limitations include the fact MSCs phenotype may vary according to the tissue source[66]. There is a suggestion by some authors that a new definition is required which incorporates the cell transcriptome, proteome and secretome[67]. However, the ISCT criteria still remains widely recognized.

Table 1-1 ISCT criteria for MSC definition

1. Adherence to tissue culture plastic in standard tissue culture conditions
2. Positive cell surface markers: CD105; CD73; CD90
3. Negative cell surface markers: CD45; CD34; CD14 or CD11b; CD79a or CD19; HLA-DR; CD31*; TER-119* * Not included in ISCT criteria but used to exclude endothelial (CD31) and erythroid cells (TER-119)
4. In vitro differentiation: osteoblasts, adipocytes, chondrocytes (demonstrated by staining of in vitro cell culture)

1.3.3 Nestin Positive Stromal Cells

Nestin-positive MSCs described by Mendez-Ferrer[68] are recognised as an important sub-population of MSC within the stem cell niche. They were further defined by Pinho et al[69] as a sub-population of CD146+ stromal cells. Nestin positive MSC are believed to

play a vital role in maintenance of haematopoietic stem cells[70]. Maintenance of low reactive oxygen species (ROS) is vitally important in HSC maintenance as an increase in ROS has been demonstrated to induce cycling and differentiation in HSC and therefore loss of HSC from their niche[71].

Mesenchymal stromal cells (MSCs) have been shown to import ROS from stem cells via connexin gap junctions, and by that to reduce ROS content in primitive cells[72]. In addition, α-smooth muscle actin positive (αSMA) macrophages have been shown to secrete prostaglandin E2 to maintain low ROS levels in stem cells by inhibiting Akt phosphorylation[73]. Together, the supporting cells contacting primitive cells serve to reduce ROS levels in stem cells, attenuating excessive proliferation and differentiation that would induce stem cell pool exhaustion[71]. More recently the role of mitochondrial transfer between cells within the HSC has been described[74], which is discussed in more detail below. The depletion of nestin positive MSC within the bone marrow leads to a reduction in the HSC population in murine models[68]. Thus confirming the vital role of nestin positive MSC within the HSC niche.

1.3.4 Bone Marrow Stromal Cell Lines

Two human bone marrow stromal cell lines, designated HS5 and HS27a, created by a replication-defective recombinant retrovirus containing human papilloma virus E6/E7 genes are postulated to represent distinct sub-populations of stromal cells[75]. $CD146^-$ HS5 secretes growth factors (GM-CSF, G-CSF, IL-6) leading to the proliferation and differentiation of CD34+ cells, whereas $CD146^+$ HS27a cells do not secrete these

growth factors, but do express activities reported to be associated with the stem cell niche and maintenance of quiescence[76]. Given treatment resistance cells in ALL have consistently been demonstrated to be quiescent[13] and due to their CD146 expression – in the work described below I selected HS27a cells as well as healthy donor bone marrow MSCs to model the ALL niche in vitro.

1.4 Leukaemic Microenvironment

1.4.1 Leukaemic Microenvironment Overview

There is increasing evidence over the past 20 years that the bone marrow microenvironment plays an important role in the development, progression and treatment resistance of many haematological malignancies including ALL. There is growing support for the hypothesis that 'cross-talk 'between stromal cells and cancer cells are directly involved in maintenance and survival of haematological malignancies.

Kumagai et al[77] showed that the ex-vivo survival ability of ALL on bone marrow-derived stromal layers reflected aggressiveness of the disease and was a powerful, independent predictor of treatment outcome. More recently Ebinger et al.[13] eloquently demonstrated via a patient derived xenograft model that the small numbers of surviving ALL cells post chemotherapy and MRD cells from patients post treatment shared the common characteristics of dormancy, treatment resistance and ability to initiate leukaemia. However, the genetic make-up of these cells was essentially unchanged from the bulk population of ALL cells at diagnosis. Further,

following removal of these few treatment resistance cells from the microenvironment and examination *ex-vivo*, the ALL cells lost their dormancy, were no longer resistance to chemotherapy and were indistinguishable from the 'bulk' treatment sensitive ALL population. Thus, suggesting the microenvironment plays a crucial role in aiding survival of the small number of ALL cells that survive following induction chemotherapy.

Further evidence for the important role of the microenvironment in treatment resistance is provided by Duan et al[12] in their B-ALL murine model. In their B-ALL cell line model they found following treatment with cytarabine or daunorubicin surviving B-ALL cells formed a protective niche with nestin positive stromal cells, which were also partially alpha smooth muscle actin positive. In contrast, Hawkins et al[78] found in their murine model that following treatment with either vincristine or dexamethasone alone or in combination with asparaginase that T-ALL cells did not form a niche of surviving ALL cells as previously observed and the very few surviving ALL cells were noted to be moving more rapidly than at diagnosis in random locations and directions. Although the presence or absence of a niche following chemotherapy may be a feature of different disease biology (B-ALL vs T-ALL), in this thesis I propose instead that niche induction may relate to the chemotherapy drug used.

Recently many mechanisms of interaction between MSCs and ALL cells have been identified demonstrating how MSCs within the niche may aid survival of ALL cells from

chemotherapy. These include soluble factors, contact dependent mechanisms and modulation of the immune system which are discussed in further detail below.

1.4.2 Mesenchymal Stromal Cells in the Leukaemic Microenvironment

(i) Chemokines and Cytokines

Haematological malignancies derive advantage from the soluble factors and extracellular proteins secreted by MSCs and other cells within the bone marrow microenvironment. Civini et al[79] demonstrated that co-culture of Acute Myeloid Leukaemia (AML) cells, also an aggressive bone marrow-based malignancy, with healthy donor MSCs led to up-regulation of a number of pro-inflammatory cytokine genes and IL-17 pathway regulated genes. These included Interleukin-8 (IL8) and chemokine ligand (CCL2). Similarly, Polak et al[80] found that co-culture of MSCs and ALL cells, via tunnelling nanotube formation, led to increased secretion of pro-inflammatory factors (IL8, CXCL10, CCL17, CCL22) which was postulated to contribute to the subsequently demonstrated steroid resistance of ALL cells in co-culture. De Vasconcellos et al[81] also found that MSCs up-regulate IL8 and CCL2 expression following exposure to ALL cells and that IL8 and CCL2 aided the adhesion of ALL cells and MSCs. Alteration of the chemokine and cytokine profile within the bone marrow microenvironment therefore appears to lead to a niche more favourable for proliferation and survival of leukaemic cells.

The CXCR4-CXCL12 axis which plays a crucial role in the interaction of MSCs and HSCs in the stem cell niche has also been shown to be 'hijacked' by leukaemic cells within the bone marrow[82,83]. It is well established that CXCR4 positive leukaemic cells migrate to specific CXCL12 positive vascular niches in the bone marrow[82]and increased expression of CXCR4 on ALL blasts in paediatric ALL has been associated with a poorer prognosis[83].

(iii) Exosomes

Exosomes are small lipid membrane extracellular vesicles of endocytic origin. They are defined by their size (50-100nm), density (1.13-1.19g/m), morphology (cup or disc shape on transmission electron microscopy) and certain enriched protein markers[84]. They are able to shuttle bioactive molecules including proteins, DNA, mRNA and non-coding RNA from one cell to another[84]. There is evidence in a number of different cancers including B-ALL that exosomes transfer messages from cancer cells to immune cells and stromal cells to enable evasion of the immune system and contribute to formation of the tumour niche[85-87].

In Chronic Lymphocytic Leukaemia (CLL), a haematological malignancy, Paggetti et al[88] demonstrated that exosomes from CLL cells stimulated MSCs to induce an inflammatory and pro-tumorigenic milieu including increased angiogenesis, thus supporting survival and outgrowth of CLL cells. In ALL, Johnson et al[87] recently demonstrated that ALL cells also secrete extracellular vesicles (ECV) consistent with

exosomes and MSCs internalized them leading to a metabolic switch from aerobic metabolism to glycolytic metabolism in the MSCs. The MSCs post exposure to ECVs also increased their secretion of lactate which the authors postulated may provide an energy source to cancer cells, termed the 'reverse Walburg effect', discussed further below.

(iv) Asparagine Secretion

ALL cells have low asparagine synthetase (ASNS) expression and asparagine biosynthesis making them extremely sensitive to asparagine depletion[89]. Therefore, Asparaginase or its derivatives are a major component of ALL induction chemotherapy. Iwamoto et al. [90] demonstrated ASNS levels were on average 20 times higher in MSCs than ALL cells and they found MSCs provided protection to ALL cells from asparaginase by increasing the concentration of asparagine in the leukaemic cell microenvironment.

(v) Wnt Pathway and Notch Signalling

MSCs have been shown to induce activation of the Wnt Signalling pathway in ALL cells and this activation contributes to survival of ALL cells following exposure to chemotherapy [91]. The authors showed that subsequent pharmacological blocking of Wnt pathway activation by MSCs in ALL cells has been demonstrated both in vivo and in vitro to sensitize ALL cells to chemotherapy.

Notch signalling has been demonstrated to play a pivotal role in the onset and development in ALL[92]. More recently a role for MSCs in Notch signalling has been described[92]. MSCs express Notch receptors and ligands through which they can interact and influence normal and leukaemia cell survival.

(vi) Integrins

Within the bone marrow ALL cells physically adhere to MSCs, partly through binding of integrins expressed on ALL cells via cell receptors such as vascular cell adhesion molecule 1 (VCAM-1) on MSCs[93]. There is also evidence to support upregulation of Very Late Antigen-4 (VLA-4) (α4β1 integrin) in leukaemia[94]. It appears that β1 integrin adhesion regulates stability and trafficking of mediators and inhibitors of apoptosis, favouring survival of ALL cells[95].

Pillozzi et al.[96] demonstrated that the co-culture of ALL cells and MSCs in direct contact led to a signalling complex of human ether-a-go-go related gene 1 channels (hERG1 channels), the β1 integrin subunit and the chemokine receptor CXC chemokine receptor-4 (CXCR4) being formed on the lymphoblast membrane. This in turn activated the ERK1/2 and PI3/Akt pro-survival signalling pathways leading to ALL cells becoming markedly resistance to chemotherapy induced apoptosis.

(vii) Tunnelling Nanotubes

Tunnelling Nanotubes (TNT) were first described in 2004[97] as a new type of cell to cell communication between rat phaechromocytoma (PC12) cells, with subsequent studies demonstrating their presence in multiple cell types including tumour cells, MSCs and immune cells [80,98-102]. They are nano-scaled, open ended membranous tubes 50-200nm in diameter, containing F-actin and several cell diameters in length. They have no contact with the substrate and hover in medium. Two distinct mechanisms describe their formation. Firstly, a cell protrudes filopodium which makes contact to neighbouring cell(s) and subsequently converts into a TNT bridge[97]. Alternatively, cells have been demonstrated to form TNTs by retaining thin threads of membrane upon dislodgement[103]. Although the function of TNTs is not entirely defined, they are capable of transferring cellular components including organelles such as mitochondria[100], autophagosomes[104] and have a role in electrical signalling [101]. There is also evidence they are capable of transferring viruses[100] and prions[105].

TNTs have recently been demonstrated[80] in vitro between ALL cells and MSCs. The bidirectional transfer of cellular contents was noted via dye transfer between ALL cells and MSCs. The formation of nanotubes led to an increase in pro-inflammatory cytokine secretion and associated corticosteroid resistance in the ALL cells. When the nanotubes were inhibited by physical or chemical means, cytokine production was reduced, and the ALL cells were re-sensitized to corticosteroids[80].

Recently a novel type of TNT with continuous microtubules (MT-TNTs) has been described between PC12 cells, a rat phaeochromocytoma cell line[102]. PC12 cells were exposed to UV light and subsequently entered the early stages of apoptosis with loss of cytochrome c. However, these cells were able to be rescued from the execution phase of apoptosis by UV-unexposed or healthy PC12 cells via formation of MT-TNTs which transferred mitochondria from the healthy cells to the UV treated cells. MT-TNTs showed different physical properties to standard TNTs including increased diameter allowing dye entry, prolonged lifespan and decreased membrane fluidity. Notably, impaired formation of MT-TNTs and 'healthy' PC12 cells carrying defective mitochondria were unable to rescue UV treated PC12 cells from apoptosis.

Rustom in a review of TNTs in 2016[106] noted the recent finding of the MT-TNTs and proposed a model describing a link between reactive oxygen species (ROS), cellular stress and the presence of either F-actin containing nanotubes (AT-TNTs) or MT-TNTs using cancer as a possible example. Rustom proposes that rising ROS leads to cellular stress and affected cells send out distress signals via a possible Fibroblast Specific Protein 1 (FSP-1/S100A4) gradient to surrounding healthy cells with a view to formation of AT-TNTs once a pre-defined level of ROS is achieved. These AT-TNTs allow cells to restore redox/metabolic homeostasis by intercellular material exchange. If ROS levels rise further, endangering proper mitochondrial function, then MT-TNTs are formed. This allows for efficient redox/metabolic rescue of stressed cells via intercellular transfer of mitochondria along MT-TNTs. Finally, if ROS levels are increased even further TNTs are broken to isolate and remove degenerative cells from

the collective and apoptosis is induced. Rustom postulates that this may be a mechanism by which cancer cells survive exposure to chemotherapeutic agents that depend on ROS induction for apoptosis of the cancer cells.

Evidence for Rustom's proposed model is provided by Moschoi et al[107] in AML when they demonstrated transfer of mitochondria from MSCs to AML cells both *in vitro* and *in vivo* following exposure to chemotherapy. Strikingly, all chemotherapy drugs used with the exception of Vincristine induced transfer of mitochondria from MSCs to AML cells. Although they postulated an endocytic mechanism was responsible for the transfer of mitochondria, MT-TNTs could also potentially explain their findings.

Marlein et al[108] more recently demonstrated that mitochondrial transfer from MSC to AML cell occurred by tunnelling nanotubes in an NADPH Oxidase 2 (NOX2) dependent fashion. The transfer of mitochondria to AML cells was enhanced by exposure to ROS or ROS inducing agents and was reduced by anti-oxidants. A subsequent paper from the same group demonstrated that Peroxisome proliferator-activated receptor-gamma coactivator (PGC) 1 alpha, the master regulator of mitochondrial biogenesis, was upregulated in MSC transferring mitochondria to AML cells[109]. Forte et al[110] also demonstrated transfer of mitochondria from MSC to AML cell post exposure to the ROS inducing chemotherapy agent, cytarabine. Notably, they used nestin positive MSC in their model and concluded that the transfer of mitochondria was to 'detoxify' the leukaemic cell from the effects of chemotherapy. Several other disease models

support the concept of tunnelling nanotube formation and mitochondrial transfer as a rescue from oxidative stress including acute lung injury, corneal hypoxia and myocardial ischaemia[111-113].

However, to date there is no definitive evidence of mitochondrial transfer from MSC to ALL cells. A recent paper in T-ALL demonstrated that mitochondrial transfer occurred from T-ALL cells to MSC following chemotherapy[114]. They demonstrated that the mitochondria transferred showed evidence of increased mitochondrial DNA damage and postulated the transfer occurred to reduce the oxidative stress of the T-ALL cell following chemotherapy. Further support for transfer of mitochondria from target cell to MSC to protect against oxidative stress is provided by Golan et al in their HSC and MSC model[74].

(viii) Immune Modulation by MSC

There is also increasing evidence that MSCs or their closely related counter-parts fibroblasts can modulate the immune response in cancer. Depending on the setting this can include both immune stimulation and immune suppression of both the innate and acquired immune system. A recent paper by Entrena et al[115] showed that MSCs from paediatric ALL patients with low-risk disease activated Natural Killer (NK) cells and improved their ALL cell specific cytotoxicity in vitro compared to healthy donor MSCs. Whereas NK cells from high risk paediatric ALL patients had the opposite effect and suppressed the activation of NK cells and ALL cell cytotoxicity.

1.5 Cancer Associated Fibroblasts

1.5.1 Fibroblasts

Fibroblasts are the most common cell type within connective tissue in animals and play an important role in the synthesis of extracellular matrix and collagen and in wound healing. They share many features with MSCs and at present remain indistinguishable from MSCs by morphology, cell surface markers, differentiation potential, gene expression profiling and immunological properties[116]. The exact relationship between MSCs and fibroblasts therefore remains to be clearly defined. Fibroblasts, like MSCs, are found within the bone marrow stroma.

1.5.2 Myofibroblasts/Activated Fibroblasts

Resting or quiescent fibroblasts undergo activation during wound healing and become myofibroblasts or activated fibroblasts post exposure to transforming growth factor beta 1 (TGF-β1) secreted by platelets[117]. As myofibroblasts they acquire contractile stress fibres, express alpha-smooth muscle actin (α-SMA) and ED-A Fibronectin and form cell to cell contacts through gap junctions. They aid in wound closure. Upon completion of wound healing myofibroblasts undergo programmed cell death and are cleared and replaced by quiescent or resting fibroblasts[117].

1.5.3 Cancer Associated Fibroblasts Overview

Cancer Associated Fibroblasts (CAFs) are a cell within the microenvironment of many cancers that play a crucial role in promoting tumour growth, progression and metastases. They are the most prominent cell type within the tumour stroma of many cancers, notably breast, prostate and pancreatic cancer[118-120]. More recently they have also been described in haematological malignancies including CLL[88], AML[121] and lymphoma[122]. CAFs share similarities with myofibroblasts or activated fibroblasts in that they express α-SMA and ED-A fibronectin consistent with the concept that tumours represent 'wounds that don't heal'[123]. However, unlike myofibroblasts, CAFs are not removed by apoptosis and their activation is not reversible[117].

1.5.4 Origin of Cancer Associated Fibroblasts

CAFs are described as originating from a number of sources including resident fibroblasts, bone marrow derived MSCs and trans-differentiating epithelial or endothelial cells through epigenetic transition [124]. They become activated by several tumour secreted factors with TGF-β1 being the most described, in keeping with their normal physiological counterpart.

Activation of CAFs is also thought to be under Redox control with different studies showing ROS play a pivotal role in the process of fibroblast activation[125,126]. ROS produced by rapidly proliferating cancer cells generates oxidative stress to surrounding stromal cells inducing their transformation to the CAF phenotype[126]. Increased TGF-β1

secretion leads to increased production of ROS by CAFs, downregulation of the gap junctions between CAFs, achievement of their myofibroblast phenotype and tumour promoting activity[127]. In support of this, antioxidant treatments have been shown to prevent CAF activation and inhibit enhancement of tumour invasion[128].

1.5.5 Role of Cancer Associated Fibroblasts in Tumour Progression and Treatment Resistance

CAFs directly stimulate tumour proliferation by secretion of growth factors, hormones and cytokines including hepatocyte growth factor (HGF), epidermal growth factor (EGF), basic fibroblast growth factor (bFGF), CXCL12 and IL-6[117]. CAFs exhibit a pro-inflammatory signature of cytokines and chemokines including CXCL1, CXCL2, IL6, IL8 and IL1β which is believed to be a gene set under the transcriptional control of the NF-KB pathway[129]. This pro-inflammatory signature recruits pro-angiogenic macrophages and promotes tumour growth. It has been demonstrated in tumours with CAFs there are increased alternatively activated or tumour associated macrophages[130].

CAFs also secrete plasminogen activators and several members of the matrix metalloproteinase (MMP) family which leads to remodelling of the extracellular matrix and tumour expansion and invasion.

There is clinical and experimental data that support the hypothesis that CAFs regulate cancer cell motility and play an important role in their metastatic spread towards

distant organs[131]. It is also believed that CAFs play an important role in modifying the microenvironment in distant metastases to aid survival of cancer cells[131].

CAFs are also believed to supply lactate, ketone bodies and glutamate as an energy source to cancer cells via a switch from oxidative to glycolytic metabolism and a so-called 'reverse Walberg effect'[132]. As described above[87] exosomes secreted from ALL cell lines were able to induce the switch from oxidative to glycolytic metabolic in MSCs with the authors commenting this was in keeping with a CAF like phenotype. Given its relevance to this thesis the metabolic properties of CAFs and their impact on cancer cell metabolism is discussed in more detail below.

1.5.6 Metabolic Properties of Cancer Associated Fibroblasts

As rapidly proliferating cancer cells generate high rates of oxygen consumption leading to a progression of a hypoxic and acidic environment, cancer cells must rapidly adapt to survive. This adaption is achieved and sustained by 'metabolic reprogramming' of both the cancer cells themselves and CAFs within the tumour bed[126,133]. In the tumour microenvironment, CAFs appear to be re-wired to fuel the massive proliferation and nutrient demands of cancer cells by undergoing transition to a catabolic state, where they directly fuel adjacent tumour cells through production and supply of lactate, pyruvate and ketone bodies[134].

ROS are known to play an important role in the metabolic reprogramming that occurs as an adaption to oxidative stress that triggers CAF differentiation[135]. Cancer cells produce high levels of ROS through mitochondrial dysfunction, upregulation of NADPH oxidases and alteration of antioxidant enzymes[136]. Therefore, ROS generates a reactive microenvironment, where the energy needed for cancer cells is sustained by CAFs, whose activated phenotype is constantly maintained.

The oxidative stress induced in CAFs leads to production of autophagosomes that fuse with lysosomes, with a consequent mitochondrial disruption and Caveolin-1 (Cav-1) degradation[137]. Cav-1 downregulation leads to the CAF shift towards a catabolic phenotype and enhanced mitochondrial activity of adjacent cancer cells[138]. Hence CAFs undergoing metabolic reprogramming switching towards a more glycolytic phenotype, whereas the cancer cells rely more on mitochondrial routes of energy production via OXPHOS[136]. Therefore aerobic glycolysis occurs predominantly in the CAFs rather than cancer as originally thought (Warburg effect) and instead the so called 'reverse Warburg effect' occurs where the CAF catabolic state fuels mitochondrial OXPHOS in the adjacent cell[134].

Further evidence for the 'reverse Warburg effect' is supplied in a recent study by Ippolito et al[139] in prostate cancer showing that CAFs enhance cancer cell mitochondrial mass and activity through two distinct mechanisms. Firstly, lactate secreted by CAF alters the NAD+/NADH ratio in cancer cells, culminating in PGC1alpha

activation and enhancement of mitochondrial mass and activity. Secondly, the prostate cancer cells 'hijack' CAF- derived functional mitochondria via tunnelling nanotubes leading to enhanced motility and invasiveness of the prostate cancer cells.

Therefore cancer cells are able to exploit CAFs metabolically to support their own growth and survival. Furthermore there is evidence CAFs are able to help cancer cells overcome pharmacological stress preventing apoptosis[140] and enhancing mitochondrial activity in cancer cells[141]. Cancer cells that acquire drug resistance are often characterised by increased mitochondrial mass, OXPHOS activity, and antioxidant capacity[136]. This has been demonstrated in AML following treatment with cytarabine, where residual leukaemic cells post treatment had a high OXPHOS status and mitochondrial mass[142].

Initially, anticancer drugs reduce tumour mass, by damaging or killing bulk population of cancer cells, however this initial cancer regression often precedes the appearance of new and more vigorous tumours due to the surviving residual cancer cells that resist the pharmacological stress via mitochondrial adaption[143]. This is in keeping with the clinical observation in ALL that patients with relapsed disease tend to have limited responses to salvage chemotherapy with very poor long-term survival[144].

Given increased ROS production and oxidative stress on stromal cells induces the CAF phenotype and subsequent metabolic reprogramming, it supports the idea that

treatment with antioxidants and or anti-inflammatories may allow inhibition of the CAF phenotype and therefore metabolic separation of CAF and cancer cell. In support of this hypothesis is evidence that treatment with anti-oxidants such as n-acetylcysteine (NAC), metformin or nitric oxide can reverse CAF phenotypes, rescuing Cav-1 expression in fibroblasts[145]. The inhibition of CAF induction using the anti-oxidant NAC and the corticosteroid, dexamethasone, will be further explored in this thesis.

1.5.7 Chemotherapy-induced Cancer Associated Fibroblasts

There is also evidence that standard chemotherapy drugs used to treat cancer can transform fibroblasts into the cancer associated fibroblast phenotype in a similar way to cancer cells. Peiris-Pages et al[146] provide in vitro evidence of chemotherapy induced modifications in fibroblastic cells including the expression of α-SMA, a glycolytic switch, activation of the JNK/AP1, HIF1, TGFβ/SMAD, STAT3 and NFkB stress-induced pathways, a greater secretion of the inflammatory cytokine interleukin 6 (IL6) to aid cancer cell survival, induction of stemness in the cancer cells and recruitment of immune cells to further support malignancy. All well described properties of CAFs.

Sun et al[147] demonstrated that the activation or damage to fibroblasts induced by chemotherapy aided treatment resistance of prostate cancer through secretion of Wnt family member wingless-type MMTV integration site family member 16B (WNT16B). Chan et al[148] also demonstrated that activation of fibroblasts with cytotoxic

chemotherapy induced a stromal cell state, characterised by enhanced ELR-motif cytokine secretion which aided cancer cell survival.

A possible explanation for the finding that chemotherapy can cause induction of a CAF phenotype is through the DNA damaging certain chemotherapies cause and subsequent ROS production. A theory that will be explored further in this thesis.

1.5.8 Evidence of Cancer Associated Fibroblasts in Acute Lymphoblastic Leukaemia

CAF have never been definitively described in ALL. However over the past two years they have been described in a number of other haematological malignancies including CLL[88] and AML[121]. Duan et al[12] described the presence of MSCs in their murine model of B-ALL consistent with a CAF phenotype. Following exposure to the ROS-inducing chemotherapy agents, cytarabine and daunorubicin, MSCs via TGF-β1 secreted by ALL cells were transformed into α-SMA expressing cells which aided survival of ALL cells via the pro-survival factor growth/differentiation factor 15 (GDF-15). They also demonstrated the presence of α-SMA positive cells in patient's post treatment trephine biopsies who failed to achieve complete remission following induction chemotherapy whereas they were absent in patients who had achieved complete remission. Furthermore, as discussed above[87] exosomes from ALL cells have been demonstrated to induce a CAF like catabolic state in MSCs.

1.5.9 Acute Lymphoblastic Leukaemia, Mesenchymal Stromal Cells and Cancer Associated Fibroblasts

In this thesis in chapter 3, I systematically defined, described and categorised the appearance and behaviours of MSC in B-ALL at diagnosis and following treatment. The UKALL14 trial specimens provided a unique opportunity to achieve this objective on a large scale given the large number of samples available, the fact treatment is uniform, and a large amount of clinical and outcome data is known.

I was able to expand MSCs from patient samples at different stages of disease and to build a bank of MSCs to be used for future experiments and in so-doing I was able to determine which factors predict successful expansion of MSCs and establish if these are linked to patient outcome.

It soon became evident that I was able to detect the development of MSC with an 'activated' or CAF-like phenotype, a phenomenon which has not be described, to date. I therefore used the initial data I generated in conjunction with clinical observations in B-ALL to refine my hypothesis and re-focus my project on the role of 'activated' MSC or CAF in ALL.

1.6 Hypothesis and Aims

The central hypothesis of this thesis is that surviving B-ALL cells following chemotherapy are protected from oxidative stress by activated mesenchymal stromal cells with a CAF-like phenotype. This protective effect is influenced both by the intrinsic genetic lesion of the ALL cell and the chemotherapeutic agent used.

Chapter 3: Isolation, expansion and characterisation of BM-MSCs from patient bone marrow specimens on the UKALL14 trial

Aims:

1. To isolate and characterise MSC from patient samples at different stages of disease on the UKALL14 trial.
2. To determine if MSC from patient specimens have characteristics consistent with a CAF phenotype.

Chapter 4: Modelling induction of a CAF phenotype in MSC following exposure to B-ALL cells

Aims

1. To determine if B-ALL cells across different genetic sub-types can induce a CAF-like phenotype in MSC *in vitro*.
2. To investigate the underlying mechanism for the induction of the ALL-CAF phenotype in MSC.

Chapter 5: Modelling induction of a CAF phenotype in MSC following exposure to chemotherapy drugs used in ALL

Aims

1. To determine if chemotherapy drugs commonly used in ALL treatment can induce an ALL-CAF phenotype in MSC *in vitro*.
2. To explore the functional significance of the ALL-CAF phenotype on ALL cell proliferation and survival following chemotherapy *in vitro*.

Chapter 6: Mesenchymal stromal cells transfer mitochondria to B-ALL cells to rescue them from oxidative stress

Aims

1. To explore the mechanism by which ALL-CAF protect ALL cells from chemotherapy induced oxidative stress, focusing on the role of tunnelling nanotubes and mitochondrial transfer.
2. To use a disseminated murine model of B-ALL to demonstrate that ALL-CAF induction, mitochondrial transfer and niche formation occur *in vivo* and is dependent on the chemotherapy drug used.

Chapter 2 Methods

2.1 Primary Cells

2.1.1 Human Specimens and Consent

Primary material was sourced from patients enrolled on the UKALL14 trial (NCT01085617). Informed consent for specimen collection and future use in ethically approved projects was given by all patients. This project was ethically approved under the application 16/LO/2055 "Genetic and functional characterization of ALL". Healthy donor specimens were collected from patients undergoing bone marrow harvest who had given their consent for excess material to be used for research.

2.1.2 Primary Mesenchymal Stromal Cell Isolation and Expansion

Mononuclear cells (MNC) from bone marrow specimens were isolated by density gradient centrifugation (Ficoll-Paque™, Amersham Biosciences, Bucks, UK). The resultant MNC were re-suspended in Mesencult© MSC basal medium supplemented with Mesencult© stimulatory supplements, 100 units/ml penicillin G, 100mg/ml streptomycin, 2mM L-glutamine and 1ng/ml basic fibroblast growth factor. Samples where the MNC had previously been stored in liquid nitrogen were thawed out as described below and re-suspended in the same media. The cells were plated in T75 – T175 flasks at a density of 1x10^5/cm^2 – 1.5x10^5 with 10-25 ml of media and 24 to 48 hours after plating, non-adherent cells were removed by washing with phosphate

buffered saline (PBS) and fresh medium added. The media was then replaced every 3-5 days.

Following 14 – 21 days in culture when MSC had reached sub-confluency, cells were washed with 10ml PBS and incubated with 2ml of Trypsin for T75 flanks for 2 minutes and 5ml for T175 flasks for 3-5 minutes. The detached cells were then collected in 10ml fresh medium, centrifuged at 1200rpm for 5 minutes, enumerated in a haem cytometer chamber and either frozen as described below for future propagation or passaged into new T75 – T175 flask at a density of 1 – 2x10^4/cm^2. The cells were passaged when they reached sub-confluence (80-90%) or frozen as described below for future experiments.

MSC used in experiments were from passage 3 – 5. Cell supernatants used were from passage 1 or 2.

2.1.3 Mesenchymal Stromal Cell Cryopreservation and Thawing

MSCs were cryopreserved by re-suspending the live cell pellet in a freezing mix consisting of 10% dimethyl sulfoxide (DMSO; ATCC) and 90% foetal bovine serum (FBS) to a concentration of $1x10^6$ cells/ml. The cell suspension was aliquoted into polypropylene cryogenic vials (Corning) and placed at -80ºC overnight in a freezing container (Nelgene, Rochester, US) filled with 100% isopropyl alcohol to achieve a

cooling rate of 1ºC/minute. On the following day, the frozen cells were transferred to liquid nitrogen for long-term storage.

To thaw cryopreserved cells the frozen vials were placed in a 37ºC water bath for 2~3 minutes. As soon as the cells were thawed, 10 ml of FBS was slowly added into the vials with gentle mixing. After centrifugation at 1200 rpm for 5 minutes without brake, the cell pellet obtained was washed again with the appropriate cell medium supplemented with 50% FBS to remove any residual DMSO. Finally, cells were re-suspended in supplemented medium and kept initially in a T25 flask at 37ºC, passaging to a T75 flask when the cells reached sub-confluency, at a cell density described above.

2.1.4 Mesenchymal Stromal Cell Characterization

Cells were assessed at the time of tissue culture passage (P2-4) to confirm success of the isolation procedure, and purity of the product obtained. Criteria set out by the International Society for Cellular Therapy (ISCT) were used to define MSCs and are summarized above in the introduction.

1. Microscopic evaluation

Cells were monitored microscopically and identified by their adherence to tissue culture plastic and their distinctive spindle-shaped appearance in vitro.

2. Flow cytometric classification

For immunophenotyping of primary MSCs, samples were analysed as detailed below in flow cytometry methods.

3. Multi-potent differentiation

Adipogenic and osteogenic differentiation of human MSCs was demonstrated using the Human Mesenchymal Stem Cell Functional Identification Kit (R&D Systems; Cat. no: SC006) as detailed below in imaging methods.

2.1.5 Macrophage Characterization

Samples with macrophages were washed with PBS 10ml x1 and incubated with 2-5ml Trypsin for 2-5 minutes. Following scrapping the bottom of the flask with a cell scrapper the detached cells were collected in 10ml PBS and then centrifuged at 1200rpm for 5 minutes. The cell pellet was then re-suspended in 1-2mls of fresh media. A cytospin was performed and cells fixed on a number of slides. The fixed cells were stained with May-Grünwald-Giemsa (MGG) stain and appropriate antibodies on individual slides.

2.2 Cell lines

2.2.1 Mesenchymal Stromal Cell and Acute Lymphoblastic Leukaemia Cell Lines

Human MSC cell line HS27a (ATCC) and the B-precursor ALL cell lines (DSMZ) SD1, SEM, 697, TOM1 and REH were grown in RPMI 1640 (Gibco) media supplemented with 10% foetal bovine serum (FBS) (Gibco) (20% for TOM1), 100 units/ml penicillin G (Gibco), 100mg/ml streptomycin (Gibco) and 2mM L-glutamine (Gibco). Murine MSC cell line MS5 (DSMZ) was grown in alpha MEM (Gibco) media supplemented with 5% FBS, 100 units/ml penicillin G (Gibco), 100mg/ml streptomycin (Gibco) and 2mM L-glutamine (Gibco).

2.2.2 Mesenchymal Stromal Cell and Acute Lymphoblastic Leukaemia Co-culture

For co-culture experiments, HS27a, MS5 or HD MSC were plated on Day 0, and 24 hours later ALL cells added at a ratio of 1 MSC:4 ALL cells with chemotherapy where appropriate. For transwell experiments, the B-ALL cells were added onto a transwell insert (0.4 – 1.0 μm) (Greiner Bio) with or without chemotherapy at 24 hours.

2.2.3 Acute Lymphoblastic Leukaemia Conditioned Media Experiments

For the conditioned media experiments, media was collected from the ALL cells post centrifugation and added to HS27a cells.

2.2.4 Mitochondrial Depletion of Cell Lines

HS27a cells or SD1 cells were cultured in media containing 0.1µg/ml ethidium bromide, 50 µg/ml uridine and 1mM sodium pyruvate for 4 weeks.

2.2.5 MTS Cell Proliferation Assay of Cell Lines

B-ALL cells with or without the addition of chemotherapy were co-cultured with either untreated or chemotherapy pre-treated HS27a. After 48 hours the viability or proliferation of the B-ALL cells was measured using the CellTiter 96® Aqueous One Solution Reagent (MTS) according to manufacturer's instructions. Absorbance was read at 570nm on a BMG FLUOstar Galaxy absorbance reader.

2.3 Chemotherapy and other Therapeutic Agents

2.3.1 Chemotherapy and Therapeutic Drugs Used

All chemotherapy drugs, nocodazole, colchicine and latrunculin-B were made into stock solutions according to manufacturer's instructions and stored at -20C. When required, they were thawed out and diluted in media (*in vitro* work) or PBS (*in vivo* work) to correct concentrations. The drugs used are listed in the ***table 2-1*** on the following page.

Table 2-1 Chemotherapy and therapeutic drugs used

Drug	Manufacturer	Mechanism of Action	When used in UKALL14
Cytarabine (AraC)	Cambridge Biosciences	DNA synthesis inhibitor	Post Phase II Consolidation
Daunorubicin (DNR)	Cambridge Biosciences	Intercalates DNA and prevents topoisomerase II progression	Post Phase I Consolidation
Dexamethasone (DEX)	Cambridge Biosciences	Corticosteroid, potent anti-inflammatory agent	Post Phase I Consolidation Maintenance
Vincristine (VCR)	Cambridge Biosciences	Microtubule damaging agent	Post Phase I Consolidation Maintenance
Nocodazole (NOC)	EMD Millipore	Microtubule damaging agent, designed as anti-helminth	Not used
Colchicine (COL)	Generon	Microtubule damaging agent, used as treatment for gout	Not used
Latrunculin-B	Cayman Chemical Company	Actin polymerisation inhibitor	Not used

2.4 Flow Cytometry

2.4.1 Flow Cytometry Preparation and Analysis

Samples were analysed using appropriate antibodies (listed below) either in combinations or as single stains after harvesting by trypsinisation, re-suspending in PBS, and incubating with the appropriate primary antibody/antibodies 4°C for 30 minutes. Flow minus one (FMO) controls were used to account for non-specific background staining. Live cells were gated according to their FSC/SSC characteristics or identified by using DAPI to exclude dead cell population. Ten thousand events from the live gate were collected on a BD FACSAria instrument (Becton Dickinson, Oxford, UK). Cells were sorted using BD FacsAria III. Data were analysed using FlowJo software (version 7.4.1). Antibodies and stains used for flow cytometry are listed in ***table 2-2***.

2.4.2 Cell viability and apoptosis assay

B-ALL cells were cultured in mono-culture or co-culture with HS27a in 6-well plates with or without AraC, VCR or DEX. At 48 hours all cells were collected and stained with CD19 before staining with Annexin V according to manufacturer's instructions, finally followed by DAPI. Using flow cytometry, the CD19+ population (B-ALL cells) was analysed for Annexin V/DAPI to determine apoptotic and dead cell populations.

2.4.3 ROS quantification

B-ALL cells were cultured with or without chemotherapy drugs. CellROX® Green (ThermoFisher C10444) staining was carried out at 24 hours, according to manufacturer's instructions and quantified by flow cytometry.

2.4.4 MitoTracker™ Assay

MSC were stained with MitoTracker™ Deep Red (ThermoFisher M22426) or MitoTracker Green™ (ThermoFisher M7514) according to manufacturer's instruction at 37°C for 30 minutes. The cells were washed twice, then left for three hours to eliminate unbound probe prior to a final wash. The stained MSC were co-cultured with ALL cells for 24 – 72 hours. Mitochondrial transfer was quantified among the CD19-expressing ALL population.

2.4.5 Fluorescence-activated Cell Sorting

Samples were incubated with the appropriate primary antibody/antibodies at 4°C for 30 minutes, and then analysed for fluorescence-activated cell sorting. Fluorescence minus one (FMO) controls were used to account for non-specific background staining. Dead cells were excluded according to forward scatter and side scatter and DAPI staining. Cells were sorted using a BD FACSARIA Fusion according to human CD90 and/or human CD19 expression.

2.5 Immunocytochemistry

2.5.1 Immunocytochemistry Staining Protocol

Cells were fixed with 4% paraformaldehyde, washed and then blocked for 2 hours with a blocking buffer containing 1% bovine serum albumin (BSA), 10% normal donkey serum (Abcam) and 0.3% Triton X-100 (Sigma Aldrich). After blocking, the relevant primary antibody was added followed by a secondary antibody for one hour each. Serial dilutions were used to determine the optimum concentration of primary antibody used. Secondary antibody dilution was performed according to the manufacturer's instructions. The nuclear stain DAPI (Santa Cruz Biotechnology) and F-actin stain Phalloidin-Atto 633 (Sigma Aldrich) stain where relevant were added for 10 minutes prior to removal and washing with PBS. Antibodies and stains used for immunocytochemistry are listed on the following page in ***Table 2-2***.

Table 2-2 Antibodies and stains used for immunocytochemistry and flow cytometry

CD19 PE	Primary	BD Biosciences	Lineage marker	FC
Annexin V	Primary	BD Biosciences	Apoptosis marker	FC
CellROX© Green	Cell Dye	Thermo Fisher	Intrinsic Cell ROS	FC
DAPI	Stain	Santa-Cruz Biotechnology	Nuclear stain	ICC/FC
Mitotracker© Deep Red	Stain	Thermo Fischer	Mitochondrial stain	FC/ICC
Mitotracker © Green	Stain	Thermo Fischer	Mitochondrial stain	FC/ICC
Alpha Smooth Muscle Actin	Primary	R&D Systems	Specific Actin stain	ICC
CD73 PE	Primary	BD Biosciences	Human MSC	FC
CD90 FITC	Primary	BD Biosciences	Human MSC	FC
CD105 PerCP-Cy 5.5	Primary	BD Biosciences	Human MSC	FC
CD45 APC	Primary	BD Biosciences	Lineage marker	FC
CD19 APC	Primary	BD Biosciences	Lineage marker	FC
HLA-DR APC	Primary	BD Biosciences	Lineage marker	FC
CD34 APC	Primary	BD Biosciences	Lineage marker	FC
CD14 APC	Primary	BD Biosciences	Lineage marker	FC
Goat anti-human FABP-4 antigen affinity-purified polyclonal antibody	Primary	R&D systems	Adipocytes	ICC
Mouse anti-human osteocalcin monoclonal antibody	Primary	R&D systems	Osteocytes	ICC
Northern Lights TM NL557-conjugated donkey anti-goat antibody	Secondary	R&D systems	N/A	ICC
Northern Lights TM NL557-conjugated donkey anti-mouse antibody	Secondary	R&D systems	N/A	ICC
Phalloidin-Atto 633	Primary	Sigma-Aldrich	F-actin	ICC

2.6 Imaging

2.6.1 Fluorescent Microscope Imaging

Images were acquired on the Zeiss axio-observer Z1 at room temperature with objectives 10xair Plan-NEOFLUAR NA 0.3, 20xair Plan-NEOFLUAR NA 0.4 and 40xair Plan-NEOFLUAR NA 0.75 using Axiovision Rel. 4.8 software and AxioCam MR Rev 3 camera. Fluorochromes used include DAPI, red fluorescent protein and cyanine5. No image adjustments were required.

2.6.2 Confocal Time Lapse Imaging

Differentially stained cells were cultured on a 35mm glass bottom dish (Maktek) coated with 20µg/ml fibronectin at 37ºC on a heated tray at 5% CO_2. Chemotherapy was added immediately prior to imaging. Images were acquired on a Zeiss LSM 880 with Airyscan with objective 63xOil Plan-apochromat NA 1.40 at a resolution of 1024 x 1024 pixels in the *x* and *y* directions and 0.5µm steps in z direction. The pinhole diameter was set at 1 airy unit. DiO and Deep Red Mitotracker were excited with the 488 and 633 lasers respectively. Transmitted Photomultiplier Tube was used in transmitted mode to generate an image. Imaging processing was done with Oxford Instruments, BITPLANE Imaris 9.1 and Carl Zeiss ZEN Black.

2.7 Molecular Biology

2.7.1 Real Time Quantitative PCR

(i) RNA extraction

Cells following isolation were pelleted, supernatant removed and 1ml of TRIzol® reagent added (AMbion by Life Technologies, 15596026) per 5-10 x 10^6 cells. The solution was transferred to an RNase-free Eppendorf tube and incubated on ice for 15-30 minutes. Chloroform (Sigma Aldrich) 0.2ml per 1ml of TRIzol® was then added to separate the RNA from DNA. The tube was shaken vigorously and then incubated on ice for 2-3 minutes. Samples were then centrifuged at 12000g for 15 minutes at 4^{o}C. The upper aqueous phase was transferred into a new RNase-free tube. Isopropanol (Sigma Aldrich) was added at a ratio of 0.5ml to 1ml of TRIzol reagent. The samples were frozen at -80°C overnight to allow the RNA to precipitate. Following thawing and washing with 70% ethanol the pellet of RNA was re-suspended in 25-50µl RNase free water and the concentration and quality measured on a NanoDrop.

(ii) cDNA Synthesis using the RT² First Strand Kit

cDNA was synthesised using the RT2 first strand kit (Qiagen - 330401) according to manufacturer's instruction. Initially a genomic DNA elimination mix (10µl/sample), included in the kit, was added to the RNA samples to eliminate genomic DNA. A reverse transcriptase mix (10µl/sample) was prepared as per the kit instructions and added to each tube. This was incubated at 42°C for 15 minutes and then the reaction was immediately stopped by incubating at 95°C for 5 minutes. RNase-free water (91

µl/sample) was then added to the reaction and mixed. The reactions were placed on ice ready for the real-time PCR protocol.

(iii) Real-Time PCR for RT² Profiler PCR Array

The PCR components mix included in the kit was prepared by mixing the SYBR Green Mastermix, cDNA synthesis reaction and RNase-free water at the appropriate ratio according to the kit instructions and number of wells required. The PCR components mix was then dispensed (25µl/well) into the provided RT² Profiler PCR Array containing a pre-defined and pre-prepared selection of primers for appropriate CAF defining targets listed in ***table 3-3*** on the following page. The array was sealed, centrifuged to remove bubbles and then run in an Applied Biosystems 7500 at cycling conditions defined in the kit protocol (1 cycle - 10 minutes 95^{o}C, 40 cycles – 15 seconds 95^{o}C and 1 minute 60^{o}C). Each sample was run in triplicates. The threshold cycle for each well was then calculated using the real-time cycler software as described in the kit protocol. The threshold cycle values were then exported to a blank Excel® spreadsheet and analysis performed with SABiosciences PCR Array Data Analysis software, provided by Qiagen.

Table 2-3 PCR Cancer Associated Fibroblasts gene targets

#	Gene Symbol	Gene RefSeq #
1	*PDGFR-2*	NM_006206
2	*PDGFR-1*	NM_002609
3	*Nbla00170*	NM_006617
4	*FSP1*	NM_002961
5	*FAPA*	NM_004460
6	*IL-6*	NM_000600
7	*CD90*	NM_006288
8	*ACTA2*	NM_001613
9	*TN-C*	NM_002160
10	*FN*	NM_002026
11	*COL1A1*	NM_000088
12	*CXCL8*	NM_000584
13	*CXCL1*	NM_001511
14	*CXCL2*	NM_002089
15	*CCL2*	NM_002982
16	*MMP1*	NM_002421
17	*VEGF*	NM_003376
18	*FGF-2*	NM_002006

2.7.2 Mitochondrial DNA Detection

DNA was extracted from cells using QIAamp® DNA Blood Mini Kit (Qiagen 51106). The DNA was amplified for detection of mitochondrial and nuclear DNA from both human and mouse using the primers in ***table 2-4*** below. Annealing temperature used was 60 degrees for 15 to 25 cycles. The PCR product was run in 2% agarose (SIGMA) gel and visualised under UV.

Table 2-4 Primers for mitochondrial DNA detection

Species	Genome	Forward Primer Seq 5'-3'	Reverse Primer Seq 5'-3'	Amplicon
Mouse	Mitochondria	CCC AGC TAC TAC CAT CAT TCA AGT	GAT GGT TTG GGA GAT TGG TTG ATG T	117
Human	Mitochondria	CCC CAC AAA CCC CAT TAC TAA ACC CA	TTT CAT CAT GCG GAG ATG TTG GAT GG	221
Mouse	Nuclear beta globin	CCA ATC TGC TCA CAC AGG ATA GAG AGG GCA GG	CCT TGA GGC TGT CCA AGT GAT TCA GGC CAT CG	494
Human	Nuclear beta globin	GAA GAG CCA AGG ACA GGT AC	GGA AAA TAG ACC AAT AGG CAG	408

2.8 Quantification of Secreted Proteins

2.8.1 ELISA

Cell supernatant was collected from the MSCs when they reached sub-confluency at passage 1-3 and stored at -80 degrees.

Semi-quantitative 'screening' multi-analyte ELISAs were performed on the thawed out 1st passage cell supernatant using custom made kits (Custom Mix-n-Match Multi-Analyte ELISArray Kit, Qiagen 336111). Subsequently single analyte quantitative ELISA kits were used on the 2nd passage cell supernatant as listed below.

Table 2-5 ELISA kits used

Sl. No.	Analyte	Company
1	CCL2/MCP-1	Invitrogen (88-7399-88)
2	CXCL1/Gro-α	Qiagen (SEH00696A)
3	CXCL2/Gro-β	R&D systems (DY276-05)
4	IL6	Invitrogen (88-7066-88)
5	IL8	Invitrogen (88-8086-88)

2.8.3 Cytometric Bead Assay

Cytometric Bead Array (BD Biosciences) was carried out according to manufacturer's instruction using human IL-6 Flex Set (BD Biosciences 558276), human IL-8 Flex Set (BD Biosciences 558277) or human MCP-1/CCL2 Flex Set (BD Biosciences 558287). Three

hundred events/analyte from the live gate were collected on a BD FACSAria instrument (Becton Dickinson, Oxford, UK). Data were analysed using FCAP Array Software Version 3.0.

2.9 *In vivo* work

2.9.1 *In vivo* Regulations and Guidelines

All animal experiments were performed according to UK Home Office approved protocols and institutional guidelines.

2.9.2 Disseminated NOD-*scid* IL2Rg^{null} (NSG) Xenografts

Disseminated SEM xenografts were established in sixteen 8-10-week-old NSG (Non obese diabetic severe combined immunodeficiency gamma) male mice (Charles River, Margate, UK) by tail vein injection of 2 x 10^6 SEM cells expressing luciferase and blue fluorescent protein. One additional NSG male mouse not injected with SEM cells was used as a baseline control for imaging and subsequent analysis as a positive control for detection of murine mitochondrial DNA by PCR.

2.9.3 *In vivo* Imaging

Seven days after tail vein injection of SEM luciferase expressing cells, engraftment was confirmed by bioluminescent imaging. Mice were shaved and injected i.p. with 200 µl of D-luciferin (Caliper Life Science, Cheshire, UK). They were then imaged under

anaesthetic (Isofluorane) under IVIS 100 Lumina (Caliper Life Sciences, Chesire, UK). The results were analysed using Living Image 3.2 software. The same protocol for in vivo imaging was used to assess leukemic burden at day +3 following treatment.

2.9.4 Chemotherapy Treatment

Ten days following tail vein injection of SEM cells, the mice were split into four treatment groups of four mice each. The different groups of mice were treated with either 200µl PBS (control), AraC 100mg/kg in 200µl PBS, VCR 0.25mg/kg in 200µl PBS or Nocodazole 9mg/kg in 200µl PBS i.p. daily for two days.

2.9.5 Sacrifice and Analysis

Two days following the final dose of treatment the mice were humanely sacrificed and bone marrow cells were extracted by isolation and crushing of the tibias and one femur. The remaining uncrushed femur was sent for histopathology. SEM cells were identified, or flow sorted by BFP expression for subsequent analysis, including intracellular ROS, mitochondrial mass (Green Mitotracker, ThermoFisher M7514) and DNA extraction for identification of murine mitochondria DNA by PCR. For isolation and expansion of murine stromal cells, residual cells post extraction of SEM cells were plated in 6 well plates at a density of 1-2 x 10^6 per ml in αMEM media supplemented with 10% FBS and Pen-Step-Glut. Seventy-two hours later the media was removed, washed with PBS and new media added. Two weeks later the adherent cells were removed with trypsin, washed with PBS and re-plated in a glass bottom plate for imaging. Following overnight culture to allow the stromal cells to adhere, the cells were fixed and stained with Phalloidin, DAPI and αSMA as previously described. The

plates were then imaged using a fluorescent microscope as described previously in methods.

2.9.6 Immunohistochemistry of Femur Sections

Immediately following humane sacrifice of the mice, one femur was removed and fixed in 10% neutral buffered formalin. The samples were decalcified in 10% formic acid for 9-10 hours then processed and embedded. Following sectioning the samples were stained with the appropriate primary and secondary antibodies.

2.10 Statistics

2.10.1 Statistics Overview

The data generated was analysed on GraphPad Prism 6 software or other software where indicated. For statistical comparison Chi-squared and unpaired student t tests were used where appropriate and are stated in the results.

Chapter 3: Isolation, Expansion and Characterisation of BM-MSCs from Patient Bone Marrow Specimens on the UKALL14 trial

3.1 Background

3.1.1 The Role of Mesenchymal Stromal Cells in Treatment Resistance in Acute Lymphoblastic Leukaemia

There is increasing evidence of the importance of the microenvironment in treatment resistance in ALL. Recent murine models have suggested that treatment resistance cells within the bone marrow are not genetically distinct from the bulk population but instead reside in a 'protective niche'[13]. MSC have emerged as vital players within the ALL protective niche[12]. A number of mechanisms have been postulated to explain their protective effect including cytokines[79], growth factors[12], exosomes[87], tunnelling nanotubes[114] and aberrant pathway signalling[92].

To explore the properties of mesenchymal stromal cells in the leukaemic bone marrow niche both before and after treatment I isolated, expanded and characterised MSC from bone marrows of patients enrolled on the UKALL14 trial with B-ALL. As discussed below, my preliminary and unexpected findings suggested that a proportion of the patient MSC had features suggestive of an activated or cancer associated fibroblast

(CAF)-like fibroblast phenotype. This led me to focus on confirming that MSC from ALL patient bone marrow specimens had morphological features, a gene expression profile and cytokine/chemokine profile consistent with an activated or CAF-like phenotype.

3.1.2 Characterisation of Cancer Associated Fibroblasts

Although there is no strict definition in the literature of an activated fibroblast/stromal cell or CAF, certain features are recognised as being characteristic. The differences between fibroblasts within the tumour bed (CAF) and fibroblasts within adjacent healthy tissue has largely been used to determine the characteristics of a CAF. These include increased presence of actin stress fibres, increased expression of alpha-smooth muscle actin (αSMA) and an enhanced secretory profile including cytokines/chemokines, growth factors and extracellular re-modelling enzymes[117].

CAF have never been definitively described in ALL, although previous publications have noted MSCs in ALL with features of CAF including αSMA expression[12] and an altered MSC metabolic profile in keeping with CAF[87]. I used fluorescent microscopy, targeted gene expression profiling and cytokine/chemokine quantification to characterise CAF within the patient bone marrow specimens.

3.2 Aims

1. To isolate and characterise MSC from patient samples at different stages of disease on the UKALL14 trial
2. To determine if MSC from patient specimens have characteristics consistent with a CAF phenotype

3.3 Results

3.3.1 Cohort of Patient Bone Marrow Specimen's Representative of UKALL14 Trial Population

Eighty-four patient bone marrow specimens from 70 patients with B-ALL on the UKALL14 trial were evaluated for the capacity to allow isolation and expansion of MSCs. These included specimens at diagnosis and following the first and second cycle of treatment. Samples were selected primarily due to availability of patient material. Healthy donor MSC from allogeneic stem cell transplant donor bone marrow specimens were expanded to be used as controls for subsequent experiments.

Table 3-1 compares relevant clinical and biological features in the cohort of samples used for isolation and expansion of MSC as compared to the entire UKALL14 trial population. It confirms that the cohort of samples selected were representative of the

entire UKALL14 trial population. Patient gender was the only variable that was significantly different between the cohort of samples used and the entire trial population. There is no obvious explanation as to why a greater percentage of samples from males were selected for my cohort and this is highly likely due to chance alone.

Table 3-1 Comparison of patient characteristics of samples selected for MSC expansion versus entire UKALL14 trial population

Baseline Characteristic		In MSC sample population	Not in MSC sample population	p-value*
		N=70	N=585	
Age, median (range)		**43.0(22 - 65)**	**46.0(23 - 65)**	**0.068****
Sex				
	Male	48 (68.6)	310 (53.0)	0.013
	Female	22 (31.4)	275 (47.0)	
Baseline WBC, median (range)		11.0(.8 - 583.1)	7.9(.11 - 889.6)	0.24**
PH status				
	PH-	51 (73.9)	392 (68.7)	0.37
	PH+	18 (26.1)	179 (31.3)	
	Missing/failed	1	14	
T(4,11)				
	Absent	62 (91.2)	497 (92.4)	0.33
	Present	6 (8.8)	41 (7.6)	
	Missing/failed	2	47	
Complexity				
	Absent	53 (96.4)	425 (95.1)	0.97***
	Present	2 (3.6)	22 (4.9)	
	Missing/failed	15	138	
HoTr/Near-haploidy				
	Absent	55 (96.5)	409 (89.7)	0.10
	Present	2 (3.5)	47 (10.3)	
	Missing/failed	13	129	
Any of the above Cytogenetic risk factors				
	Absent	28 (50.0)	186 (39.6)	0.13
	Present	28 (50.0)	284 (60.4)	
	Missing/failed	14	115	
High risk baseline				
	Standard risk	13 (19.4)	64 (11.5)	0.064
	High risk	54 (80.6)	492 (88.5)	
	Unknown, assumed standard	13 (19.4)	64 (11.5)	0.064

*Chi-squared unless otherwise stated
**Wilcoxon Mann Whitney test
***Fisher's exact test

Table 3-2 shows a comparison of the relevant clinical and biological features in the cohort of samples used for isolation and expansion of MSC as compared to the UKALL14 trial population but in the diagnostic specimens only. The only variables that were significantly different between the two populations being baseline white cell count and low-hypodiploid/near haploid in the diagnostic specimens. The difference in baseline white count is likely explained by the greater availability of patient material from patients with higher presenting white blood counts. There is no obvious biological reason for the absence of samples with hypotriploid near haploid in my cohort, although patients with low-hypodiploid/near haploid typically display low white cell counts at presentation[149].

Overall, I would consider my patient cohort to be representative of the entire trial population and to include a representative range of the common genetic abnormalities described in B-ALL.

Table 3-2 Comparison of patient characteristics in diagnostic samples selected for MSC expansion versus entire UKALL14 population

Baseline Characteristic		In MSC sample population	Not in MSC sample population	p-value*
		N=37	N=618	
Age, median (range)		**40.0(26 - 63)**	**46.0(22 - 65)**	**0.058****
Sex				
	Male	24 (64.9)	334 (54.0)	0.20
	Female	13 (35.1)	284 (46.0)	
Baseline WBC, median (range)		26.8(1.2 - 210.6)	7.7(.11 - 889.6)	0.001**
PH status				
	PH-	23 (63.9)	420 (69.5)	0.48
	PH+	13 (36.1)	184 (30.5)	
	Missing/failed	1	14	
T(4,11)				
	Absent	32 (88.9)	527 (92.5)	0.30***
	Present	4 (11.1)	43 (7.5)	
	Missing/failed	1	48	
Complexity				
	Absent	29 (93.5)	449 (95.3)	0.45***
	Present	2 (6.5)	22 (4.7)	
	Missing/failed	6	147	
HoTr/Near-haploidy				
	Absent	32 (100.0)	432 (89.8)	0.036***
	Present	0 (0.0)	49 (10.2)	
	Missing/failed	5	137	
Any of the above Cytogenetic risk factors				
	Absent	13 (40.6)	201 (40.7)	0.99
	Present	19 (59.4)	293 (59.3)	
	Missing/failed	5	124	
High risk baseline				
	Standard risk	6 (17.1)	71 (12.1)	0.18
	High risk	29 (82.9)	517 (87.9)	
	Unknown, assumed standard	2	30	

***Chi-squared unless otherwise stated**
****Wilcoxon Mann Whitney test**
*****Fisher's exact test**

3.3.2 Factors Predicting Isolation and Expansion of Mesenchymal Stromal Cells from Patient's Bone Marrows

I defined 'isolation of MSC' as the identification of cells with MSC morphology at any stage during culture and 'expansion of MSC' as the ability to expand MSCs beyond the second passage of growth. It was possible to isolate MSC from 68/84 (81%) of patient samples and expand MSCs from 37/84 (44%) patient samples. ***Table 3-3*** summarises the factors predicting successful expansion.

Technical considerations were the most impactful. MSCs were more successfully isolated (90.4% vs 65.6%, Chi-Squared test p = 0.005) and expanded (59.6% vs 18.8%, p = 0.0002) from fresh compared to frozen specimens. Age, dichotomised by the UKALL14 risk score cut-off of older or younger than 40 years, had no impact. The ease of isolation or expansion also did not appear to relate to different cytogenetic groups although the number of samples in some sub-groups were small making it difficult to draw any definitive conclusions.

The stage of therapy did appear to impact the ability to expand MSCs. I was able to isolate and expand MSC from diagnostic specimens in a smaller proportion than from patients at the end of Phase I and Phase II of therapy. However, these differences were not statistically significant with the exception of expansion of post phase 1 MSC versus diagnostic MSC (64.7% vs 29.7%, Chi-Squared test, p = 0.015).

Table 3-3 Factors predicting MSC isolation and expansion

		MSC Isolated	MSC Expanded
All Samples		68/84 (81.0%)	37/84 (44%)
Technical Factors			
Sample Type	Fresh	47/52 (90.4%)**	31/52 (59.6%)***
	Frozen	21/32 (65.6%)	6/32 (18.8%)
Biological Factors			
Age (need to add 3)	Age < 40	28/37 (75.7%)	16/37 (43.2%)
	Age > 40	40/47 (85.1%)	21/47 (44.7%)
Cytogenetics	BCR-ABL positive	16/22 (72.7%)	8/22 (36%)
	MLL-AF4 positive	5/7 (71.4%)	2/7 (28.6%)
	Complex karyotype	2/2 (100%)	1/2 (50%)
	HoTr/Near haploidy	2/3 (66.7%)	0/3 (0%)
	Any of above cytogenetic risk factors	25/34 (73.5%)	11/34 (32.4%)
Therapeutic Factors			
Stage of Treatment	Diagnostic	27/37 (73.0%)	11/37 (29.7%)
	Post Phase I	16/17 (94.1%)	11/17 (64.7%)*
	Post Phase II	25/30 (83.3%)	15/30 (50.0%)

3.3.3 Mesenchymal Stromal Cell Characterisation

I then sought to confirm that the MSC isolated were adherent consistent with the previously discussed ISCT criteria[65].

(i) Plastic adherence

Primary ALL-derived MSCs successfully expanded were all clearly adherent to the cell culture flask.

(ii) Immunophenotype

I demonstrated by flow cytometry that a subset (n=5) of the primary ALL-derived MSCs at passage 2-3 including diagnostic and follow-up specimens expressed CD73, CD90 and CD105 as demonstrated in the representative example of dot plots in ***Figure 3-1***. I utilized a 'dump gate' conjugated to allophycocyanin (APC) to show absence of expression of the lineage markers CD14, CD19, HLA-DR, CD45 and CD34. Although there was auto-fluorescence in the APC channel as demonstrated in the FMO (APC), there was no significant shift in the APC channel following addition of the lineage markers conjugated to APC with less than 1% of cells being positive. All samples analysed showed greater than 90% of cells expressed CD73 and CD90. CD105 expression was more variable, as shown in figure 1 with expression varying between 67 – 90.8%. Overall though the absence of lineage markers in the primary MSCs and expression profile was consistent with an MSC phenotype.

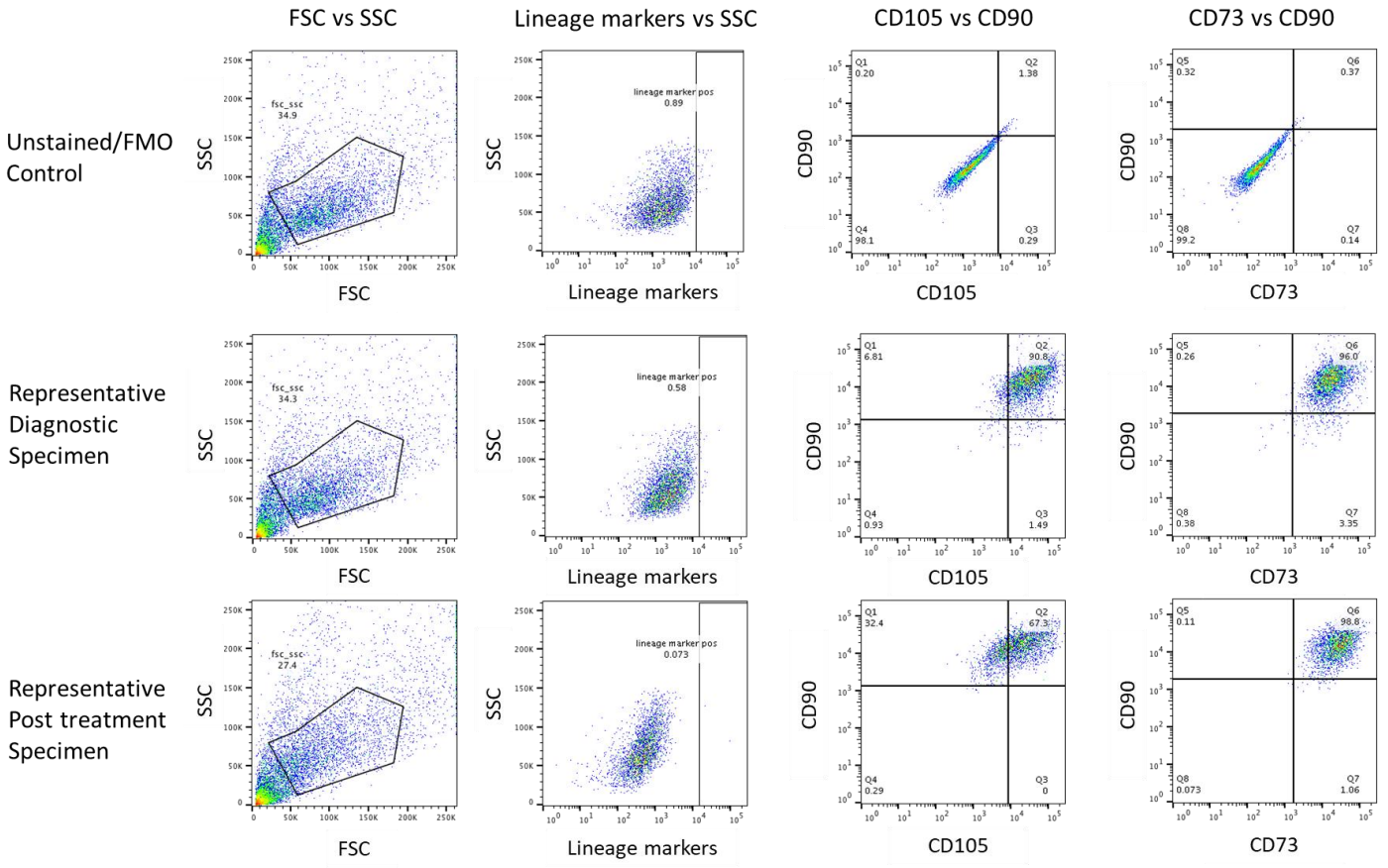

Figure 3-1: MSC phenotype. A representative example of diagnostic and post treatment specimens. Live MSC populations were gated according to their FSC and SSC characteristics. MSC populations were shown to be negative for lineage markers, with a FMO used as the negative control. MSC populations were shown to co-express CD73, CD90 and CD105.

(iii) Differentiation Potential

Using the mesenchymal differentiation kit, I demonstrated the ability of a subset (n = 5) of the primary ALL-derived MSCs including healthy donor, diagnostic and follow-up specimens to differentiate into adipocytes and osteocytes. Representative examples are shown in ***Figure 3-2***.

Therefore, the sub-set of primary ALL-derived MSC tested displayed appropriate MSC-defining ISCT criteria.

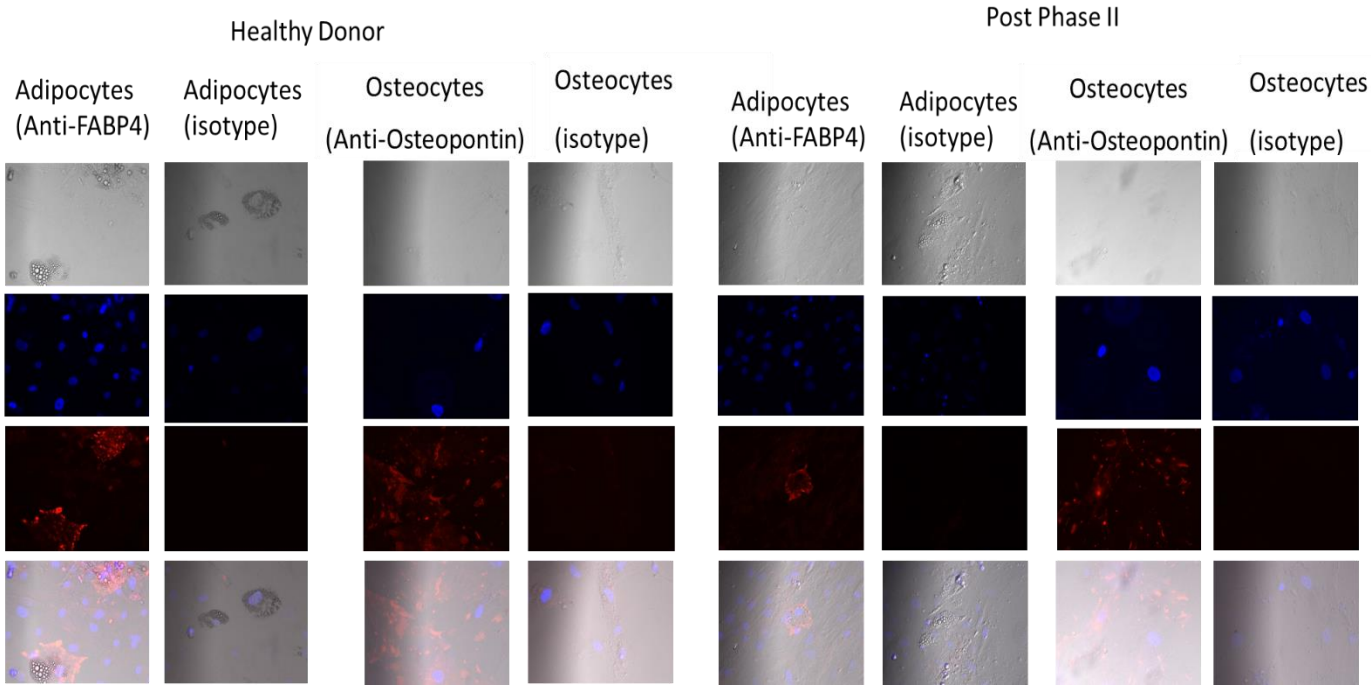

Figure 3-2: MSC differentiation. Representative images demonstrating adipocytic and osteocytic differentiation of both healthy donor and post treatment BM-MSCs, using the Human Mesenchymal Stem Cell Functional Identification Kit (R&D Systems, MN, USA).

DAPI Anti-FABP4 Anti-Osteopontin

3.3.4 Isolation and Characterisation of Unexpected Macrophage Population

An unexpected finding in 26 out of 41 (63%) post-treatment samples where MSC were successfully isolated was the growth of large numbers of rounded cells with cytoplasmic projections. ***Table 3-4*** documents the frequency of occurrence of the rounded cells in specimens by stage of therapy.

Table 3-4: Isolation of round cell population by stage of treatment

Stage of Treatment	Samples with round cells (All Samples)	Samples with round cells (MSC able to be isolated)	Samples with round cells (MSC able to be expanded)
Healthy Donor	0/5 (0%)	0/5 (0%)	0/5 (0%)
Diagnostic	0/37 (0%)	0/27 (0%)	0/11 (0%)
Post Phase I	6/17 (35.3%)	6/16 (37.5%)	3/11 (27.3%)
Post Phase 2	20/30 (66.7%)	20/25 (80%)**	10/15 (66.7%)

These cells were never noted in diagnostic or healthy donor specimens and were more frequently seen after the second phase of therapy than the first phase of therapy (80% vs 38%, p = 0.006). The cells were not noted in second and subsequent passages of the MSCs, at least in part because they were very poorly removed by trypsin and remained adherent to the plastic, by comparison to the MSCs which were readily removed with trypsin.

As demonstrated in ***figure 3-3*** when the large round cells were present in the MSC cultures, MSC also frequently had altered morphology, being larger with prominent cytoplasmic projections.

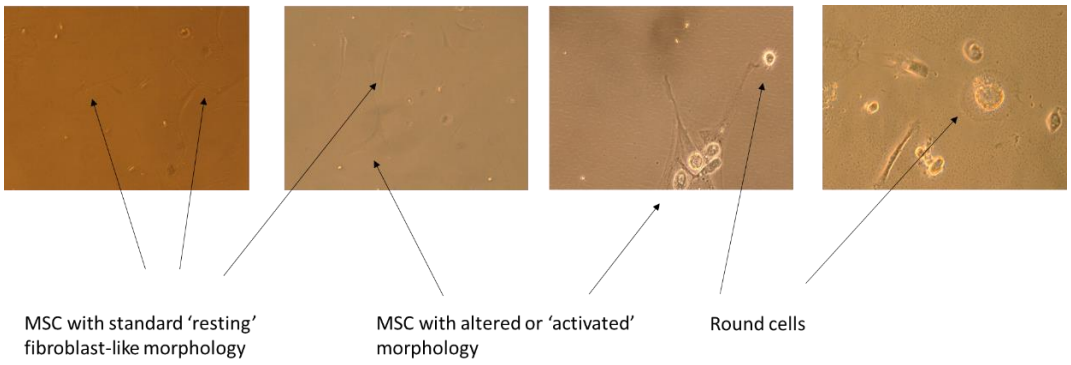

Figure 3-3: Light microscopy round cell population. Representative light microscopy of both round cell population and MSC with altered or 'activated' morphology in primary patient MSC cultures. MSC with an activated appearance are larger and broader. MSC with a 'normal' or non-activated are also demonstrated with spindle-like morphology. Both cell populations are identified with arrows.

To characterise and identify this alternative cell population the cells were removed by scraping and additional prolonged trypsinisation. They were stained after cytospin preparation as demonstrated in ***figure 3-4***. May Grunwald Giemsa staining revealed morphology that was in keeping with macrophages or dendritic cells.

Immunohistochemistry revealed CD68 (not shown), CD11b and CD163 expression confirming the presence of macrophages. CD163 is described as a specific marker for type 2 or alternative macrophages[150] which, in the context of cancer, are termed tumour associated macrophages (TAMs).

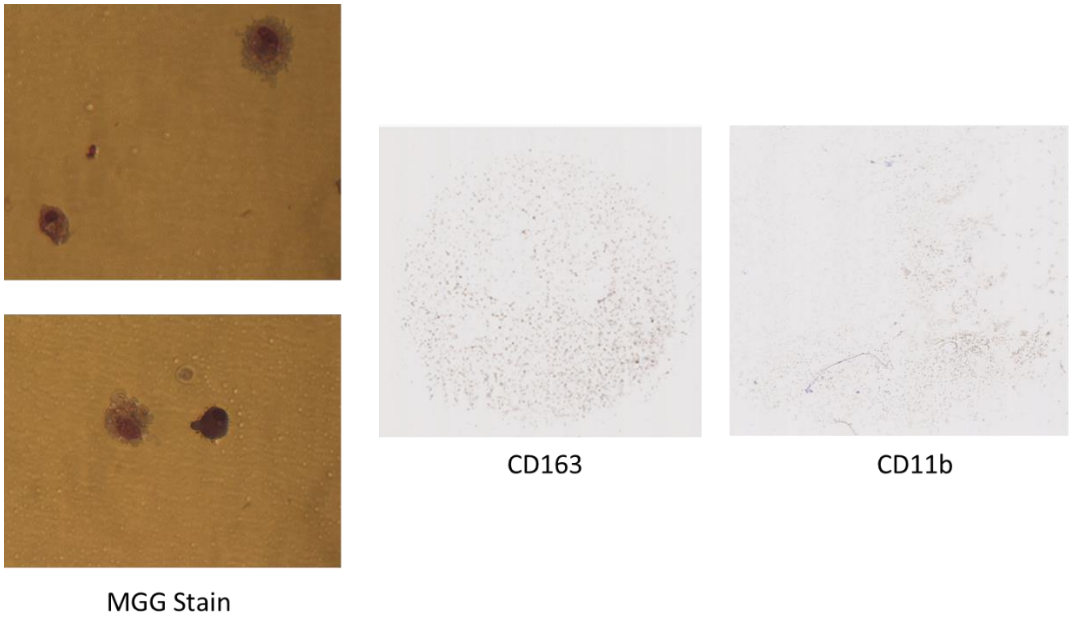

Figure 3-4: MGG staining and immunocytochemistry identifies macrophages as round cell population. Representative images of an MGG stain of the round cell population found in MSC cultures confirming they have the morphological appearances of macrophages. Subsequent immunocytochemistry confirms the cells express CD163 and CD11b (brown = expression of relative antigen) thus confirming the round cell population as macrophages.

3.3.5 Mesenchymal Stromal Cell Secretion Profile

Given that the macrophages appeared to be viable, even proliferating in conditions optimized only for MSC growth I hypothesized that the MSCs may be secreting soluble factors such as growth factors or cytokines to aid their survival. I used semi-quantitative ELISAs from the supernatant of the first passage to screen for relevant soluble mediators in order to narrow down the appropriate factors to precisely quantitate as shown in ***table 3-5***. The first passage supernatant was used as I felt this would most closely represent the true *in vivo* secretion profile. However, results from the semi-quantitative ELISA were solely a screen due to the possibility of macrophages also secreting the cytokines or chemokines tested.

Table 3-5: Semi-quantitative ELISA of primary MSC supernatant

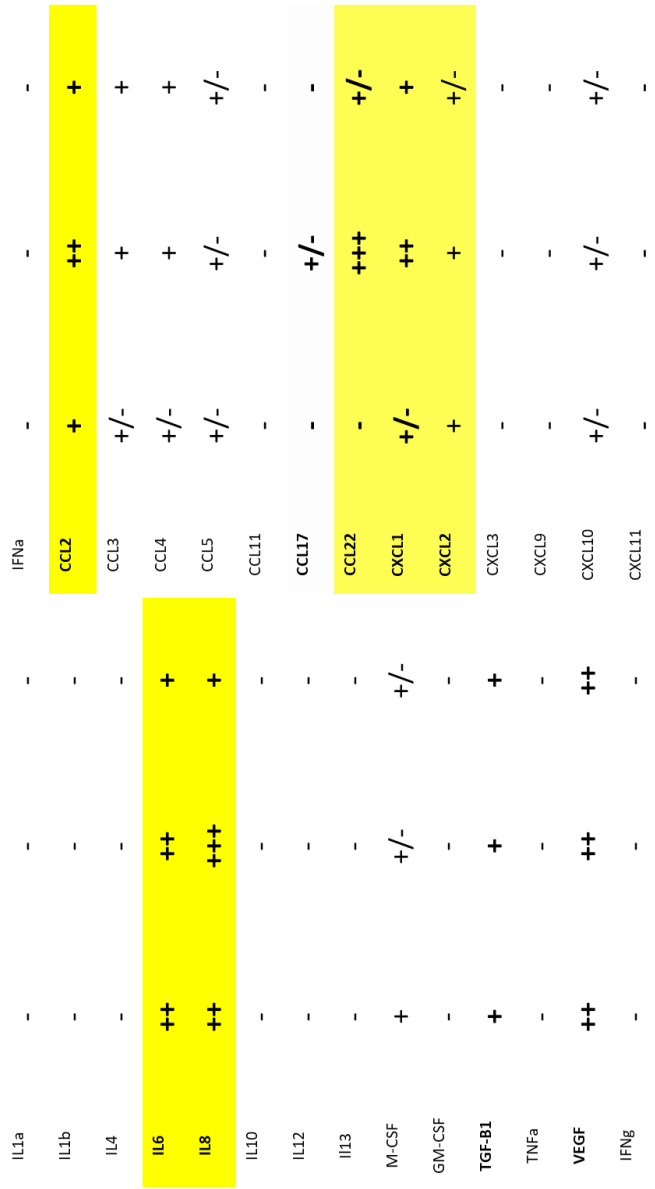

	Diagnostic	FU M+	FU M-
IL1a	-	-	-
IL1b	-	-	-
IL4	-	-	-
IL6	++	++	+
IL8	++	+++	+
IL10	-	-	-
IL12	-	-	-
Il13	-	-	-
M-CSF	+	+/-	+/-
GM-CSF	-	-	-
TGF-B1	+	+	+
TNFa	-	-	-
VEGF	++	++	++
IFNg	-	-	-

	Diagnostic	FU M+	FU M-
IFNa	-	-	-
CCL2	+	++	+
CCL3	+/-	+	+
CCL4	+/-	+	+
CCL5	+/-	+/-	+/-
CCL11	-	-	-
CCL17	-	+/-	-
CCL22	-	+++	+/-
CXCL1	+/-	++	+
CXCL2	+	+	+/-
CXCL3	-	-	-
CXCL9	-	-	-
CXCL10	+/-	+/-	+/-
CXCL11	-	-	-

Table 3-5: Semi-quantitative ELISA of primary MSC supernatant. The table shows relative levels of cytokines/chemokines as measured by optical density using a screening semi-quantitative ELISA kit (Qiagen, optical density measured but no standard curve measured/created). Cytokine/chemokine levels are stated as no target protein detectable (-), low level (+), moderate level (++), high level (+++). The groups compared are the average of three samples and include primary patient MSC supernatant diagnostic specimens (diagnostic), follow-up specimen with macrophages (FU M+) and follow-up specimen without macrophages (FU M-). The cytokines highlighted in yellow (IL6, IL8, CCL2, CCL22, CXCL1, CXCL2) appeared to be present at greater levels in the supernatant of follow-up samples with macrophages as compared to follow-up samples with macrophages. Therefore these cytokines were selected to perform quantitative ELISAs on larger numbers of primary MSC. .specimens.

Next, I carried out quantitative ELISAs for IL6, IL8, CCL2, CCL22, CXCL1 and CXCL2 on the basis of differential secretion of these cytokines between the samples containing macrophages and those without. I used available supernatant from the second passage of MSC patient samples. Macrophages were absent from the second passage as discussed above and confirmed by the high purity of MSC demonstrated by flow cytometry (in ***figure 3-1***). Therefore, we could be certain that the cytokines or chemokines were only secreted by MSC. I compared soluble factor levels between healthy donor specimens, diagnostic specimens, post phase I treatment and post phase II treatment (which contained the greatest proportion of samples with macrophages).

The soluble factors are shown in ***figure 3-5***, quantified in pg/ml and separated by stage of treatment and relevant cytokine/chemokine. CCL22 is not shown as the levels were undetectable in all samples and therefore it was highly likely secreted by the macrophages in the first passage. Although the mean secretion level of all chemokines and cytokines was higher in the second cycle of treatment specimens than both the first cycle specimens and healthy donor specimens, the difference between first cycle and second cycle of treatment only reached statistical significance for IL8 (unpaired student t test, $p = 0.04$) and did not reach statistical significance for any cytokines/chemokines when comparing healthy donor and second cycle treatment specimens. Similarly, the mean of all cytokines/chemokines was greater in the

diagnostic specimens as compared to healthy donor specimens, with the exception of CCL2, but none of the differences reached statistical significance.

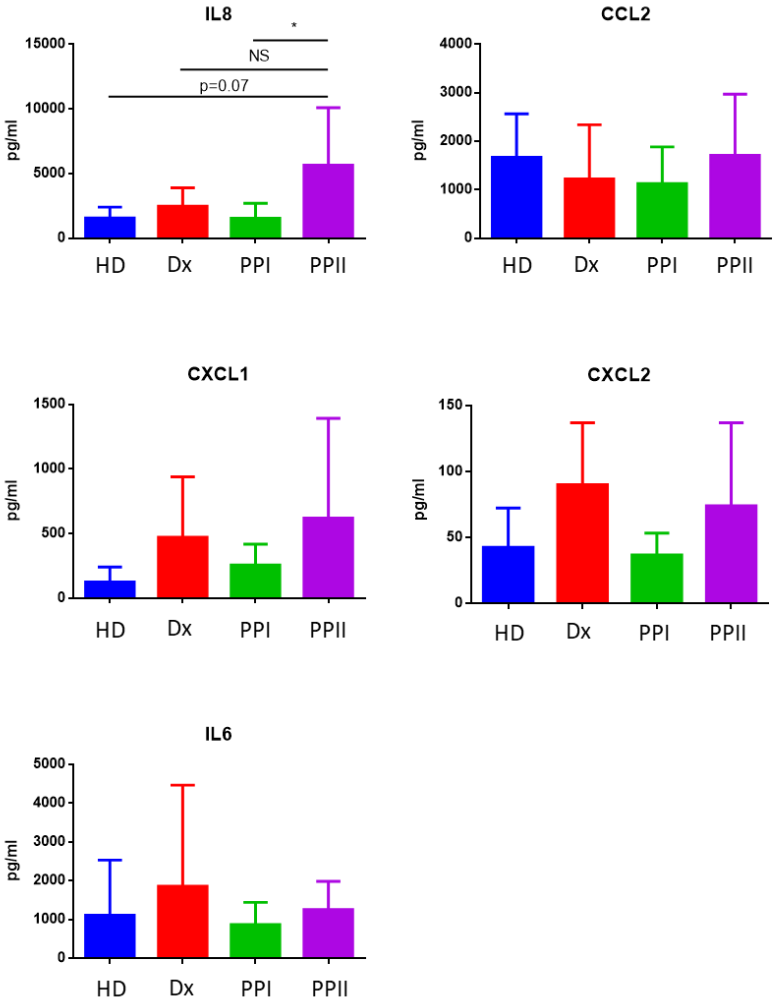

Figure 3-5: Primary MSC cytokine secretion by stage of therapy. The graphs show cytokines and chemokines secreted by MSC isolated from the normal healthy donor bone marrow or primary patient ALL specimens at diagnosis and after first and second course of chemotherapy. Each bar graph shows a different cytokine/chemokine as per the title. Bars show mean +/- SE of primary patient specimen cytokine/chemokine levels (HD n = 5, Dx n = 6, PPI n = 8, PPII n = 8). Cytokine/chemokine level in the supernatant is measured in pg/ml shown on the Y axis. Healthy donor specimens (HD, blue), Diagnostic specimens (Dx, red), after first course specimens (PPI, green), after second course specimens (PPII, purple) are shown on the X axis. Statistical significance as depicted: IL8 PPI vs PPII, P = 0.04; IL8 HD vs PPII, P = 0.07. There were no other statistically significant differences.

3.3.6 Determination of Whether Cancer Associated Fibroblasts are Present in Primary Samples

Given the presence of tumour associated macrophages in follow-up specimens and the associated enhanced cytokine/chemokine secretion profile of a proportion of the MSCs, I postulated the presence of activated MSC or CAF in the primary specimens.

To explore this hypothesis further, three samples from each time point with available material were selected to represent a mixture of cytokine secretion profiles, for imaging and targeted gene expression profiling based on genes described to be upregulated in CAFs[117,151].

Figure 3-6 shows phalloidin and DAPI staining of the patient samples compared to those from healthy donor MSC. The samples with clear morphological changes including prominent F-actin containing stress fibres are indicated by red box around the images. I didn't quantify the immunocytochemistry images, which likely would have been helpful in providing quantification of the number of activated MSC in the primary patient specimens. In the future I plan to try different methods of quantifying the number or percentage of activated MSC by different measure of immunofluorescence. Measurement options I plan to explore include measuring the size of individual MSC (given activated MSC tend to be flatter and broader) or variability in the immunofluorescence within an individual cell (as activated MSC have

prominent actin stress fibres which are brightly immunofluorescent in contrast to non-activated MSC which have a more uniform distribution of actin).

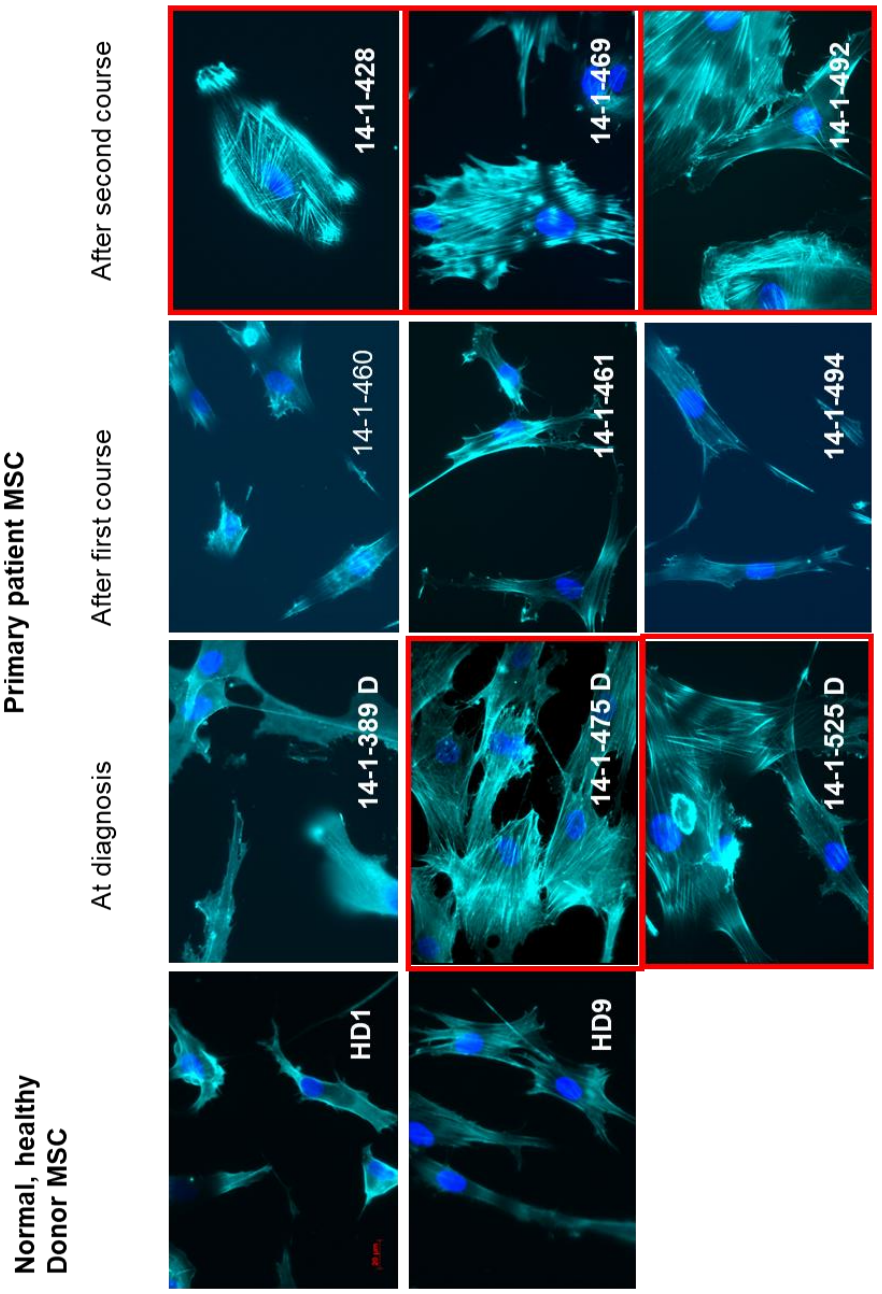

Figure 3-6: Primary MSC show activated or CAF-like appearance. Photomicrographs at 40X magnification, showing phalloidin and DAPI staining of MSC isolated from primary patient ALL or health controls. Unique (UPN) or healthy donor number (HDN) are shown. The images with red borders show the ALL-CAF phenotype.

To examine the gene changes associated with MSC activation, I performed a targeted, 18-gene expression profile RQ-PCR of MSC isolated from normal healthy donors served as baseline controls. ***Figure 3-7*** shows upregulation of growth factors, extracellular remodelling, cancer-associated fibroblast-related genes, and chemokines and cytokines genes within the same MSCs also showing the prominent morphological changes as indicated by the red boxes around the specimen numbers. Among the key characteristics of the directly isolated primary patient activated MSC were a 16-64 fold increase in transcription of Nbla00170 (nestin), a pro-inflammatory pattern of cytokine secretion, up-regulation of the extracellular matrix remodelling enzyme matrix metalloproteinase 1 (MMP1) and up-regulation of growth factors basic fibroblast growth factor (bFGF) and vascular endothelial growth factor (VEGF). This is consistent with an activated fibroblast or CAF profile, described in solid organ malignancies[117,151].

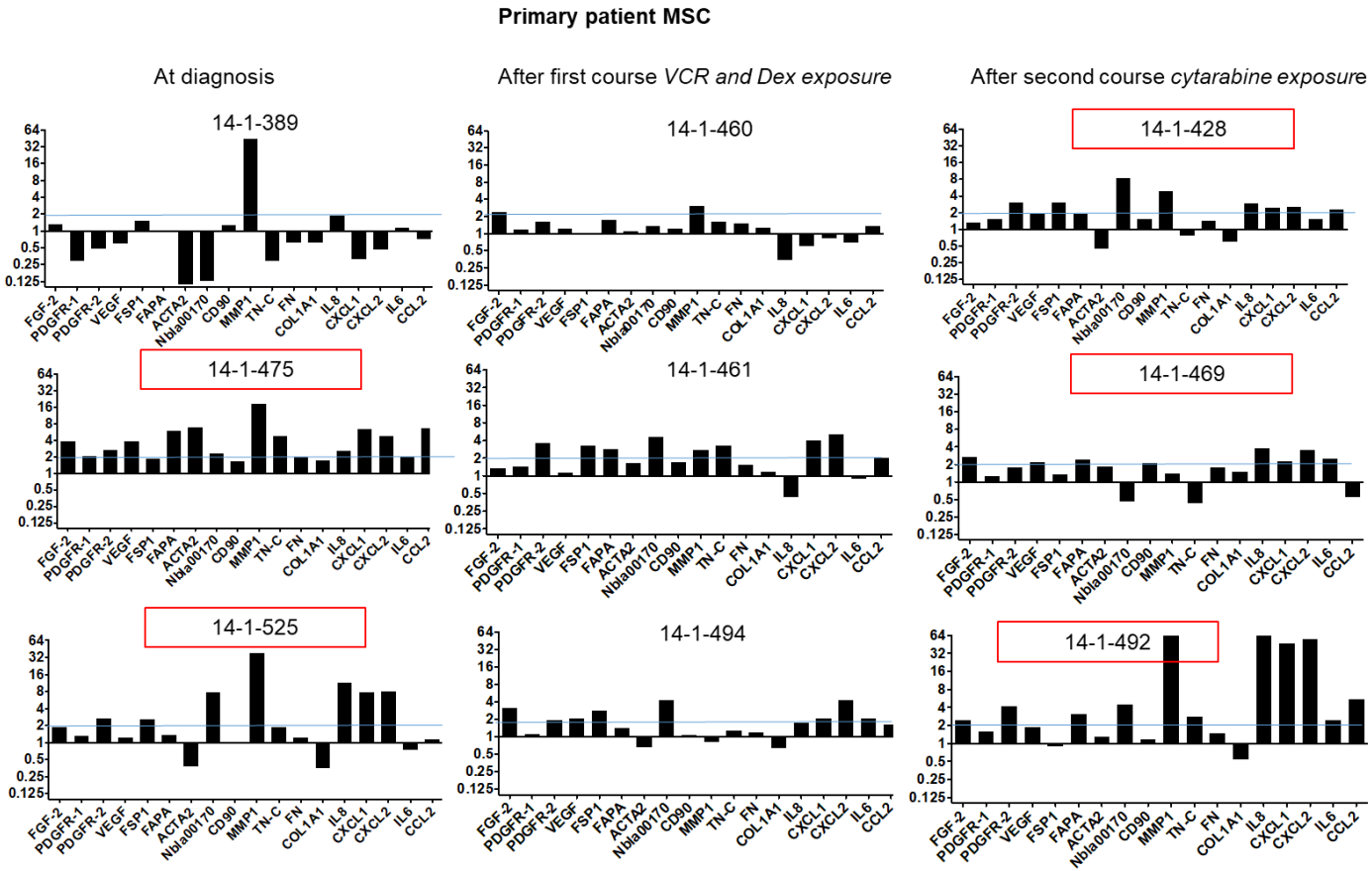

Figure 3-7: Primary MSC show upregulation of CAF relevant genes. Gene expression profile showing fold upregulation (Y axis) of 18 selected genes in the patient specimens - at diagnosis and after first and second course of chemotherapy - compared to mean baseline of 3 normal healthy donors MSC isolated from primary patient ALL. UPN is indicated with each panel. Red box around UPN indicates specimen with morphological changes. Gene names are shown on the X axis. Blue line is drawn at 2-fold upregulation.

3.4 Discussion

I have shown that MSC can be isolated and expanded from a cohort of B-ALL patient bone marrow specimens both at diagnosis and following treatment. MSC display appropriate defining characteristics according to ISCT criteria.

Unsurprisingly, technical factors predicted ease of isolation and expansion, with MSC easier to isolate and expand from fresh samples as compared to frozen specimens. I was able to expand MSC at different stages of treatment in sufficient numbers from a proportion of patients to be used for subsequent characterisation. However, my data shows that MSC may be more challenging to expand from patient samples at diagnosis as compared to following treatment. This suggests that MSC may be more difficult to expand from patient bone marrow at diagnosis when they have large numbers of leukaemic cells as compared to post treatment when the majority of leukaemic cells in almost all patients have been eradicated by chemotherapy. This may mean that leukaemic cells have a deleterious effect on stromal cell survival or proliferation either *in vivo* or *ex vivo*. Alternatively, the reduced rates of isolation and expansion of MSC from diagnostic specimens, may relate to a lower relative frequency of MSC within the total cellular population of the bone marrow at diagnosis. Especially given that patient's marrows at diagnosis are often 'packed' with leukaemic cells.

The unexpected presence of large numbers of tumour associated macrophages in the follow-up specimens is likely explained by the altered secretion profile of the MSCs.

The increased secretion of pro-inflammatory factors by MSCs within the samples containing macrophages provides support for this theory as there is evidence in other malignancies that IL8, CXCL1, CXCL2 and CCL2 secreted by fibroblasts can act as a chemo-attractant for myeloid derived cells including macrophages and CCL2 and IL6 can lead to a conversion of these to a type 2 or tumour associated macrophages (TAM) [152,153].

The absence of macrophages in diagnostic specimens is surprising given some of the diagnostic MSCs also appear to have an enhanced secretion profile of aforementioned soluble factors compared to healthy donor specimens. A possible explanation for this is that the bone marrow in ALL at diagnosis is heavily infiltrated with ALL blasts and there is marked reduction in normal haematopoiesis including myeloid derived cells as they are 'crowded out' of the bone marrow. Therefore, monocytes and macrophages are likely to be present in much smaller numbers given the 'lack of space' within the bone marrow. Alternatively, the presence and growth of macrophages may be dependent on an effect of chemotherapy.

Further evidence supporting chemotherapy modulating the presence of macrophages in patient's samples is that we observed a significantly higher proportion of samples with macrophages post the second phase of treatment as compared to the first phase. This is unlikely explained by the burden of disease as the vast majority of patient (>90%) achieve remission, defined as less than 5% blasts in the bone marrow, post the

first cycle of chemotherapy. Notably, the chemotherapy agents used in the first phase are different to the agents used in the second phase suggesting that the presence of macrophages may depend on the combination of chemotherapy drugs used.

I was then able to demonstrate that MSC from primary bone marrow specimens of patients undergoing treatment for B-ALL can adopt an activated phenotype with gross cytoskeletal changes, gene expression changes and secretion of high levels of pro-inflammatory cytokine secretion. The MSC which we extracted directly from primary patient specimens seem closely morphologically and functionally related to cancer associated fibroblasts (CAF). CAF have not previously been identified as playing a particular role in acute leukaemia, whilst they are the most abundant mesenchymal cell types present within most human carcinomas.

Notably, the presence of CAF-like MSC appeared to relate closely to the presence of macrophages within the specimens. There is a well described link between the presence of CAF and TAM in solid organ malignancy and haematological malignancy including lymphoid malignancies such as lymphoma[130,154,155]. The presence of CAF and TAM were more frequent following the second cycle of treatment than the first cycle. Notably, the combination of drugs used is different in the first cycle compared to the second. Daunorubicin (which intercalates DNA and prevents topoisomerase II progression), vincristine (a microtubule damaging agent) and dexamethasone (a corticosteroid) form the backbone of the first cycle but are not present in cycle 2.

Whereas blocks of cytarabine (a DNA synthesis inhibitor) feature in cycle 2 but not cycle 1. This suggests that the presence of CAFs may depend on the chemotherapy drugs used. This will be further explored in chapter 5.

Given the morphological appearance of the CAF and the pro-inflammatory secretion profile, an alternative explanation could be that a proportion of the stromal cells could be senescent. Cellular senescence defines an irreversible cell cycle arrest and therefore arrested cellular division. Other features of senescent cells include cytoskeletal change, an enhanced secretory of cytokines, growth factors and tissue remodelling enzymes (known as senescence associated secretory phenotype) and upregulation of p16INK4a and p21[156]. Senescence can be induced prematurely in actively dividing cells by application of stimuli associated with proliferative stress (oncogenes) or by direct DNA damage (ionizing radiation, reactive oxygen species, chemotherapeutics)[156].

Senescence of the MSCs could either have occurred *in vivo* or be a result of proliferation senescence, an inevitable consequence of serial passaging of primary cells due to telomere shortening. However supernatant (passage 2), imaging (passage 4) and gene expression profile (passage 4) were all performed at the same passage for all specimens and MSC continued to proliferate for several passages following passage 4. Therefore, the differences observed between specimens is unlikely to be primarily due to replication senescence. Furthermore, there was no apparent difference in ease of isolation or expansion of MSC between samples with an activated or CAF phenotype

and those without, suggesting the activated phenotype is unlikely due to a greater proportion of senescent MSC *in vivo*. However, it is difficult to exclude the possibility that a proportion of the MSC may be senescent, especially given activated fibroblasts and senescent fibroblasts are both induced by DNA from oxidative stress and chemotherapeutics.

One of the major limitations is the lack of access to longitudinal, serial specimens in the same patients. This would enable more meaningful comparison of the changes noted before and after treatment. However, the availability of primary patient material and the challenges of expanding MSC make this a very challenging task. Therefore, I consider the work, although intriguing, to be predominantly hypothesis generating rather than definitive. Hence, in chapter 4 and 5 I turn to modelling the process *in vitro* by investigating the effects of both chemotherapy and B-ALL cells on MSC in isolation. Although I found the presence of macrophages in a proportion of the primary specimens intriguing, I elected to focus on MSC given the overall aims of my project and their more well described role in treatment resistance in B-ALL.

Chapter 4: Modelling induction of a CAF phenotype in MSC following exposure to B-ALL cells

4.1 Background

4.1.1 Cancer Associated Fibroblasts in Malignancy

CAFs are well described in several solid organ malignancies and are increasingly recognised to also play a role in haematological malignancies including chronic lymphocytic leukaemia[88] and lymphoma[157]. The cell of origin is postulated to either be local fibroblasts or other stromal cells within the vicinity of the tumour[117] or possibly MSC from distant sites especially the bone marrow[158].

Fibroblasts or MSC are believed to become activated by exposure to oxidative stress, growth factors such as TGFβ1 or exosomes secreted from tumour cells[87,88,117]. In normal 'healthy tissue', a similar process is believed to occur due to tissue damage and fibroblasts undergo a similar transformation to play an important role in wound healing. Following wound healing, activated fibroblasts undergo apoptosis or are cleared from the wound site and do not persist. In contrast, under continuous exposure to reactive oxygen species, growth factors or exosomes from tumour cells the activated fibroblasts/MSC are believed to undergo epigenetic change leading to the more permanent CAF state.

CAF persist and proliferate within the tumour bed, aiding cancer cell proliferation, spread and treatment resistance via secretion of cytokines, growth factors, alteration of the extracellular matrix and by providing metabolic support to the tumour cells. This has led to the description of cancer as a 'wound that doesn't heal'.

4.2 Aims

1. To determine if B-ALL cells across different genetic sub-types can induce a CAF-like phenotype in MSC *in vitro*
2. To investigate the underlying mechanism for the induction of the ALL-CAF phenotype in MSC

4.3 Results

4.3.1 B-ALL and MSC *in vitro* Co-culture Design

I designed a model to explore if B-ALL cells *in vitro* could induce the ALL-CAF phenotype in MSC that we had observed in the primary specimens. I initially used a cell line model co-culturing stromal cells with different B-ALL cell lines as depicted in ***Figure 4-1***. I selected HS27a cells (a human papilloma virus 16 E6/7 transformed human bone marrow stromal line) as this MSC cell line is postulated to represent a sub-population of CD146+ MSC important in maintenance of haematopoietic stem cells (HSC) within

their niche and is therefore more likely to be representative of stromal cells in the postulated treatment resistant leukaemic niche[76]. Furthermore, my preliminary work with transforming growth factor beta 1 (TGF-β1) (an accepted inducer of fibroblasts or activated stromal cells) suggested that they produced a more reliable phenotype of an activated or CAF-like MSC than HS5 (also a human papilloma virus 16 E6/7 transformed human bone marrow stromal line), an alternative human MSC cell line.

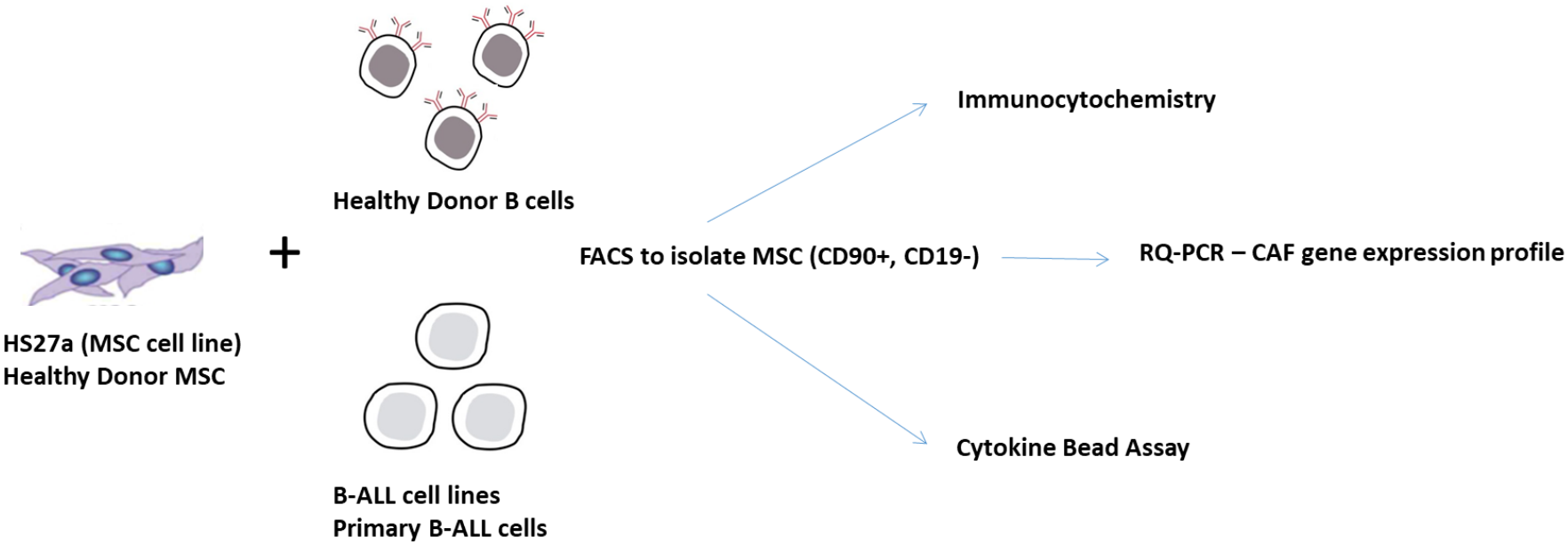

Figure 4-1: Model of CAF induction *in vitro.* Cartoon image demonstrating the co-culture experimental model of MSC with ALL cells and planned outputs to assess for a CAF phenotype including immunocytochemistry, gene expression profile and cytokine secretion.

I co-cultured HS27a cells with five different B-precursor ALL cell lines SEM[159], REH[160], TOM-1[161], SD1[162], and 697[163], chosen to represent the spectrum of common genetic abnormalities found in ALL (see ***table 4-1***). The outputs to assess for transformation to an activated or CAF phenotype included immunocytochemistry for characteristic morphological changes, RQ-PCR of CAF defining genes as previously described and secretion of relevant cytokines or chemokines, thus consistent with our approach in the primary specimens. For gene expression analysis of the targeted CAF related genes, MSC were sorted following co-culture as demonstrated by the representative example of the sorting strategy in ***Figure 4-2***. The MSC were CD90 positive, CD19 negative and were also clearly separated from ALL cells according to forward and side scatter.

Table 4-1: B-ALL cell lines used in co-culture model.

Cell line	Karyotype	Other known lesions
SD-1	t(9;22) *BCR-ABL1 (e1-a2)*	No abnormality identified in a set of genes covered by MLPA P335-100R kit
REH	*ETV6-RUNX1*	Homozygous deletion of *CDKN2A-5, CDKN2A-2a* and *CDKN2B-2*; heterozygous deletion of *ETV-6-1, ETV-6-2, ETV-6-3, ETV-6-5* and *ETV-6-8*; heterozygous deletion of *BTG1-2*; heterozygous deletion of *IL3RA-1*
697	Near diploid karyotype	Expression of fusion gene TCF3-PBX (E2A-PBX)
TOM-1	t(9;22) *BCR-ABL1 (e1-a2)*	
SEM	t(4;11) *KMT2A-AFF1*	

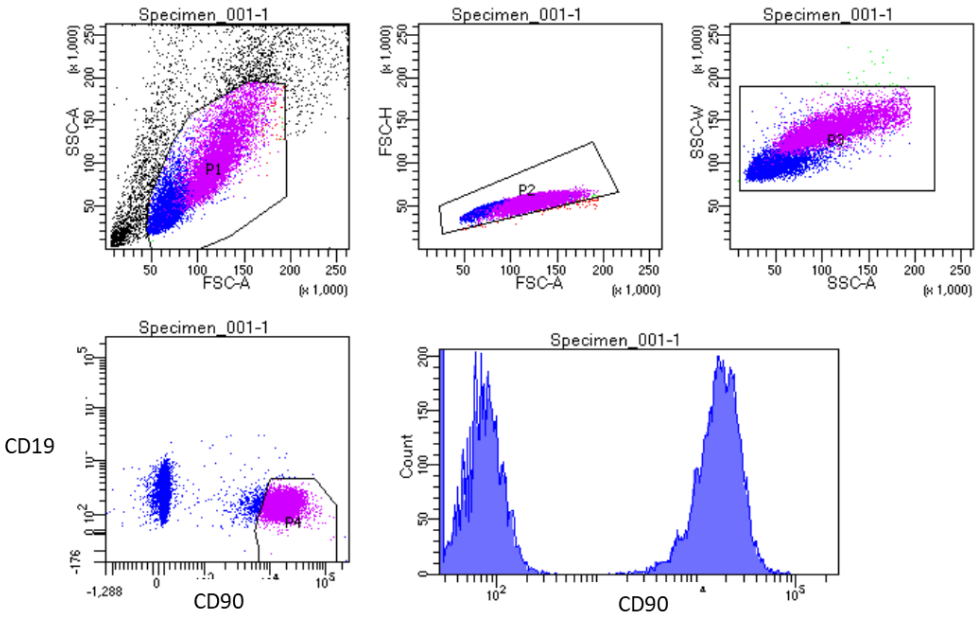

Tube: 1

Population	#Events	%Parent	%Total
All Events	15,192	####	100.0
P1	11,640	76.6	76.6
P2	11,519	99.0	75.8
P3	11,493	99.8	75.7
P4	5,693	49.5	37.5

Figure 4-2: FACS sorting strategy to isolate HS27a after co-culture with ALL cells. The image shows the sorting strategy used to isolate HS27a cells in the co-culture with B-ALL cell lines. Cells were initially gated according to their forward and side scatter and doublets excluded by FSC-A versus FSC-H. MSCs were then separated from B-ALL by nature of their CD90 expression and lack of CD19 expression. To ensure the purity of the HS27a population isolated the P4 gate was drawn at a high fluorescence intensity of the CD90 conjugated fluorochrome. Sorted HS27a cells are purple dots in the image.

4.3.2 A Sub-set of B-cell Acute Lymphoblastic Leukaemia Cell Lines Induce an ALL-CAF Phenotype in HS27a *in vitro*

Figure 4-3 shows the relationship between cytomorphology after phalloidin staining and gene expression profile. After 5 days of co-culture with normal B cells, SEM or REH cells, the HS27a showed minimal morphological changes and no significant change in gene expression profile. By contrast, after co-culture with 697, TOM1 and SD1 cells, HS27a stromal cells took on the typical appearance of ALL-CAF. The gene expression panel revealed a similar, but more profound upregulation of CAF-related genes than we had observed in the primary samples. This was most apparent following co-culture with SD1 cells, where similar to the primary specimens, there was upregulation of growth factors (FGF-2, VEGF), extracellular matrix remodelling enzymes (most notably MMP1) and up to 500-fold upregulation of some cytokine genes. Therefore, a subset of B-ALL cell lines appeared able to induce ALL-CAF (697, TOM1, SD1) whereas others were not (SEM, REH). Based on these findings for future experiments, I designated SEM cells as “non-ALL-CAF inducers” and SD1 cells as “ALL-CAF-inducers”. Importantly, both of these cell lines are derived from clinically aggressive B-ALL, carrying t(4:11) and t(9;22) translocations, respectively.

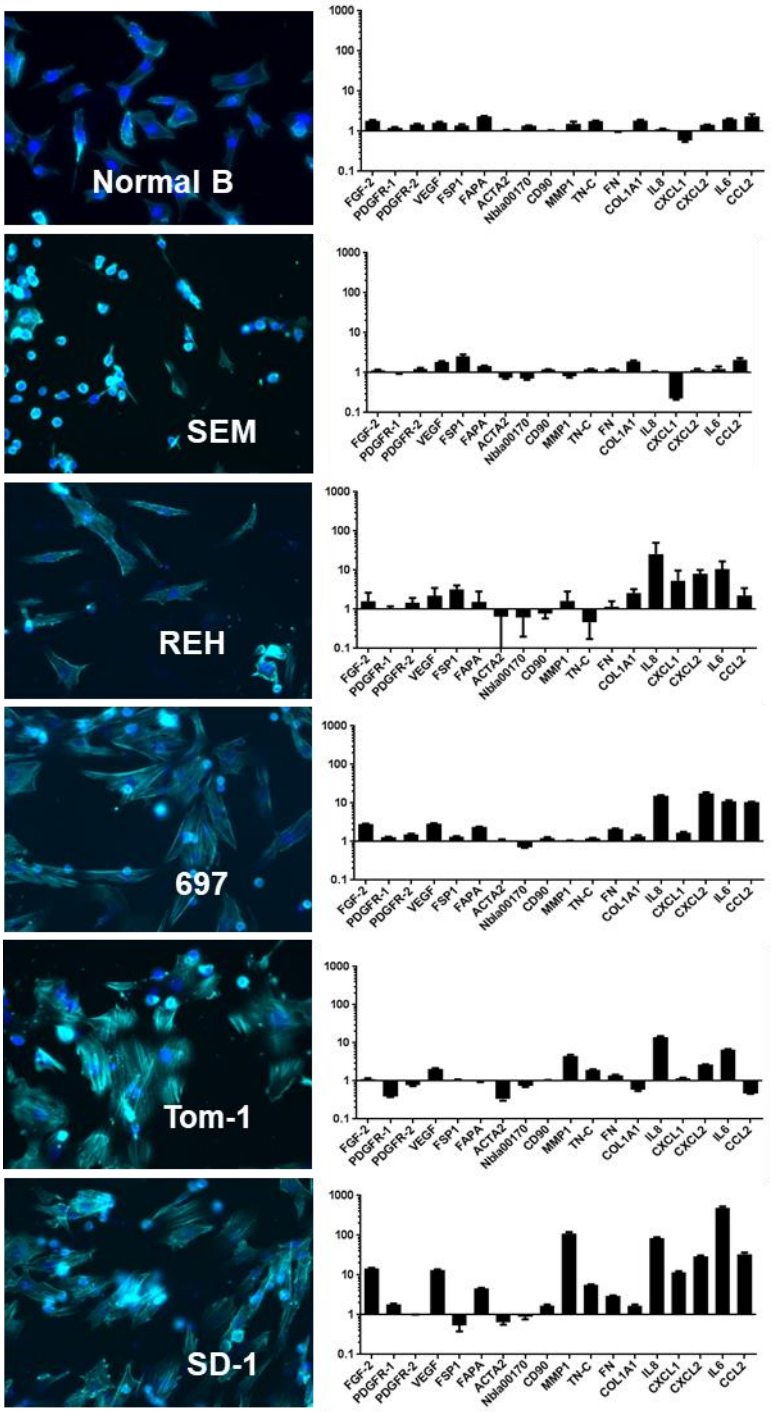

Figure 4-3: A proportion of B-ALL cell lines generate ALL-CAF from HS27a.
Photomicrographs at 20X magnification, of phalloidin (cyan) and DAPI (blue) staining of HS27a cells after five days co-culture with five B-ALL cell lines SEM t(4;11), REH (*ETV6-RUNX1*), 697 (*TCF3-PBX*), Tom-1 (*BCR-ABL1,* p190)) SD-1 (*BCR-ABL1,* p190) or a healthy donor, mature B-cell control. The corresponding HS27a gene expression panel showing fold upregulation of HS27a co-cultured with the denoted B-ALL cell line compared to HS27a in monoculture.

I then explored whether the altered morphology and altered gene expression profile induced in the MSC corresponded to an enhanced secretory profile. I used a cytokine bead assay to compare IL8, IL6 and CCL2 production in the supernatant of both mono-culture and co-culture of B-ALL cell lines and HS27a. I selected both an ALL-CAF inducer (SD1) and a non-ALL-CAF inducer (SEM) to act as a control. The soluble targets selected were based on the soluble targets secreted at the highest levels in the primary specimens. ***Figure 4-4*** shows that little or no IL8, IL6 or CCL2 were generated when HS27A, SEM or SD1 were cultured alone, nor when HS27A were co-cultured with non-CAF inducing SEM cells. By contrast, IL8, CCL2, and IL6, were generated in abundance when HS27a cells were co-cultured with SD1 CAF-inducer cells, thus confirming that a subset of the B-ALL cell lines was able to induce a CAF phenotype in MSC.

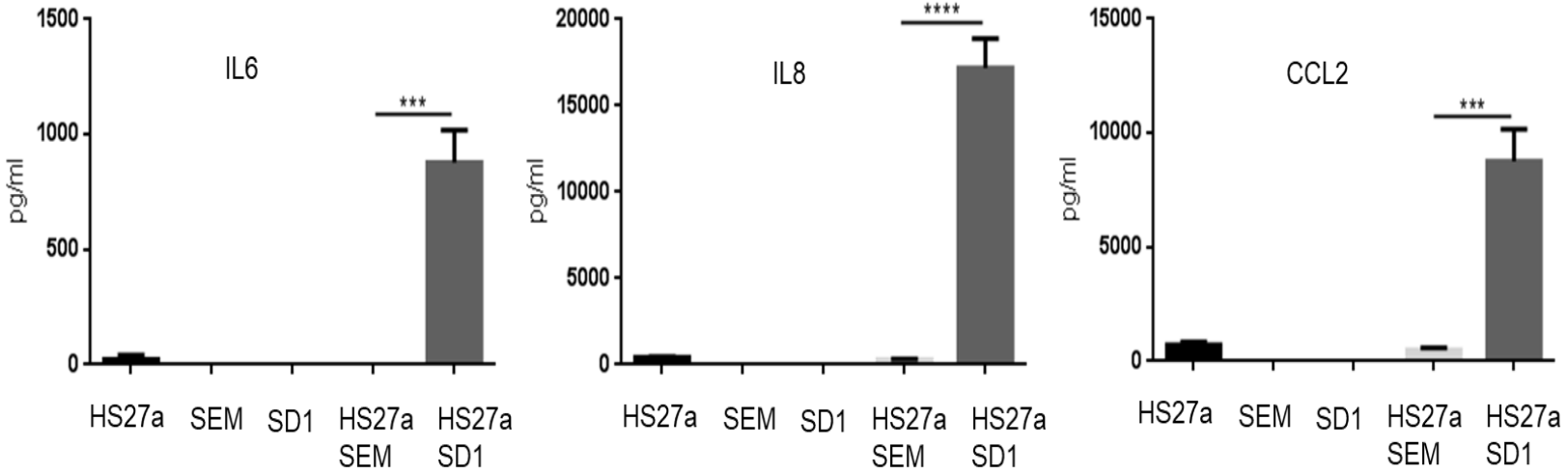

Figure 4-4: Cytokine Bead Assay of supernatant of B-ALL cell lines and HS27a mono-culture and co-culture. Cytokine bead assays for IL6, IL8 and CCL2 (Y axis, pg/ml) during monoculture of HS27 (black bars), SEM and SD1 cells and co-culture of SEM with HS27a and SD1 with HS27a (grey bars), as indicated on the X axis. Bars show mean and standard error of the mean of 3 independent experiments. Statistical significance IL6, P = 0.0004, IL8, P < 0.0001, CCL2, P = 0.0005 using an unpaired t-test is shown for the comparison between HS27a with SEM and HS27a with SD1.

The same phenotype had been previously observed in the primary specimens, with appropriate cytomorphology, gene expression and secretory profile. There was a possible relationship to the underling genetic abnormality of the B-ALL cell, with cell lines harbouring *BCR-ABL1*/*t9;22* (TOM1, SD1) capable of inducing ALL-CAF whereas *KMT2A-AFF1/t4;11* (SEM) and *ETV6-RUNX1/t12;21* (REH) were not.

4.3.3 Primary B-cell Acute Lymphoblastic Leukaemia Cells Induce an ALL-CAF Phenotype in Healthy Donor Mesenchymal Stromal Cells

I then sought to confirm that primary B-ALL cells from patient bone marrow specimens at diagnosis could also induce an activated or CAF phenotype in healthy donor MSC *in vitro,* using the same experimental model depicted in ***figure 4-1***. Given the observation in the cell line model that *BCR-ABL1* cell lines induced the ALL-CAF phenotype, I selected 3 primary samples known to harbour *BCR-ABL1* translocations and included a patient sample from which we had previously isolated ALL-CAF (14-1-475). I included one further sample with no known driver genetic abnormality (B-other ALL, 14-1-456). As my outputs to assess for induction of an ALL-CAF phenotype I used morphological changes and secretion profiles observed in the cell line model and ALL-CAF isolated from primary samples.

Primary ALL specimens variably induced ALL-CAF morphology in two different normal healthy donor MSC as shown in ***figure 4-5***. The sole non-*BCR-ABL1* primary sample (14-1-456) induced CAF morphology in HD1 MSC but not in HD9 MSC whereas the *BCR-ABL1* primary samples consistently induced CAF morphology in both HD MSC (images were not taken, in error, for the co-culture of HD9 and 14-1-475).

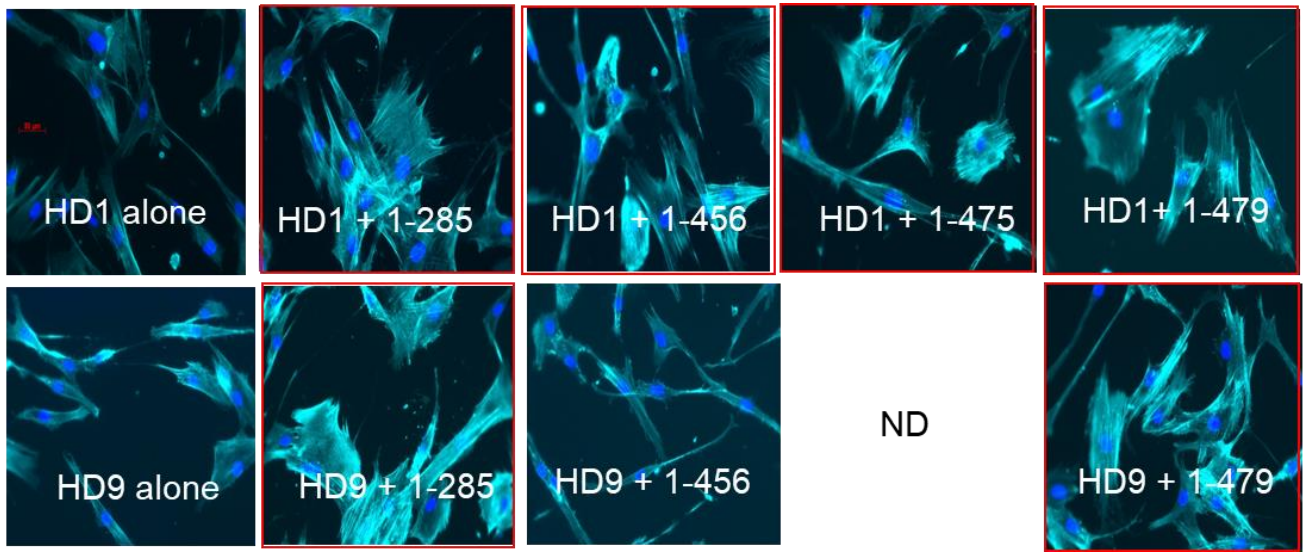

Figure 4-5: Primary B-ALL cells induce ALL-CAF morphological changes in healthy donor MSC. Photomicrographs at 20X magnification, of phalloidin and DAPI staining of two healthy MSC after exposure to primary ALL specimens, UPN as indicated. Red boxes indicate morphology consistent with CAF.

We then assessed whether the primary B-ALL cells could also induce an enhanced secretory profile in the HD MSC. Figure 6 shows that increased IL8, IL6 and CCL2 were also secreted by two different healthy donor MSC in response to the CAF-inducing specimens seen in ***figure 4-6***. Notably the only co-culture (HD9 + 14-1-456) where ALL-CAF morphology was not induced was associated with the lowest level of IL6, IL8 and CCL2 production. This was also the sole non-*BCR-ABL1* primary sample used. Therefore, both B-ALL cell lines and primary B-ALL cells can induce the ALL-CAF phenotype in both HS27a and healthy donor MSC.

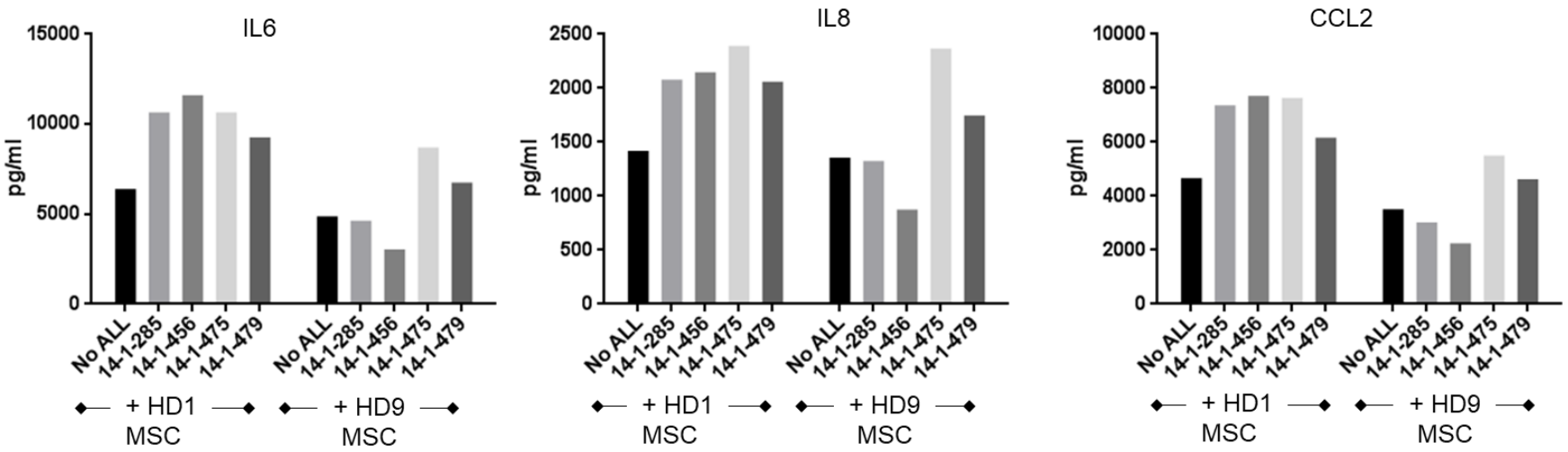

Figure 4-6: Primary B-ALL cells induce enhanced secretory profile in healthy donor MSC. Cytokine bead assays for IL6, IL8 and CCL2 (pg/ml, Y axis) of HD1 and HD9 MSC at baseline or following exposure to four primary ALL specimens, UPNs as indicated on the X axis.

4.3.4 ALL-CAF Induction in HS27a is Due to a Soluble Mediator

I next sought to determine the mechanism behind the activation of the stromal cells by a sub-set of B-ALL cells. As previously discussed, growth factors, oxidative stress and exosomes have all been postulated as mechanisms to explain the activation of fibroblasts or MSC. I chose to focus on oxidative stress or reactive oxygen species (ROS) for two reasons. Firstly, the presence of *BCR-ABL1* in B-ALL cells predicted induction of the ALL-CAF phenotype both in our cell line and primary cell model. The *BCR-ABL1* translocation is known to induce increased ROS production in cells[164]. Second, we had observed MSC with an ALL-CAF phenotype in patient specimens post treatment as well as at diagnosis. Chemotherapy drugs used in B-ALL, such as cytarabine and daunorubicin, are known to induce ROS in exposed cells (further explored in chapter 5), suggesting that MSC exposure to increased levels of ROS, either due to ROS inducing genetic lesions in the B-ALL cell or induced by chemotherapy drugs, could be a common mechanism to explain induction of the ALL-CAF phenotype.

To investigate this hypothesis, I initially confirmed that the transformation was due to a soluble mediator and not contact-dependent, using a transwell to separate the MSC from the B-ALL cells. ***Figure 4-7*** confirms that, in a transwell, the CAF-inducer SD1 induces the same morphological changes, gene expression profile and cytokine/chemokine secretion profile in HS27a, as when the cells are in contact. However, the non-CAF inducer SEM, does not induce these changes in the HS27a in transwell, as expected. Therefore, the transformation to ALL-CAF was not contact-dependent, confirming that a soluble mediator was responsible for development of the ALL-CAF phenotype.

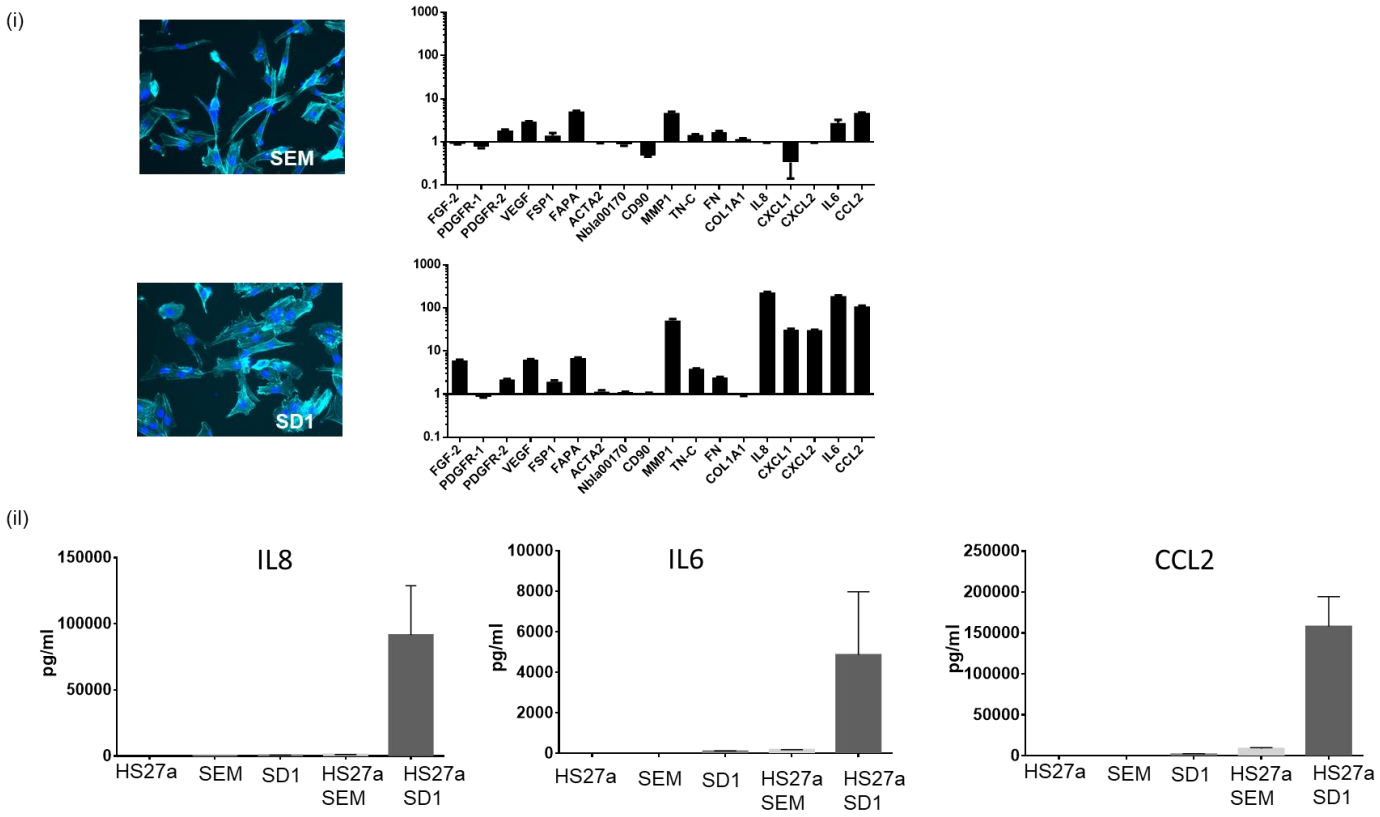

Figure 4-7 B-ALL cells induce ALL-CAF from HS27a via a soluble mechanism. (i) Photomicrographs at 20X magnification of phalloidin (cyan) and DAPI (blue) staining of HS27a cells after five days of co-culture with two B-ALL cell lines SEM and SD-1 (*BCR-ABL1,* p190) separated by a transwell. The corresponding HS27a gene expression panel showing fold upregulation of HS27a co-cultured with the denoted B-ALL cell line separated by transwell compared to HS27a in monoculture. (ii) Cytokine bead assays for IL6, IL8 and CCL2 (Y axis, pg/ml) during monoculture of HS27 (black bars), SEM and SD1 cells and co-culture of SEM with HS27a and SD1 with HS27a separated by transwell (grey bars), as indicated on the X axis. Bars show mean and standard error of the mean of 3 independent experiments.

4.3.5 ALL-CAF Phenotype Induction is Dependent on Reactive Oxygen Species Exposure

To explore if ROS was the soluble mediator responsible for the ALL cell induced transformation of MSC to ALL-CAF, I measured intracellular ROS using CELLROX Green® by flow cytometry and calculated the mean fluorescence intensity (MFI) in the ALL cell lines used in my model (***figure 4-8***). CellROX® Green Reagent is a novel fluorogenic probe for measuring oxidative stress in live cells. The cell-permeant dye is weakly fluorescent while in a reduced state and exhibits bright green photostable fluorescence upon oxidation by reactive oxygen species (ROS) and subsequent binding to DNA, with absorption/emission maxima of ~ 485/520 nm. CellROX® green only becomes fluorescent with subsequent binding to DNA, limiting its presence to the nucleus or mitochondria. There is some evidence it more reliably detects superoxide, but not hydrogen peroxide-induced hydroxyl radicals[165].

I compared the ROS levels in B-ALL cell lines able to induce CAFs and compared the levels to those B-ALL cell lines that were unable to. All 3 of the B-ALL cell lines (SD1, TOM1, 697) able to induce CAFs had higher levels of intracellular ROS than the cell lines unable to induce CAFs. Notably, SD1 cells had the highest ROS levels and induced the greatest upregulation of relevant CAF related genes in the previous RQ-PCR panel.

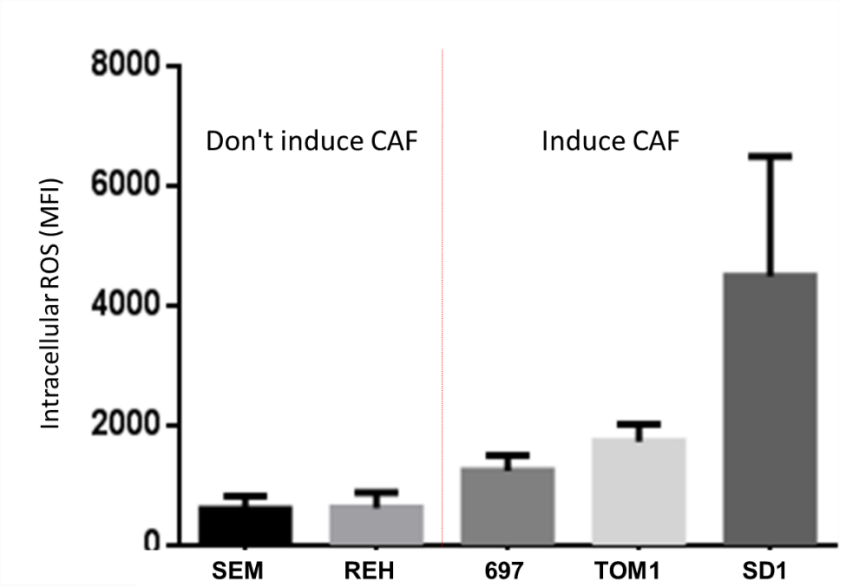

Figure 4-8: B-ALL cell lines that induce ALL-CAF have higher levels of intracellular ROS. Intracellular ROS by CellROX® assay via flow cytometry (Y axis) at baseline in SEM, REH, 697, Tom-1 and SD-1 cells.

I then explored if perturbations in ROS using hydrogen peroxide (H_2O_2) and the ROS scavenger, N-acetylcysteine (NAC) could alter the transformation of HS27a to ALL-CAF as shown in ***Figure 4-9***. I first exposed HS27a cells to the ROS H_2O_2 for 48 hours (***Figure 4-9(i)***) and confirmed that HS27a underwent morphological changes consistent with an ALL-CAF. I also noted significantly enhanced IL6 and IL8 but not CCL2 secretion (***Figure 4-9(ii)***). I then explored whether N-acetylcysteine (NAC) a ROS scavenger could inhibit the transformation of HS27a to ALL-CAF post exposure to SD1 conditioned media (***Figure 4-9(iii)***). I first confirmed exposure to NAC led to no independent change in the cytomorphology of HS27a. As expected, and shown in the images, when HS27a were exposed to SD1 conditioned media they underwent transformation to ALL-CAF. However, the addition of NAC ameliorated this transformation to ALL-CAF confirming a ROS dependent phenomenon.

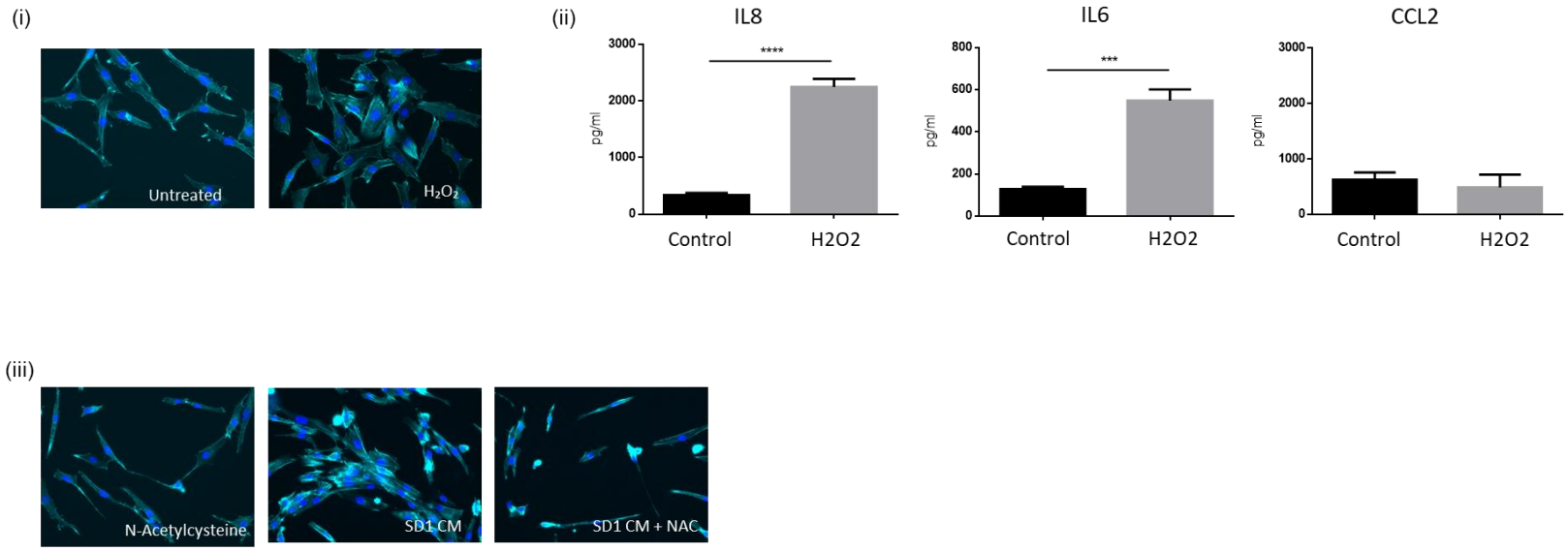

Figure 4-9 ALL-CAF phenotype induced by ROS and inhibited by N-acetylcysteine. (i) Photomicrographs at 20X magnification of phalloidin (cyan) and DAPI (blue) staining of HS27a cells after exposure to hydrogen peroxide (H2O2) and an untreated control. (ii) Cytokine bead assays for IL6, IL8 and CCL2 (Y axis, pg/ml) of HS27a in an untreated control (black bars) and exposed to H2O2 (grey bars), as indicated on the X axis. Bars show mean and standard error of the mean of 3 independent experiments. Statistical significance as depicted: IL8, $P < 0.0001$ and IL6, $P = 0.0002$. (iii) Photomicrographs at 20X magnification, of phalloidin and DAPI staining of HS27a cells culture in SD1 conditioned media (SD1 CM) with and without N-acetyl cysteine (NAC) compared to HS27a in media with N-acetyl cysteine.

To provide further support for this hypothesis, given ROS is predominantly produced in the mitochondria, I depleted mitochondria from the SD1 cells using low concentration ethidium bromide. Ethidium bromide at low concentration depletes mitochondria in cells by selective depletion of mitochondrial DNA and not nuclear DNA[166] due to the differing membrane potentials and therefore permeability of the nucleus and mitochondria. Several authors and I have confirmed the validity of this approach in depleting mitochondria in target cells (further explored in chapter 6). I confirmed that the SD1 cells retained viability after ethidium bromide treatment using trypan blue exclusion and then compared the ability of the ethidium bromide-treated SD1 cells to induce ALL-CAF in HS27a cells, as compared to untreated SD1. As shown in ***figure 4-10*** the ethidium bromide treated SD1 cells were unable to induce ALL-CAF cytomorphology changes in HS27a and there was a significant reduction in the secretion of relevant cytokines/chemokines except for IL6 as compared to untreated SD1 cells, suggesting that mitochondria-generated ROS is essential in the transformation of HS27a to ALL-CAF.

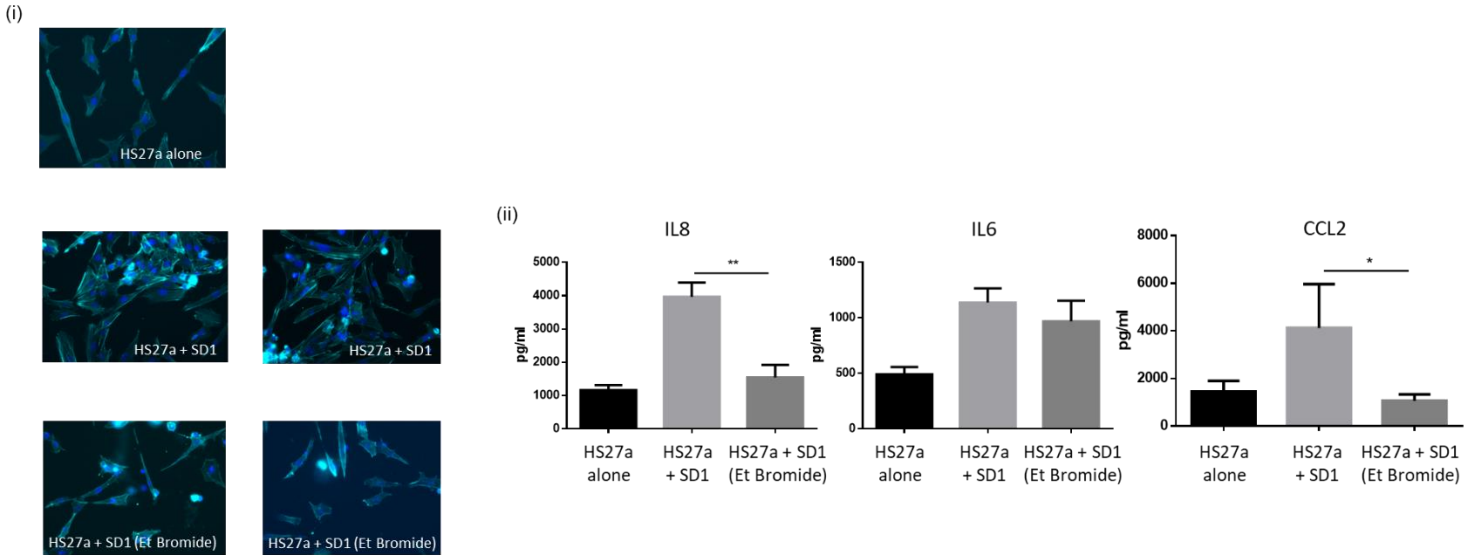

Figure 4-10: SD1 cells depleted of mitochondria are unable to activate HS27a. (i) Photomicrographs at 20X magnification of phalloidin (cyan) and DAPI (blue) staining of mono-culture of HS27a cells (HS27a alone), co-culture of HS27a with untreated SD1 cells (HS27a + SD1) and co-culture with SD1 cells treated with ethidium bromide (SD1 + Et Bromide). (ii) Cytokine bead assays for IL6, IL8 and CCL2 (Y axis, pg/ml) of HS27a in mono-culture (black bars) and in co-culture with untreated SD1 cells (light grey bars) and in co-culture with ethidium bromide treated SD1 cells (dark grey bars), as indicated on the X axis. Bars show mean and standard error of the mean of 3 independent experiments. Statistical significance as depicted: IL8, P = 0.0019 and CCL2, P = 0.04.

4.4 Discussion

I have demonstrated that a subset of B-ALL cell lines can induce the same ALL-CAF phenotype *in vitro* we had observed in a proportion of the MSC expanded from primary samples. Furthermore, I was also able to demonstrate induction of ALL-CAF using B-ALL cells from primary samples on healthy donor MSC. As with the ALL-CAF we had isolated from patient primary samples this was defined by cytomorphological changes, upregulation of CAF-relevant genes and an enhanced secretory profile.

The ability of B-ALL cells to induce these changes in MSC appears to relate to the underlying genetic abnormality of the ALL cell. *BCR-ABL1* positive cell lines and primary cells appear capable of inducing these changes whereas B-ALL cell lines positive for *ETV6-RUNX1* or *KMT2A-AFF1* were not. Notably, patient sample 14-1-475 from which I isolated ALL-CAF is *BCR-ABL1* positive, whereas sample 14-1-389 from which I did not isolate ALL-CAF has a *KMT2A-AFF1* re-arrangement. While it is difficult to draw conclusions from small numbers of samples, my data suggest that specific genetic lesions within the ALL cell may be important in determining the B-ALL cell's interaction and ability to induce activation or the ALL-CAF phenotype in MSC.

My data strongly suggests that MSC undergo transformation to ALL-CAF following exposure to increased ROS levels. The intrinsic ROS level of the B-ALL cell appears to predict whether MSC in co-culture undergo transformation. I was able to replicate the phenotype of ALL-CAF by exposing MSC to H_2O_2 and inhibit the transformation to ALL-

CAF by using either the ROS scavenger - NAC - or by depleting the ALL cell of mitochondria, the organelle which produces the majority of ROS within a cell. This suggests that ROS plays a vital role in induction of the ALL-CAF phenotype. In keeping with this is the knowledge that *BCR-ABL1*, the genetic lesion that appeared to reliably predict induction of ALL-CAF, is known to increase ROS levels within cells. This is also in keeping with previous findings in solid organ malignancy that oxidative stress induces activation in fibroblasts or stromal cells and chronic ROS exposure can lead to transformation to CAF[117]. My final experiment of depleting mitochondria also suggests that ROS produced by the mitochondria is likely important in inducing the ALL-CAF phenotype.

In the next chapter, I sought to explore if chemotherapy could directly induce the ALL-CAF phenotype in stromal cells and to evaluate the role of chemotherapy-induced ROS in this phenomenon.

Chapter 5: Modelling induction of a CAF phenotype in MSC post exposure to chemotherapy drugs used in ALL

5.1 Background

5.1.1 Chemotherapy-induced Cancer Associated Fibroblasts

While it has long been recognised that cancer cells can induce the transition of a stromal cell to a CAF as discussed in the previous chapter, it has only recently been recognised that chemotherapy may induce a similar phenotype in MSC or fibroblasts. Peiris-Pages et al[146] provided in vitro evidence of chemotherapy induced modifications in fibroblastic cells consistent with a CAF phenotype including α-SMA expression, an enhanced cytokine secretory profile and recruitment of immune cells to support cancer cell survival. Sun et al[147] and Chan[148] et al provided further evidence that chemotherapy can activate stromal cells, inducing a state characterised by enhanced cytokine secretion which aided cancer cell survival. Interestingly, the activation of stromal cells was very dependent on the dose of the chemotherapy drug used, with only higher concentrations of chemotherapy inducing the activated state which aided cancer cell survival.

Duan et al[12] in their murine ALL niche model also describe MSCs that, following exposure to daunorubicin or cytarabine and interaction with ALL cells, developed a

phenotype very much consistent with an activated fibroblast or CAF with α-SMA expression and transition to this phenotype dependent on TGF-β1.

5.2 Aims

1. To determine if chemotherapy drugs commonly used in ALL treatment can induce an ALL-CAF phenotype in MSC *in vitro*
2. To explore the functional significance of the ALL-CAF phenotype on ALL cell proliferation and survival following chemotherapy *in vitro*

5.3 Results

5.3.1 Chemotherapy Drug Selection and Dose Identification

I initially sought to determine if four chemotherapy agents (Daunorubicin (DNR), Cytarabine (AraC), Vincristine (VCR) and Dexamethasone (DEX)), commonly used in the treatment of adult ALL, were also able to induce ALL-CAF. These drugs were selected for two reasons. Firstly, they are all used as non-investigational medicinal products (IMPs) on the UKALL14 trial treatment regimens in either the first or second phase of treatment, the stages of treatment from which we had expanded primary MSC in chapter 3. Secondly, DNR and AraC were both observed to induce MSC with a CAF-like phenotype described by Duan et al[12] and are known to induce ROS through DNA

damage of target cells[167]. Therefore, I predicted they would also induce the ALL-CAF phenotype *in vitro*. VCR works by damaging microtubules and DEX is a potent corticosteroid with anti-inflammatory properties with neither described as increasing ROS in target cells.

The appropriate doses of DNR, AraC, VCR and DEX were established by identifying the doses of chemotherapy that reduced the proliferation of the B-ALL cell line, SEM, by approximately 50% at 72 hours as demonstrated in ***figure 5-1***. I selected doses of AraC 200nM, DNR 8nM, DEX 200nM and VCR 1.6nM. The doses selected were comparable to the median concentration reported as achievable in humans treated for ALL[168,169].

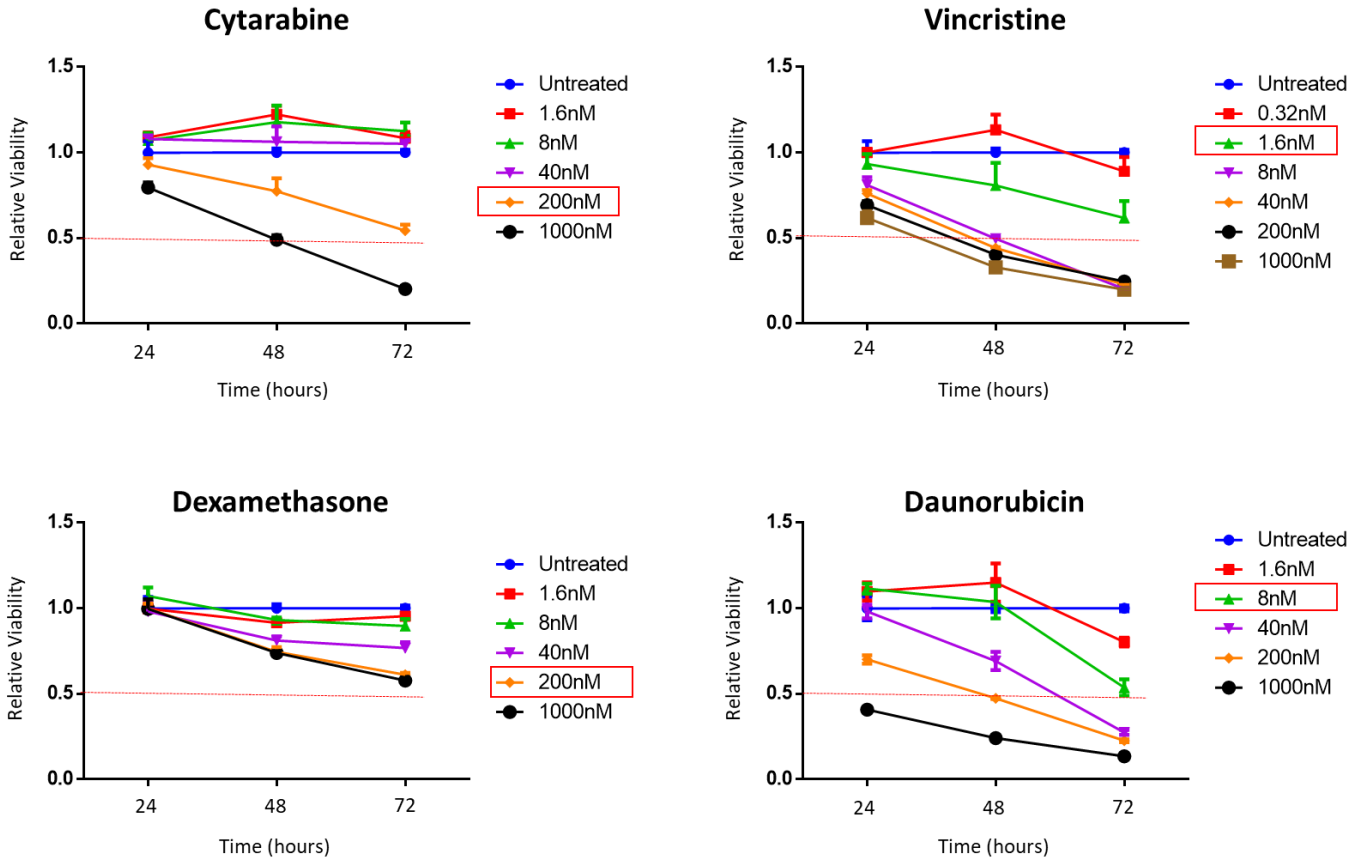

Figure 5-1: Identification of appropriate chemotherapy doses. MTS assay of ALL cell (SEM) viability compared to an untreated control (Y axis) following exposure to relevant chemotherapy agent at stated time points (X axis). Bars show mean and standard error of the mean of 3 independent experiments. Concentrations of chemotherapy drugs are colour coded and listed in the key.

5.3.2 Cytarabine and Daunorubicin Induce an ALL-CAF phenotype in Mesenchymal Stromal Cells

I then exposed both the MSC cell line, HS27a and healthy donor MSC to all four chemotherapy drugs at the calculated concentration for 96 hours. As in the primary samples and B-ALL cell line model, I used immunocytochemistry, a targeted gene expression profile and cytokine/chemokine secretion as outputs to assess for induction of the ALL-CAF phenotype.

After exposure to AraC and DNR for 96 hours, typical activated MSC or ALL-CAF cytomorphology was observed in both HS27a and normal healthy donor MSC (***figure 5-2***). By contrast, VCR exposure resulted in an enlarged, flattened morphology, but with a marked diminution in intracellular connections and no increase in actin stress fibres. DEX caused no discernible cytomorphological change. AraC and DNR, but not VCR or DEX, also lead to increased αSMA expression, in keeping with the findings from the murine model of Duan et al[12].

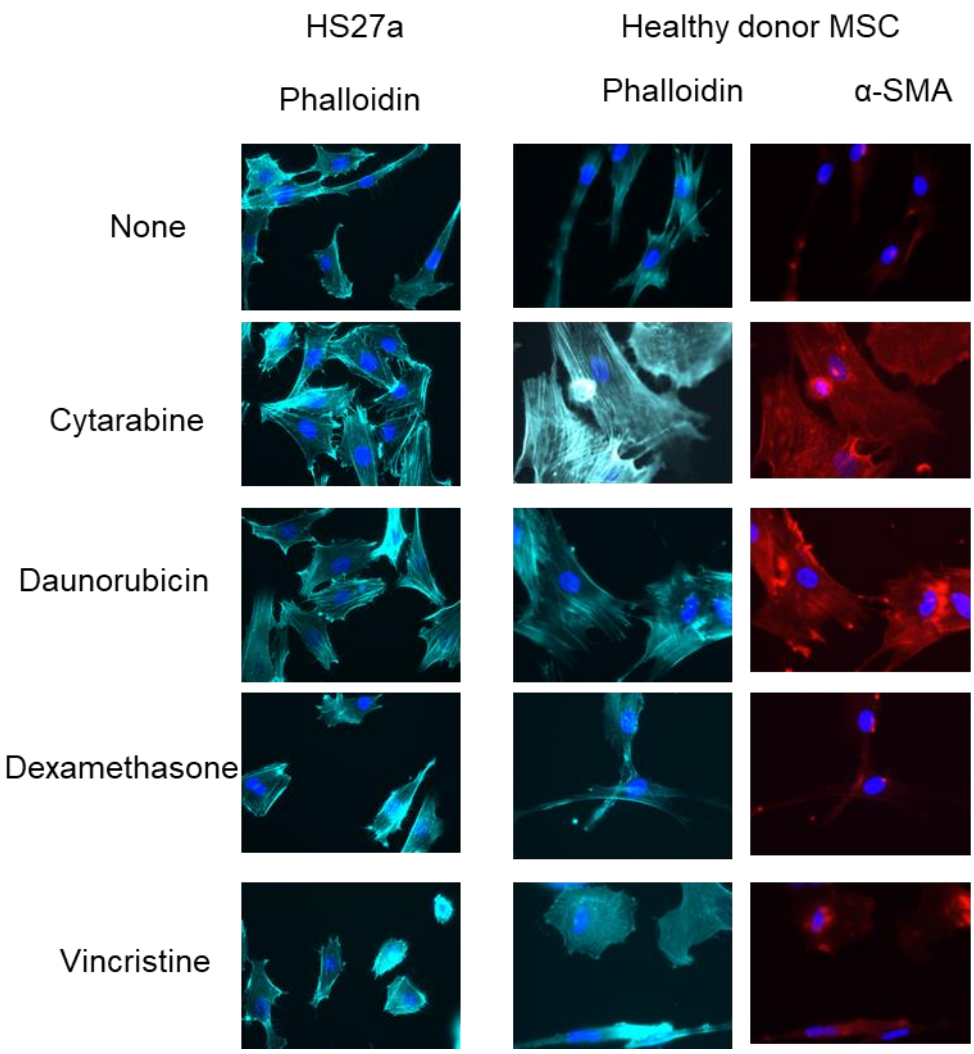

Figure 5-2: Cytarabine and daunorubicin generate ALL-CAF. Photomicrographs, at 40X magnification, showing phalloidin (cyan) and DAPI (blue) staining of HS27a cells at baseline or after exposure to the chemotherapy agents indicated on the left, or of phalloidin and DAPI staining plus αSMA (red) staining of normal, healthy donor MSC at baseline of or after exposure to the chemotherapy agents indicated.

The expression profile of key activated MSC marker genes in HS27a, relative to untreated control, is shown in ***figure 5-3***. AraC and DNR generated a gene expression profile similar to the primary samples containing ALL-CAF. This included chemokine and cytokine gene upregulation and particularly prominent MMP-1 upregulation. VCR exposure upregulated chemokine and cytokine gene expression modestly, but not cytoskeletal and ECM remodelling and growth factor gene expression. After DEX, there was striking downregulation of MMP-1. Among cytokine and chemokine genes, there was modest downregulation of CXCL1 and CCL2 expression.

The corresponding cytokine and chemokine protein expression by cytokine bead assay (***figure 5-4***) confirm the pro-inflammatory impact of AraC, DNR and VCR, by contrast to anti-inflammatory impact of DEX. This was in keeping with the gene expression profile.

Therefore AraC and DNR were capable of inducing the ALL-CAF phenotype in vitro with characteristic morphology, gene expression profile and cytokine secretion. VCR induced some features of ALL-CAF but the cytoskeleton of the cell was markedly altered presumably due to its microtubule damaging mechanism of action. DEX did not induce features consistent with ALL-CAF and notably reduced secretion of the relevant cytokines, likely due to its anti-inflammatory properties.

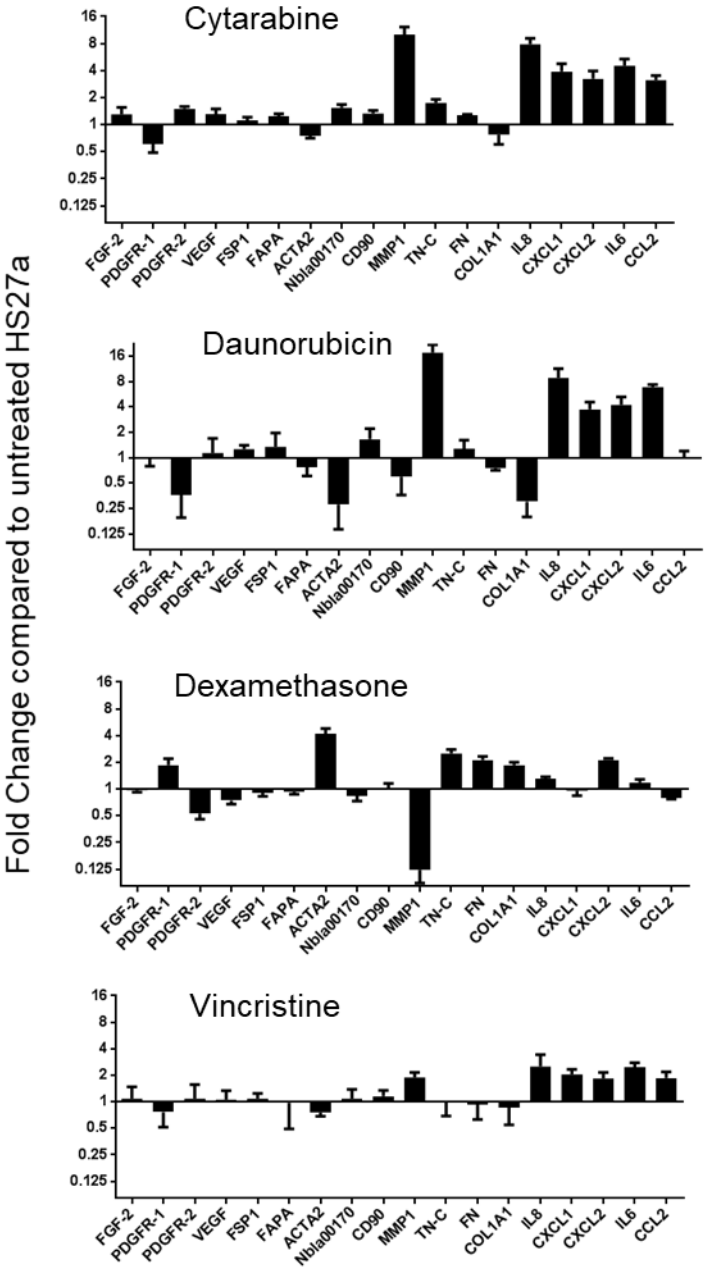

Figure 5-3: Targeted gene expression profile of HS27a following exposure to chemotherapy drugs. The 18-panel gene expression profile of showing fold upregulation in HS27a cells after exposure to each of the chemotherapy drugs indicated, compared to untreated HS27a. Bars show mean and standard error of the mean of 3 independent experiments.

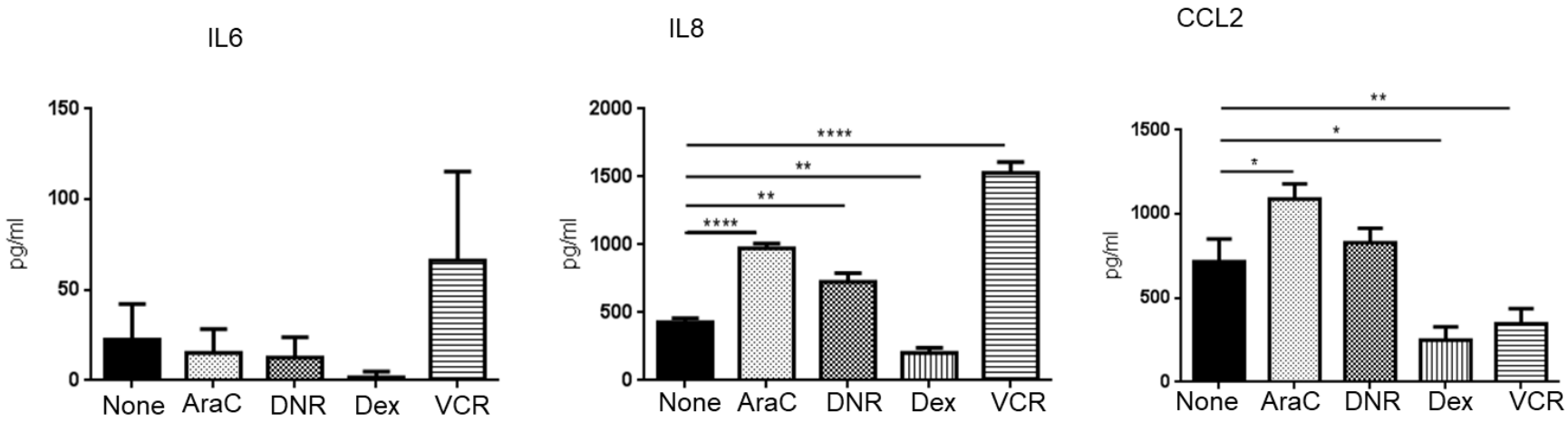

Figure 5-4: Cytokine/Chemokine secretion of HS27a following exposure to chemotherapy drugs. Cytokine bead assays for IL6, IL8 and CCL2 (pg/ml, Y axis) following exposure of HS27a to the chemotherapy drugs indicated below. Bars show means and standard error of the mean. Black bars = no chemotherapy. AraC = cytarabine, light dotted bars, DNR = daunorubicin, dark hatched bars, Dex = dexamethasone, vertical striped bars, and VCR = vincristine, horizontal striped bars. All statistically significant comparisons (by unpaired t-test) are as depicted: IL8, none versus cytarabine, $P < 0.0001$, IL8, none versus daunorubicin, $P= 0.002$, IL8, none versus dexamethasone, $P= 0.001$, IL8, none versus vincristine, $P < 0.0001$. CCL2 none versus cytarabine, $P= 0.0169$, CCL2, none versus dexamethasone, $P = 0.0166$, CCL2, none versus vincristine, $P= 0.0065$.

5.3.3 Chemotherapy Induced Alterations in Mesenchymal Stromal Cells Occur in Presence of Acute Lymphoblastic Leukaemia Cells

I next sought to confirm that the changes observed in the MSC following chemotherapy also occurred if B-ALL cells were also present. As shown in ***figure 5-5,*** I co-cultured healthy donor MSC with either the non-ALL CAF inducer SEM or the CAF inducer SD1 and then exposed the co-culture to AraC, VCR or media only. As expected, both SD1 cells and AraC exposure induced the typical cytomorphological appearance of ALL-CAF and also led to apparent enhanced contact of B-ALL cells with MSC as shown in the images. In contrast, VCR exposure led to the previously observed alteration of the cytoskeleton of the MSC, regardless of the B-ALL cell line used, with very few B-ALL cells in contact with the MSC and hence the majority were washed away during the staining process.

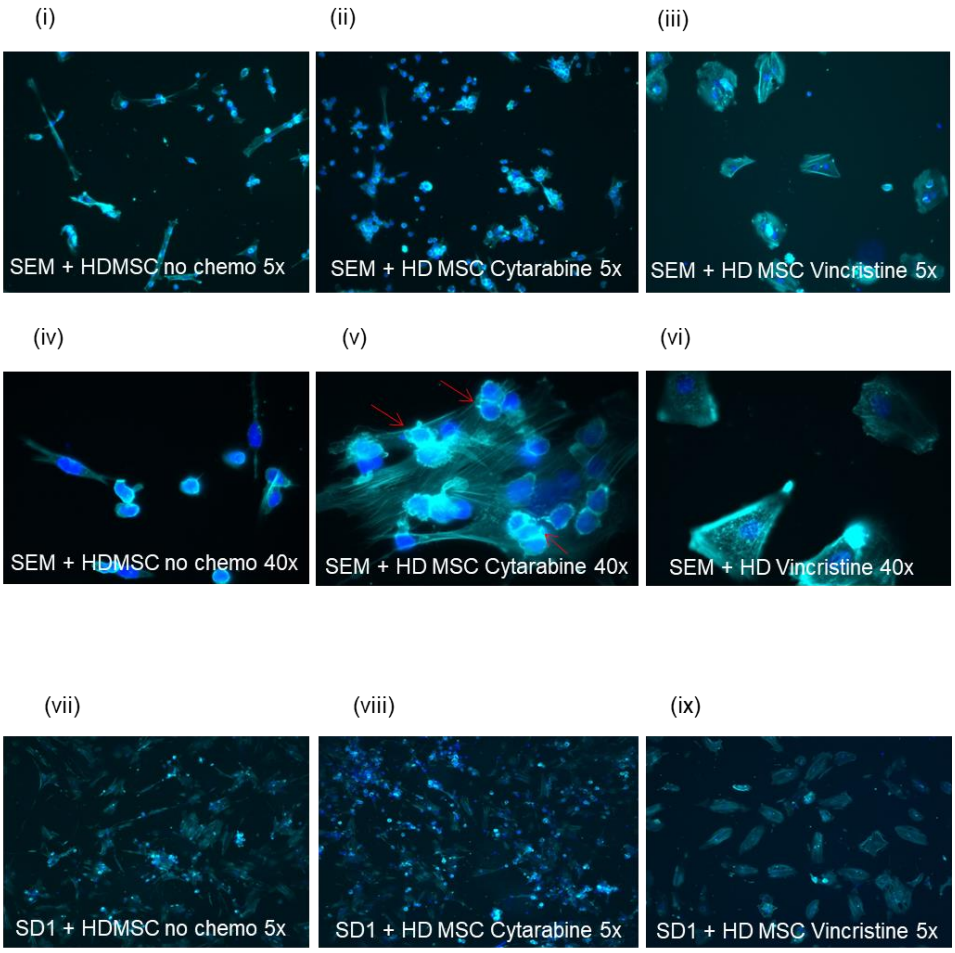

Figure 5-5: Immunocytochemistry of HS27a in co-culture with B-ALL cells following chemotherapy exposure. Photomicrographs of phalloidin (MSC) and DAPI (SEM) staining of (i) SEM + healthy donor MSC cells 5X (ii), SEM + healthy donor MSC cells with cytarabine 5X (iii) SEM + healthy donor cells with vincristine 5X (iv) SEM + healthy donor MSC cells (v) SEM + healthy donor MSC cells with cytarabine 40X, red arrows indicate SEM (DAPI) in physical contact with MSC (vi) SEM + healthy donor cells with vincristine 40X (vii) SD1 + healthy donor MSC cells 5X (viii) SEM + healthy donor MSC cells with cytarabine 5X (ix) SD1 + healthy donor.

5.3.4 Chemotherapy Induced Activation of Mesenchymal Stromal Cell is Reactive Oxygen Species Dependent

I then sought to confirm that, ALL-CAF induction following chemotherapy was ROS dependent, as I had observed from co-culture with the B-ALL cell lines. As discussed above, AraC and DNR but not VCR or DEX, are known to induce ROS in target cells. I first confirmed this by exposing SEM cells (selected for their low baseline ROS) to the four chemotherapy drugs and then measured the intracellular ROS of the SEM cells by flow cytometry (***figure 5-6***). This confirmed that AraC and DNR increased the intracellular ROS in target cells whereas VCR had no effect and DEX lowered the intracellular ROS.

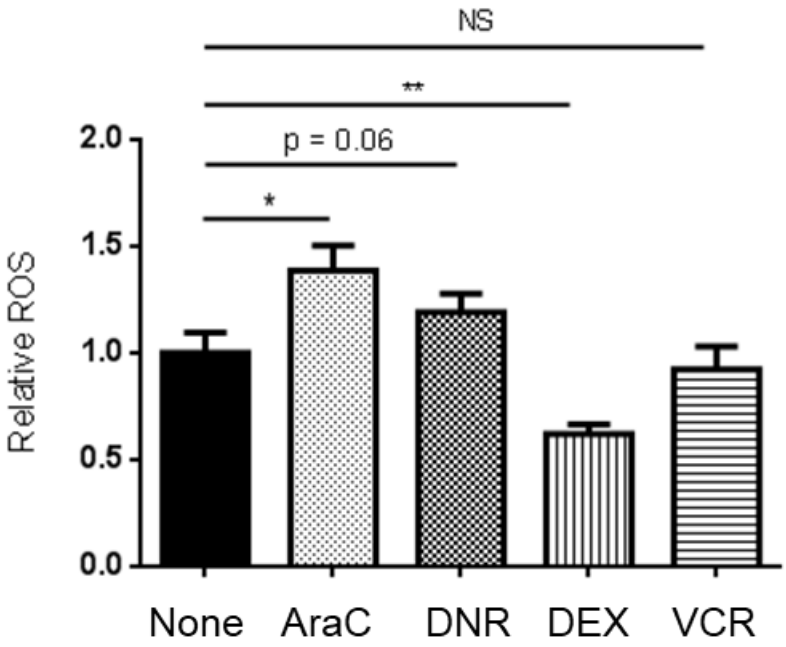

Figure 5-6: ROS levels SEM cells following chemotherapy exposure. ROS levels relative to untreated SEM baseline (1.0), Y axis, after exposure to chemotherapy agents indicated on the X axis Bars show mean +/-SE of 3 independent experiments. All statistically significant comparisons (by unpaired t-test) are as depicted: (i) ROS level, none versus AraC, P= 0.0115, none vs. DNR 0.06, none vs. DEX, P = 0.0035.

Thus, in keeping with my findings that AraC and DNR induced the ALL-CAF phenotype but VCR and DEX did not. To further confirm the role of ROS in chemotherapy induced activation of MSC into ALL-CAF, I attempted to block the effect by the addition of the antioxidant, N-acetyl cysteine (NAC) which was added to HS27a at the same time as exposure to AraC and DNR (***figure 5-7***). As previously observed, AraC and DNR induced ALL-CAF morphology in HS27a. The addition of NAC to AraC or DNR prevented the morphological transformation of HS27a to ALL-CAF. However the addition of NAC did not lead to any significant reduction in the median level of relevant cytokine secretion of HS27a cells post exposure to AraC and DNR compared to AraC and DNR alone. Notably, the HS27a cytokine secretion did not increase after exposure to AraC and DNR alone to the degree previously observed in one of the replicates, thus I suspect technical issues may have occurred. I plan to repeat this experiment to confirm or refute my suspicion of technical issues affecting the results.

Given that I had demonstrated DEX also lowered ROS in target cells, I then explored if DEX could also perturb AraC and DNR induced changes in the HS27a (***figure 5-8***). The addition of DEX to AraC and DNR prevented the transformation of HS27a to ALL-CAF morphology. Furthermore, the addition of DEX led to a significant reduction in HS27a secretion of almost all the relevant cytokines or chemokines. This provides a potential explanation for the primary MSC cytokine secretion differences observed in chapter 3 between phase I and 2 specimens. In phase I DEX is given with DNR whereas in phase II AraC is given without DEX. Overall, this confirmed that ROS inducing chemotherapy was inducing an activated state or ALL-CAF phenotype in the MSC, which could be

inhibited by reduction in ROS through NAC or using the anti-inflammatory corticosteroid, DEX.

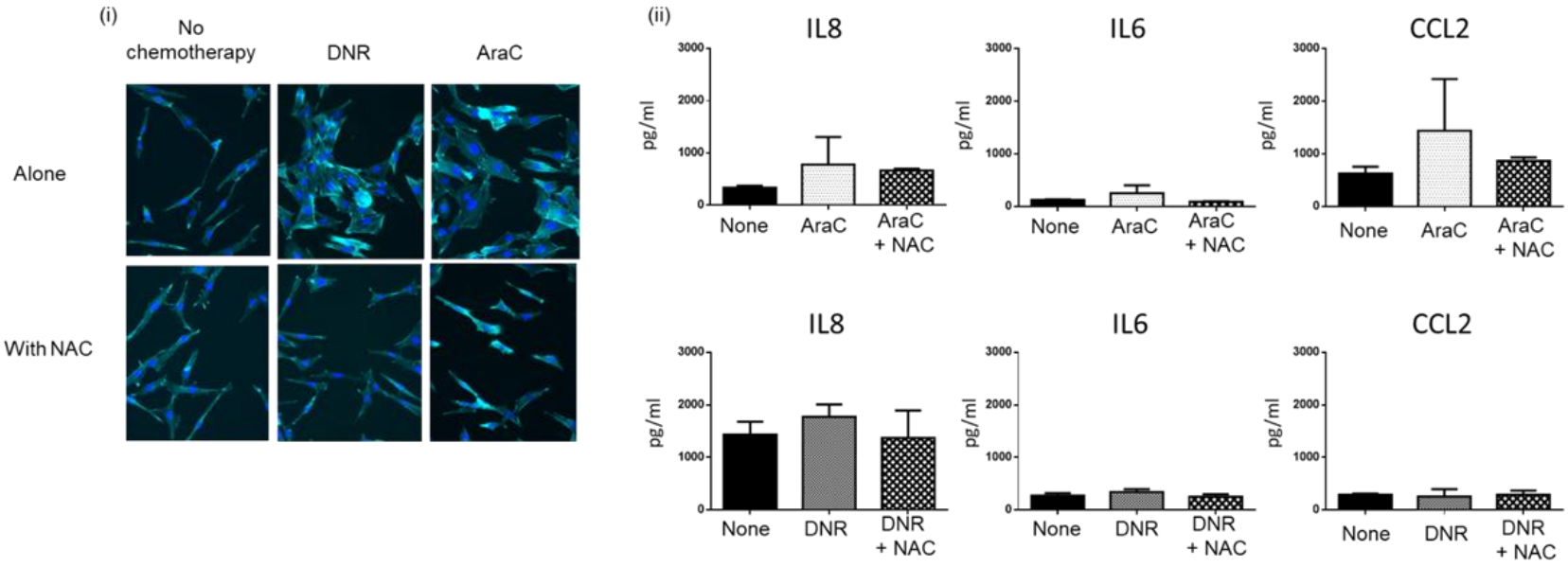

Figure 5-7: NAC abrogates chemotherapy induced activation of HS27a. (i) 20x Phallodin (cyan)/DAPI (blue) staining of HS27a MSC exposed alone or exposed to DNR or AraC with or without NAC 5mM. The images show the addition of NAC abrogates the activated MSC appearance that occurs after the addition of AraC or DNR. (ii) Cytokine bead assays for IL6, IL8 and CCL2 (pg/ml, Y axis) following exposure of HS27a to the chemotherapy drugs indicated below with and without NAC compared to an untreated control (none) as indicated on the X axis. Bars show mean +/-SE of 3 independent experiments. None of the differences observed were statistically significant.

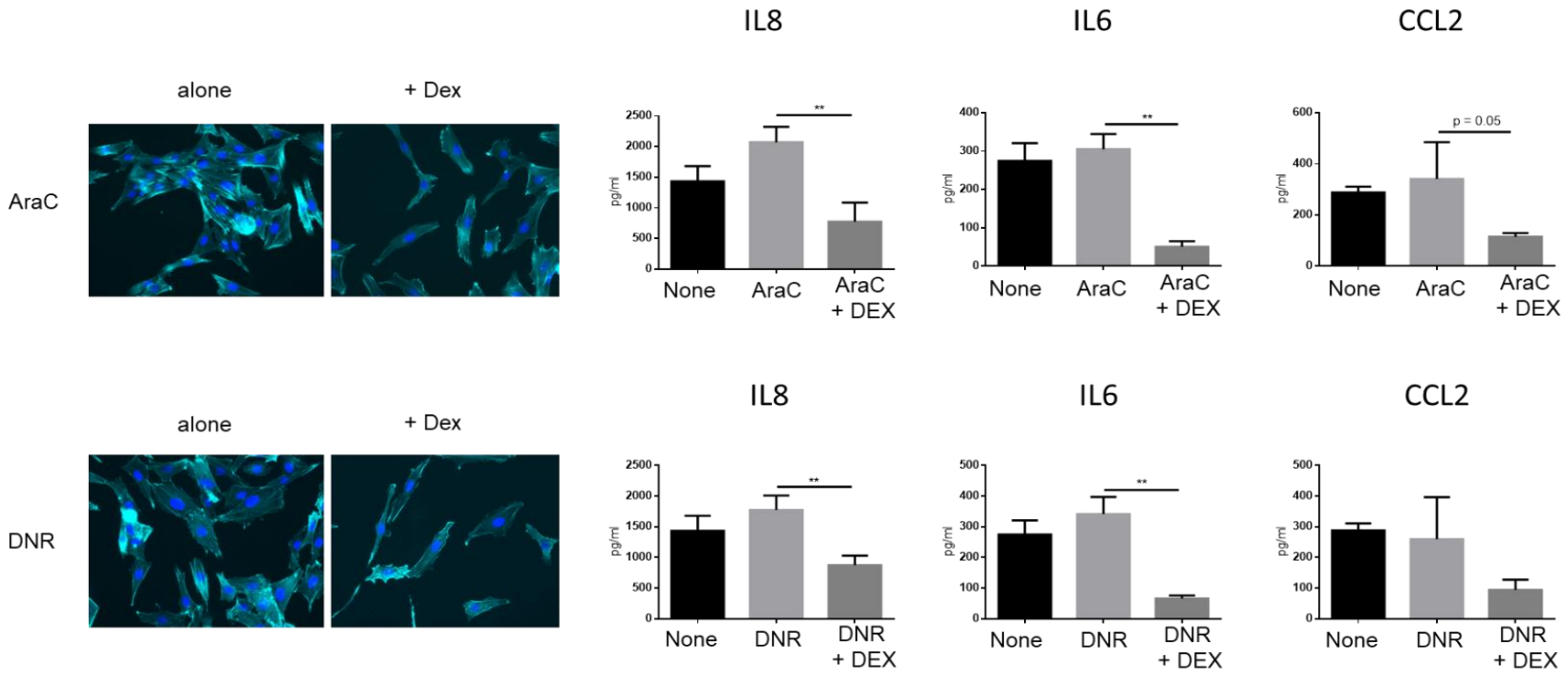

Figure 5-8: Dexamethasone abrogates chemotherapy induced activation of HS27a. (i) 20x Phallodin (cyan)/DAPI (blue) staining of HS27a MSC exposed to DNR or AraC with or without DEX. (ii) Cytokine bead assays for IL6, IL8 and CCL2 (pg/ml, Y axis) following exposure of HS27a to the chemotherapy drugs indicated below with and without DEX compared to an untreated control (None) as indicated on the X axis. Bars show mean +/- SE of 3 independent experiments. All statistically significant comparisons (by unpaired t-test) are as depicted: AraC vs AraC + DEX: IL8 P =0.0049, IL6 P = 0.005, CCL2 P =0.05; DNR vs DNR + DEX: IL8 P = 0.0053, IL6 P = 0.001.

5.3.5 Mesenchymal Stromal Cell Viability Largely Unaffected by Chemotherapy Drugs at Doses used

Given the marked differences in the HS27a phenotype following exposure to different chemotherapy drugs, I then aimed to understand how prior exposure of MSC to the chemotherapy agents might impact subsequent B-ALL response to therapy. Initially I sought to exclude the possibility that the doses of chemotherapy used were impacting on the survival and proliferation of the MSCs. Using the same method that I initially used to establish the appropriate doses of chemotherapy earlier in the chapter, escalating doses of chemotherapy were added to the HS27a cells and MTS assay performed at 24, 48 and 72 hours as demonstrated in ***figure 5-9.*** At the doses previously established for AraC (200nM), VCR (1.6nM) and DEX (200nM) there was no effect on HS27a proliferation at any of the time-points. Unexpectedly, the 8nM established dose of DNR enhanced HS27a proliferation as compared to an untreated control. Given the possibility that the enhanced proliferation of HS27a cells may confound the co-culture experiments DNR was excluded from the subsequent experiments.

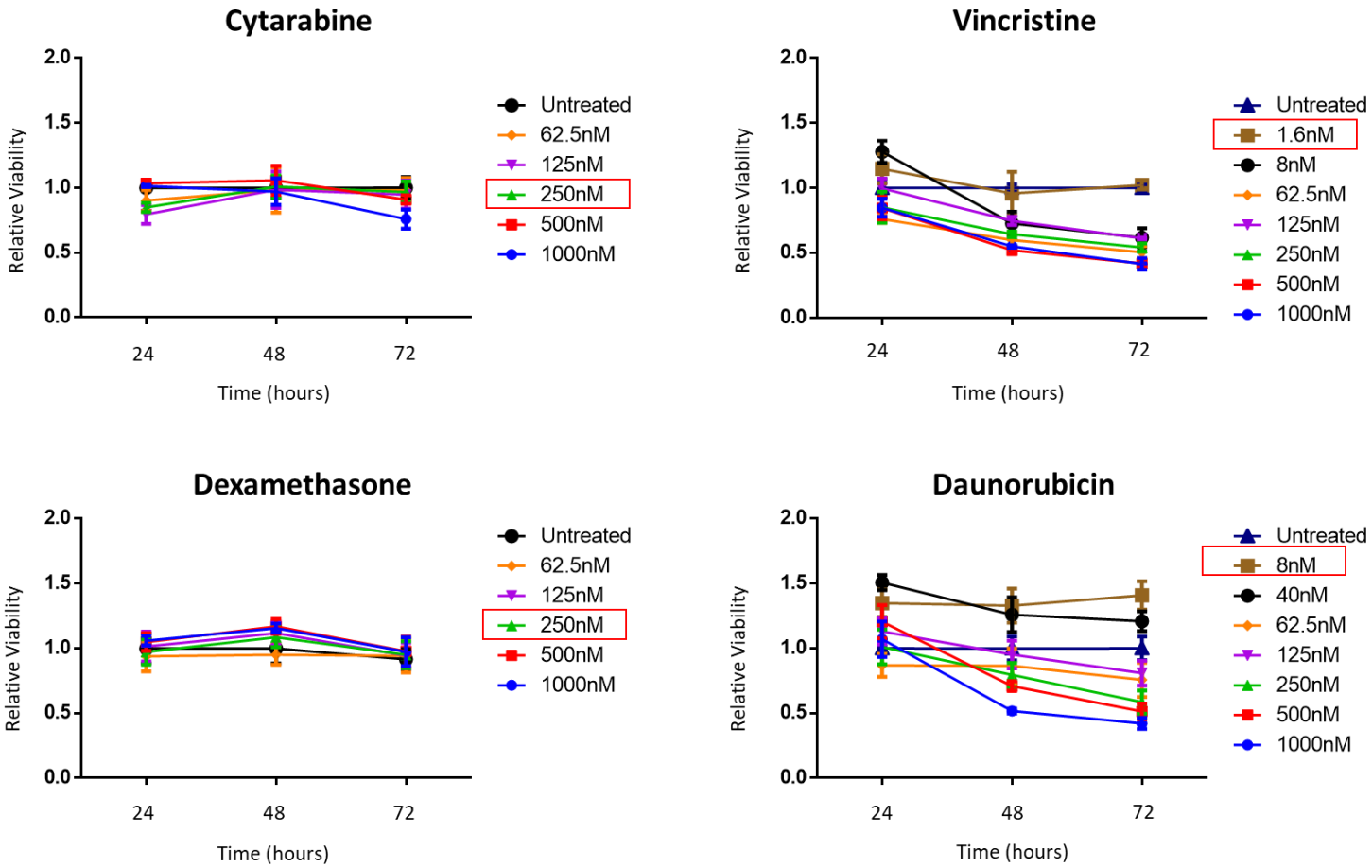

Figure 5-9: HS27a viability following exposure to chemotherapy. MTS assay of MSC cell (HS27a) viability compared to an untreated control (Y axis) following exposure to relevant chemotherapy agent at stated time points (X axis). Bars show mean and standard error of the mean of 3 independent experiments. Concentrations of chemotherapy drugs are colour coded and listed in the key.

5.3.6 Chemotherapy Drugs differentially alter Mesenchymal Stromal Cell Mediated Protection of Acute Lymphoblastic Leukaemia Cells

I then determined the impact of pre-treating MSCs with different chemotherapy drugs on B-ALL cell chemo-sensitivity in co-culture. I initially primed HS27a by exposure to AraC, VCR or DEX for 24 hours. After the chemotherapy agents were washed off, I then quantified the survival of a co-cultured B-ALL cell line SEM (specifically chosen for its low intrinsic ROS levels and known AraC susceptibility) exposed to the same agents.

As shown in ***figure 5-10i-iii***, a clear pattern of reduced response to AraC, DEX or VCR was seen at 48 hours when the MSC were primed with AraC (red arrows) but not with the other agents, thus suggesting that the different effects of the chemotherapy drugs on MSC had functional significance in terms of their ability to protect B-ALL cells from chemotherapy. Importantly, when the experiment was repeated using a transwell set-up (***figure 10iv***) the functional impact of priming of the HS27a with different chemotherapy drugs on protection of B-ALL cells from chemotherapy was not seen, confirming that a contact dependent mechanism was responsible.

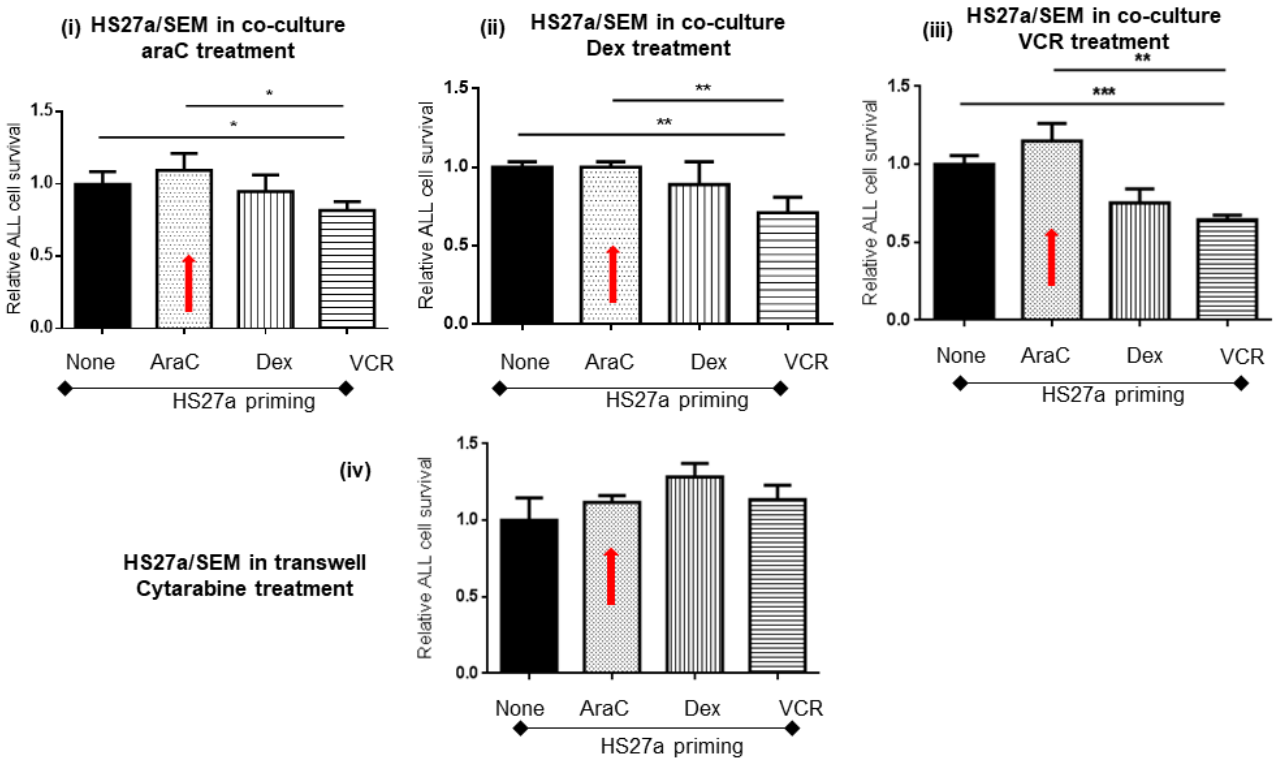

Figure 5-10: Viability of SEM cells in co-culture with differentially pre-primed HS27a. MTS assays showing relative viability of SEM cells (Y axis) after treatment with (i) AraC (ii) DEX (iii) VCR for 48 hours, after co-culture with HS27a cells previously 'primed' by chemotherapy pre-treatment denoted on the X axis. Data are shown relative to unprimed HS27a, set at 1. AraC primed HS27a are highlighted throughout with a red arrow. All statistically significant comparisons (by unpaired t-test) are as depicted: (i) no pre-treatment vs. VCR, P = 0.041, AraC vs. VCR, P = 0.022. (ii) no pre-treatment vs. VCR, P = 0.0087, AraC vs. VCR, P = 0.0087. (iii) no pre-treatment vs. VCR, P = 0.0006, AraC vs. VCR, P = 0.0017 (iv) MTS assay showing relative viability of SEM cells (Y axis) after transwell-culture with primed HS27a cells as denoted on the X axis. Data are relative to unprimed HS27a, set at 1. There are no statistically significant differences. All data are mean +/- SE of 3 independent experiments

To confirm these findings using a different technique, we compared the viability of SEM cells in mono-culture versus co-culture with HS27a post exposure to AraC, VCR and DEX. For analysis I used flow cytometry-based measurement of apoptosis and cell death by annexin V and DAPI respectively (***figure 5-11***). Whilst all three drugs caused significant and similar SEM cell death in mono-culture, as expected, co-culture of SEM ALL with HS27a MSC lowered AraC-driven cell death by two thirds, VCR by about one half but DEX, not at all. These data show that the protection provided by MSC to B-ALL cells is greater with the ROS-inducing chemotherapy agent AraC than the non-ROS inducing drugs VCR and DEX.

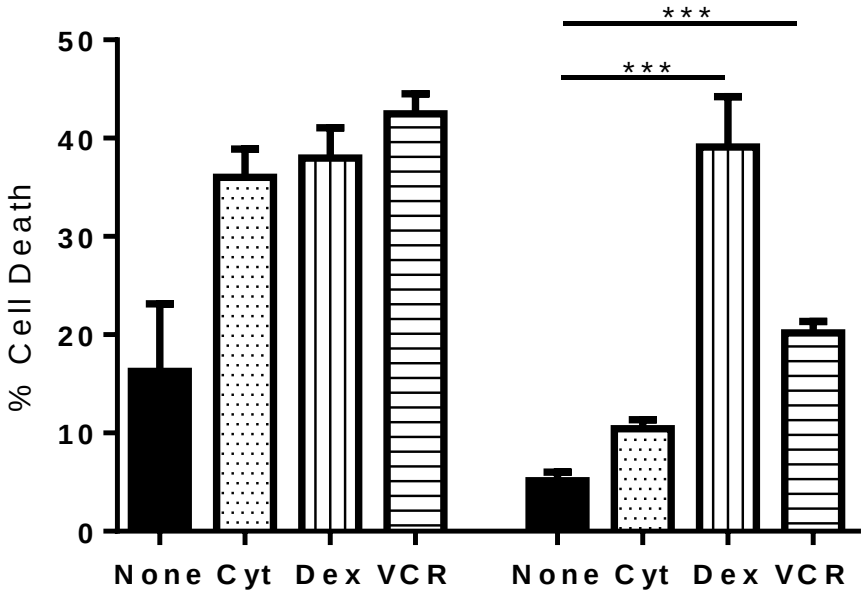

Figure 5-11: Viability of SEM cells in mono-culture versus co-culture with HS27a
Percentage cell death (DAPI+, Y axis) of SEM cells exposed to the chemotherapy agents indicated either in monoculture or during co-culture with HS27a cells, all indicated on the X axis. Bars show mean +/- SE of 3 independent experiments. All statistically significant comparisons (by unpaired t-test) are as depicted: % cell death, HS27a AraC vs. DEX, P = 0.0007, HS27a AraC vs. VCR, P = 0.0003.

5.4 Discussion

I was able to confirm that chemotherapy drugs commonly used in B-ALL treatment can induce the ALL-CAF phenotype in both the MSC cell line HS27a and healthy donor MSC. The ALL-CAF induced by chemotherapy had similar cytomorphology, gene expression profile and enhanced cytokine secretion we had observed in the primary patient specimens and MSC co-culture with the B-ALL cells. Importantly, amongst the chemotherapy drugs used, only the DNA damaging agents, AraC and DNR, induced this MSC phenotype. VCR induced distinct morphological changes, including alteration of the MSC shape and loss of cytoplasmic projections, likely due to its microtubule damaging mechanism of action. DEX induced a markedly different gene expression profile to the DNA damaging agents and notably reduced cytokine secretion by the HS27a.

Importantly, the differential morphological changes in the MSC observed following AraC or VCR exposure, were also seen when MSC were co-cultured with B-ALL cells. These changes occurred regardless of whether the MSC were cultured with a B-ALL cell line ‘CAF-inducer’ or ‘non-CAF inducer’. Interestingly, MSC with ALL-CAF morphology appeared to have enhanced contact with B-ALL cells compared to both the untreated control but especially the VCR treated co-culture, where contact between MSC and ALL cells was reduced.

I was able to inhibit DNR and AraC-induced activation of HS27a by the addition of the ROS scavenger, NAC, consistent with the B-ALL cell findings that the induction of the ALL-CAF phenotype was ROS dependent. Furthermore, DEX, a potent anti-inflammatory agent which reduced ROS in target cells, also abrogated induction of the ALL-CAF phenotype. This provides a potential explanation for the differences we observed in the MSC isolated from patients at different stages of treatment. In phase I, the ROS inducing agent DNR is given with DEX and the majority of the MSC isolated did not display an activated phenotype or enhanced cytokine or chemokine secretion. In phase II, the ROS inducing agent AraC is given without any DEX or alternative corticosteroid and in contrast to phase I, we isolated ALL-CAF from most specimens with an enhanced cytokine and chemokine secretion profile.

Importantly, the differing effects of the chemotherapy drugs on MSC, had functional significance. ALL cells on HS27a cells pre-treated with AraC, were able to proliferate and survive chemotherapy more readily than ALL cells on HS27a pre-treated with either DEX or VCR. Interestingly, this is consistent with recent findings in Acute Myeloid Leukaemia where enhanced leukaemia cell killing following addition of steroids to AraC or DNR in vitro is only observed when MSC are present (ref), suggesting that DEX is having a detrimental effect on MSC mediated protection of leukaemia cells.

Finally, the differential effect on ALL cell proliferation and chemoresistance following MSC pre-treatment with different chemotherapy drugs, is lost if MSC and ALL cells are separated by a transwell. This suggests that a contact dependent mechanism is responsible for the differences observed and contrasts with data from solid organ malignancy[148] where enhanced cytokine secretion by stromal cells after chemotherapy aided cancer cell proliferation and chemo-resistance. Notably, in this work, the secretion of "ELR+ motif " cytokines/chemokines - which include IL8/CXCL1/CXCL2 (observed in the primary specimens), was determined to aid cancer cell proliferation and chemotherapy resistance via binding to their cognate receptors on the tumour cells. ALL cells have limited expression of the relevant receptors, CXCR1 and CXCR2[170], and therefore the tumour cells may be unable to derive the same benefits observed in solid organ malignancy.

I also demonstrated that, although AraC, VCR and DEX have similar anti- ALL properties at the selected doses in mono-culture, their impact in co-culture with MSC differs. MSC clearly provided enhanced protection against AraC for the ALL cells as compared to VCR or DEX.

This is in keeping with the work of Gerby et al[171] in which pre-leukaemic T-ALL 'stem cells' were cultured in a niche-like environment with MSC and then tested for sensitivity against 1904 FDA approved compounds. The pre-leukaemic cells were sensitive to less than 5% of the compounds tested, which was defined by greater than

50% pre-leukaemic cell death. Notably, the pre-leukaemic stem cells were uniformly sensitive to all 14 microtubule damaging drugs and 15 corticosteroids tested, in contrast to their resistance to the large majority of the other 1904 compounds tested. The authors then attempted to demonstrate specificity of the effective compounds for T-ALL by repeating the experiments using primary AML cells with MSC. However somewhat surprisingly, in the niche model the AML cells were equally sensitive to microtubule damaging drugs and corticosteroids, agents which are not used routinely in the treatment of AML. The reasons for these findings was not clear at the time of publication of this paper, but the data from my work suggest an explanation – that the effectiveness of these agents is also due in part to their effect on stromal cells.

Further evidence that DEX may perturb the protective leukaemic MSC niche is provided by a recent paper by Bertoli et al[172]. In a clinical trial the authors demonstrated the unexpected benefit of dexamethasone given with induction chemotherapy in AML in reducing the risk of relapse and improving long-term disease free survival. The authors' subsequent *in vitro* work to explain the benefit of DEX revealed that the addition of DEX to DNR or AraC did not enhance AML cell killing in mono-culture but did significantly enhance AML cell death in co-culture with MSC. Thus suggesting that the benefit of DEX is due to an effect on MSC mediated protection of leukaemic cells rather than a direct effect on the leukaemic cells. Thus the work by Gerby et al in T-ALL and Bertoli et al in AML is consistent with my findings in B-ALL, suggesting that the differing effects of chemotherapy on the stromal niche

may not be a disease specific phenomenon but may be relevant to other bone marrow based malignancies such as T-ALL and AML.

In the next chapter, I sought to elucidate the contact dependent mechanism responsible for the chemo-protective effect of ALL-CAF on B-ALL cells.

Chapter 6: Mesenchymal Stromal Cells Transfer Mitochondria to B-ALL cells to Rescue them from Oxidative Stress

6.1 Background

The essential role of MSC and fibroblasts in wound healing has long been recognised and more recently this has been extended to the findings of several groups that MSC can rescue cells under oxidative stress[111,112]. The rescue mechanisms described include uptake of ROS, secretion of antioxidants and transfer of mitochondria from MSC to the cell under oxidative stress[71,72,74]. Several groups have demonstrated that mitochondria transfer occurs via tunnelling nanotubes (TNT), which are open ended actin and/or microtubule containing membrane connections between cells.

Mitochondrial transfer has been demonstrated in a diverse range of disease models including acute myeloid leukaemia[107,108], multiple myeloma[173], healthy haematopoietic stem cell nice[74], acute lung injury[112], cardiac ischaemia[113] and retinal ischaemia[111], suggesting that this is a conserved function of MSC across different organ systems. It appears especially pertinent in the haematopoietic stem cell niche where MSC are

known to tightly control ROS in haematopoietic stem cells to maintain them in a quiescent state[74].

Recently, Marlein et al demonstrated that the transfer of mitochondria from MSC to leukaemic cells is driven by ROS production from NADPH Oxidase 2 (NOX2) in the leukaemic cell[173]. Rustom, the author who provided the original description of TNT[97], suggested recently that the role of TNT is likely to be, at least in part, a rescue mechanism for cells under oxidative stress[106]. TNT have been described in B-ALL[80] between MSC and B-ALL cells, their presence being associated with enhanced cytokine/chemokine secretion and resistance to treatment. However mitochondrial transfer in B-ALL has never been described.

6.2 Aims

1. To explore the mechanism by which ALL-CAF protect ALL cells from chemotherapy induced oxidative stress, focusing on the role of tunnelling nanotubes and mitochondrial transfer
2. To use a disseminated murine model of B-ALL to demonstrate that ALL-CAF induction, mitochondrial transfer and niche formation occur *in vivo* and is dependent on the chemotherapy drug used

6.3 Results

6.3.1 Mesenchymal Stromal Cells Lower Reactive Oxygen Species and Protect Acute Lymphoblastic Leukaemia Cells from Cytarabine

Given that ALL-CAF were induced by exposure to increasing ROS levels, I hypothesised that activated MSC or ALL-CAF may be a necessary adaption to control ROS, including in B-ALL cells in co-culture. I initially investigated this by quantifying intracellular ROS, apoptosis and cell death of SEM ALL cells after AraC therapy, either alone or in co-culture with HS27a MSC.

The measurement of intracellular ROS in the B-ALL cells was achieved by use of CellROX™ Green which is a fluorogenic probe which exhibits bright green photostable fluorescence upon oxidation by ROS and binding to DNA with absorption/emission maxima of 485/520nm. Thus, allowing measurement of the mean fluorescence intensity (MFI) in this channel by flow cytometry in the CD19+ population (SEM ALL cells) as shown in the representative example in ***figure* 6-*1***. Apoptosis and cell death were assessed by annexin V and DAPI positivity in the CD19 positive population (SEM ALL cells), also by flow cytometry (***figure 6-2***).

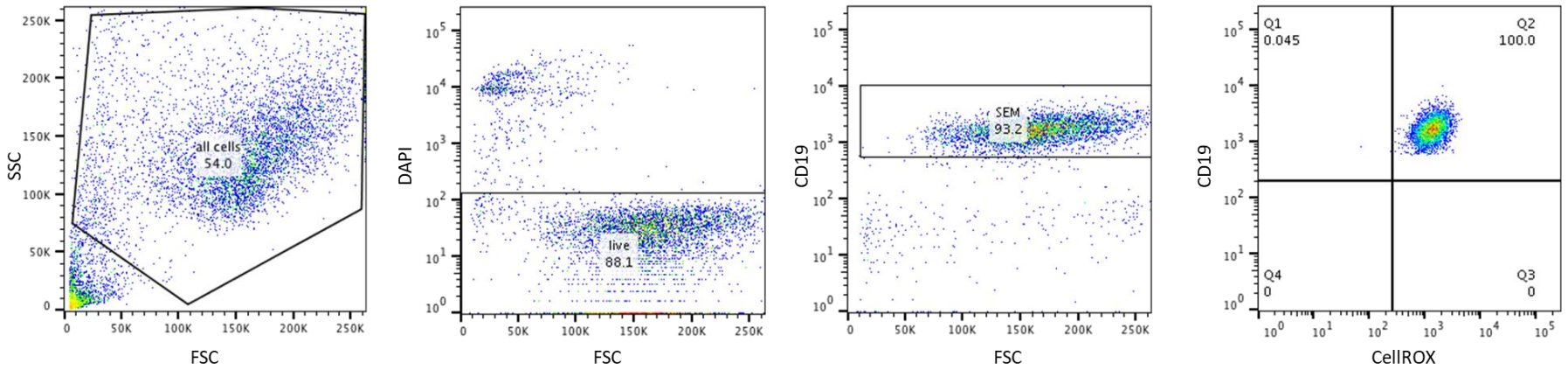

Figure 6-1: Gating Strategy for measurement of intracellular ROS. The flow cytometry dot plots demonstrate the gating strategy for measuring the MFI of Cell ROX© in ALL (SEM) cells. ALL cells are identified according to FSC and SSC, their viability by DAPI and finally by their CD19 expression.

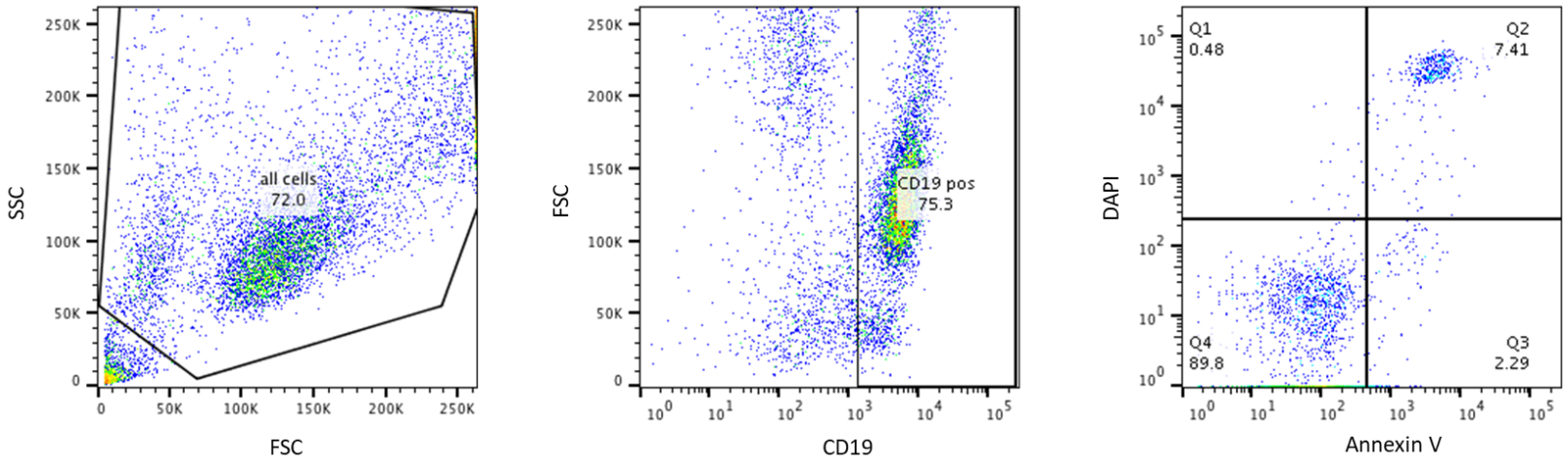

Figure 6-2: Gating Strategy for measurement of apoptosis and cell death. The flow cytometry dot plots demonstrate the gating strategy for identifying the percentage of apoptotic and dead ALL (SEM) cells. ALL cells are initially gated according to FSC and SSC and their CD19 expression. DAPI and annexin V are then used to measure cell death (annexin V +/DAPI +) and apoptosis (annexin V+/DAPI-).

Figure 6-3 (i) shows that as expected AraC significantly increased ROS in SEM cells in monoculture. However ROS levels in the SEM cells were significantly lowered in co-culture with HS27a and remained lower than baseline following the addition of AraC (conditions in which we had previously demonstrated induction of ALL-CAF). Thus confirming HS27a were indeed lowering ROS in ALL cells, including in the presence of AraC.

The corresponding graphs ***Figure 6-3 (ii,iii)*** show SEM cell apoptosis and death in mono-culture and co-culture with MSC. Importantly the MSC-mediated control of ALL cell ROS corresponded to a significant reduction in AraC-mediated SEM cell apoptosis and cell death. ***Figure 6-3 (iv)*** shows that cell-cell contact was critical for this effect – the 'chemo-protection' of SEM by HS27a was completely lost if the two cell populations were not in direct contact. Therefore, MSC in my co-culture model were reducing ROS in the B-ALL cells, in conditions where I had demonstrated the induction of ALL-CAF, and this corresponded to a reduction in SEM (ALL) cell death.

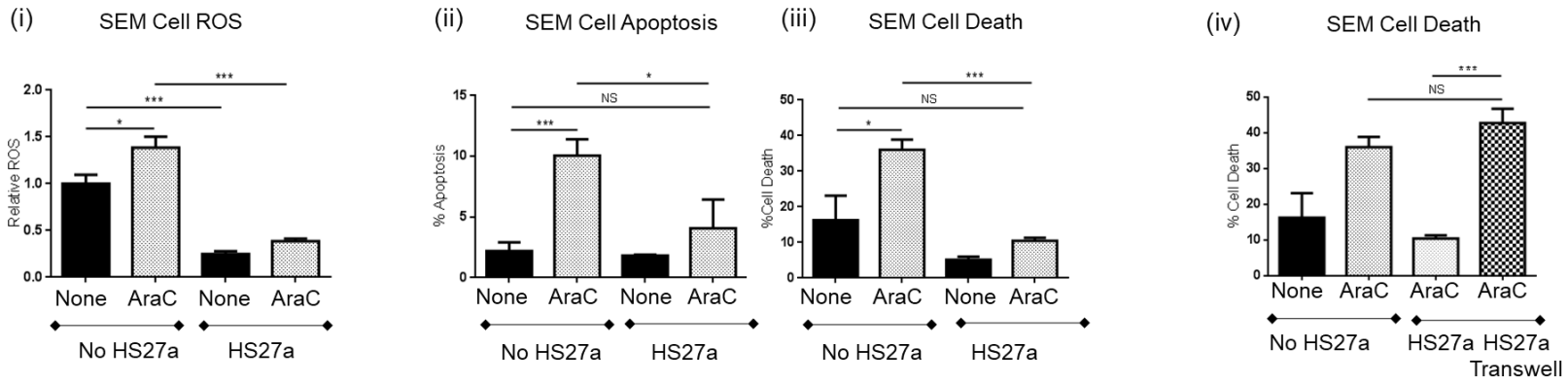

Figure 6-3: HS27a reduce ROS in SEM cells and protect them from cell death via a contact dependent mechanism. (i) CellROX® ROS assay showing mitochondrial mass (Y axis) of SEM cells in monoculture, baseline set at 1.0 or after co-culture with HS27a cells +/-AraC (X axis). Statistically significant comparisons (by unpaired t-test) are as depicted: No HS27a none vs. AraC, P = 0.0115, No HS27a none vs. HS27a none, P = 0.0002, No HS27a AraC vs. HS27a AraC, p = 0.0001. (ii) % apoptosis (annexinV+, DAPI-, Y axis) of SEM cells in monoculture, baseline set at 1.0 or after co-culture with HS27a cells +/- AraC (X axis). All statistically significant comparisons (by unpaired t-test) are as depicted: No HS27a none vs. AraC, p = 0.0009, No HS27a AraC vs. HS27a AraC, p = 0.0189. (iii) Cell death (DAPI+, Y axis) of SEM cells in monoculture, baseline set at 1.0 or after co-culture with HS27a cells +/- AraC. All statistically significant comparisons (by unpaired t-test) are as depicted: No HS27a none vs. AraC, P = 0.0102, no HS27a AraC vs. HS27a AraC, P = 0.0001. (iv) Cell death (DAPI+, Y axis) of SEM cells in monoculture +/- AraC compared with SEM co-cultured in contact with HS27a cells or in a transwell, both with AraC (X axis). All statistically significant comparisons (by unpaired t-test) are as depicted: HS27a AraC vs HS27a transwell AraC, P = 0.0002.

I next sought to confirm that the increase in ROS induced by AraC in SEM cells in monoculture was important in its cytotoxic effect and that the reduction in ROS was relevant in the MSC protection provided to the ALL cells. To investigate this I used the ROS scavenger, N-acetylcysteine (NAC), to block AraC induced ROS induction in the SEM cells in mono-culture and measured intracellular ROS in the SEM cells via flow cytometry. ***Figure 6-4 (i)*** shows that as expected the addition of AraC to SEM cell increased the intracellular ROS but this effect could be ameliorated with NAC. Importantly the addition of NAC corresponded to a significant reduction in AraC induced apoptosis and a small but non-significant reduction in cell death (***figure 6-4 (ii),(iii)***). Thus confirming that AraC cytotoxicity was at least in part due to ROS induction and that MSC induced reduction in ROS was likely important in ALL cell protection from AraC.

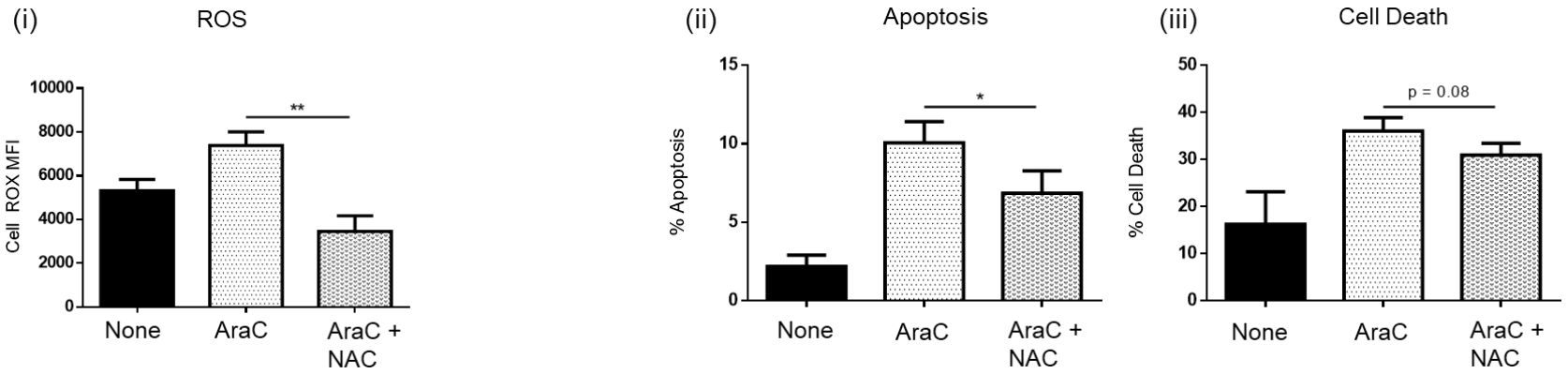

Figure 6-4: NAC rescues ALL cells from cytarabine induced apoptosis. (i)ROS levels, (ii) apoptosis and (iii) cell death (Y axis) with no treatment, AraC treatment or AraC treatment + NAC (X axis). Bars show mean +/- SE of 3 independent experiments**.** Significant reductions in ROS (p= 0.002), and apoptosis (p= 0.0479), and a non-significant reduction in cell death ((p = 0.08) by unpaired t-test are shown

6.3.2 Mesenchymal Stromal Cells Transfer Mitochondria to Acute Lymphoblastic Leukaemia Cells

Next, I investigated the mechanism for the ROS-induced, contact dependent, MSC-mediated chemo-protection of ALL cells. I hypothesised that mitochondrial transfer between activated MSC and B-ALL cells, via tunnelling nanotubes (TNT), could explain the ALL-CAF-mediated protection of ALL cells from ROS-inducing chemotherapy. I based this hypothesis on the evidence discussed in the background, that mitochondrial transfer from MSC to cells under oxidative stress have been demonstrated in a number of different disease models, including cancer models.

First, to investigate this, I used a MitoTracker™ assay in which a fluorescent dye irreversibly labels mitochondria, to quantitate mitochondrial transfer from MSC to B-ALL cell. MSC were initially labelled with the Mitotracker™ Deep Red dye and following repeated and prolonged washing to prevent passive transfer of the dye, co-cultured with B-ALL cells. The uptake of the MitoTracker™ Deep Red dye in the B-ALL cells was then measured by flow cytometry and the mean fluorescence intensity calculated in the CD19+ population (ALL cells) as shown in the representative example in ***Figure 6-5***.

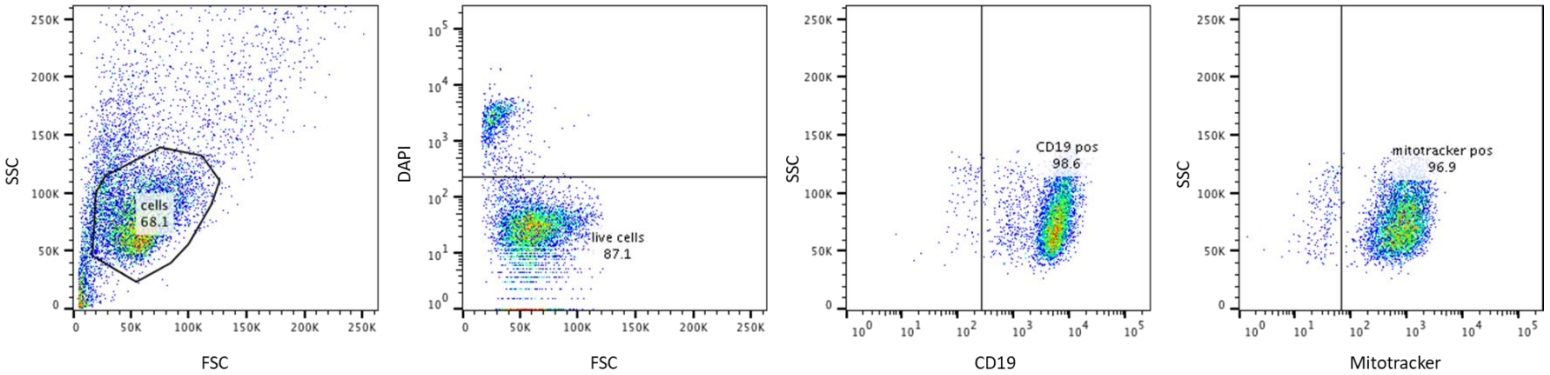

Figure 6-5: Gating Strategy for measurement of MitoTracker™ uptake in ALL cells. The flow cytometry dot plots demonstrate the gating strategy for measuring the MFI of the MitoTracker™ dye in ALL (SEM) cells. ALL cells are gated according to FSC and SSC, their viability by DAPI and finally by their CD19 expression.

Figure 6-6 (i) shows that mitochondrial transfer to B-ALL cells occurred after HS27a cells were co-cultured with 2 different B-ALL cell lines (SEM and SD1). Cell-cell contact was obligatory, as the transfer was abolished by transwell. This also excludes the possibility that the dye transfer was passive and not representative of true mitochondria transfer.

I suspected the mitochondrial transfer was a ROS-driven phenomenon based on my own findings and data from the literature[108]. To initially investigate this, I used the MitoTracker™ flow cytometry based assay to compare mitochondrial transfer from MSC to the 5 ALL cell lines used in Chapter 4, in which we had previously measured intracellular ROS levels.

In ***Figure 6-6 (ii)***, the B-ALL cell lines are placed in order from left to right of lowest (SEM) to highest (SD1) baseline intracellular ROS, relative to healthy donor B-cells (previously shown in chapter 4). The figure shows that mitochondrial transfer from MSC to B-ALL cells occurs in the ALL cell lines in proportion to baseline ROS with the exception of TOM1. The transfer is greater to all the B-ALL cell lines tested than to healthy donor B-cells.

In order to confirm mitochondrial transfer also occurred to primary ALL specimens, the experiment was repeated using patient ALL cells with normal B cells as a control and healthy donor MSC as the potential mitochondrial donors. In ***figure 6-6 (iii)***

mitochondrial transfer from MSC is shown to all 3 primary ALL cell samples tested by the presence of an increased deep red MitoTracker™ MFI as compared to healthy donor B-cells. Notably, two of the three primary B-ALL specimens selected (14-1-475, 14-1-525) were from patient samples in which I isolated ALL-CAF in chapter 3.

To provide further evidence that the mitochondrial transfer was related to elevated ROS levels and induction of the ALL-CAF phenotype, I compared mitochondrial transfer after ROS-inducing chemotherapy known to induce ALL-CAF, AraC with the non ROS – inducing chemotherapies, VCR and DEX. As predicted ***Figure 6-6 (iv)*** shows that AraC, but not VCR or DEX, stimulated the mitochondrial transfer to SEM ALL cells. Thus strongly suggesting that ROS induction was indeed important in induction of mitochondrial transfer, in keeping with previous findings in other disease models.

I then sought to confirm that by lowering ROS, either through the use of the ROS scavenger NAC or the corticosteroid DEX, that I could reduce mitochondrial transfer from MSC to ALL cell following ROS inducing chemotherapy. As anticipated ***figure 6-6 (v,vi)*** show that the ROS scavenger NAC, which I had previously shown inhibited ALL-CAF induction, significantly abrogated both AraC and DNR-stimulated mitochondrial transfer to SEM ALL cells. Likewise, the addition of DEX ***(figure 6-6 vii)***, which lowers ROS in ALL cells and also abrogates the ALL-CAF phenotype, significantly reduced the AraC-stimulated mitochondria transfer to SEM ALL cells.

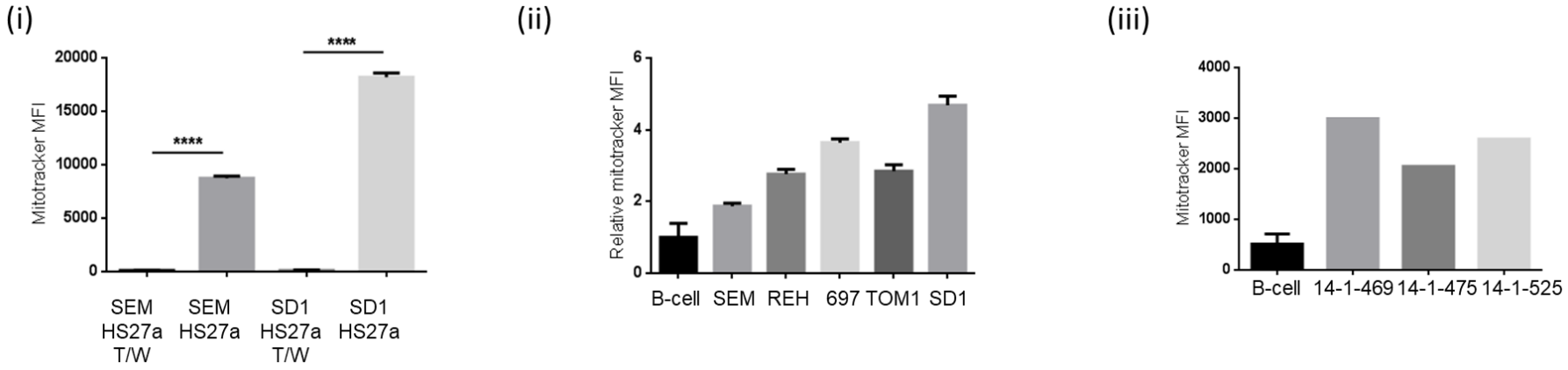

Figure 6-6: Mitochondrial transfer from MSC to ALL occurs in vitro relative to ROS level of ALL cell. (i) Mitochondrial transfer by MitoTracker™ assay (MFI, Y axis), from HS27a to SEM and SD1 ALL cells in contact or in transwell (X axis). All data are mean +/- SE of 3 independent experiments. All statistically significant comparisons (by unpaired t-test) are as depicted: SEM HS27a versus HS27a transwell, $P < 0.0001$, SD1 HS27a versus transwell, $P < 0.0001$. (ii) Mitochondrial transfer by MitoTracker™ assay (MFI, Y axis), from HS27a MSC to healthy donor B-cells or SEM, REH, 697, TOM1 and SD1 B-ALL cell lines (X axis) (3 independent experiments) (iii) Mitochondrial transfer by MitoTracker™ assay (MFI, Y axis), from healthy donor MSC to healthy donor B-cells (3 independent experiments) or patient ALL cells identified by UKALL14 trial number (UPN) (X axis).

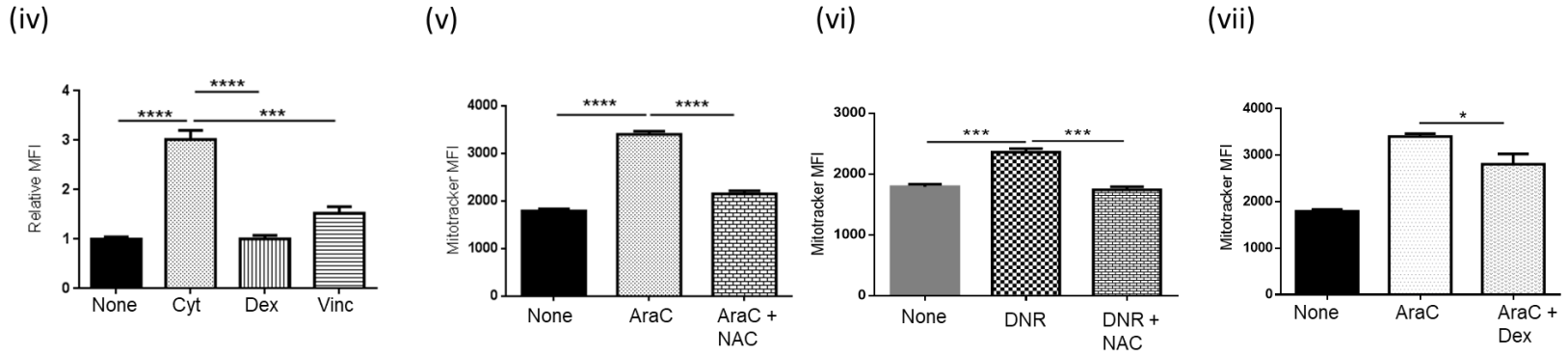

Figure 6-6: Mitochondrial transfer from MSC to ALL occurs in vitro relative to ROS level of ALL cell continued from previous page. (iv) Mitochondrial transfer by MitoTracker™ assay (MFI, Y axis) from HS27a to SEM after co-culture and either no treatment or treatment with AraC, VCR or DEX. All statistically significant comparisons (by unpaired t-test) are as depicted: no treatment vs. AraC, $P < 0.0001$, AraC vs. DEX, $P < 0.0001$, AraC vs. VCR, $P = 0.0003$. (v) Mitochondrial transfer by MitoTracker™ assay (MFI, Y axis) of SEM cells in co-culture with HS27a MSC after no treatment, AraC treatment or AraC plus NAC 5mM. All statistically significant comparisons (by unpaired t-test) are as depicted: no treatment vs. AraC treatment, $P < 0.0001$, AraC treatment vs AraC plus NAC, $P < 0.0001$. (vi) Mitochondrial mass by mitotracker assay (MFI, Y axis) of SEM cells in co-culture with HS27a MSC after no treatment, DNR treatment or DNR plus NAC 5mM. All statistically significant comparisons (by unpaired t-test) are as depicted: no treatment vs DNR treatment, $P = 0.0002$, DNR treatment vs DNR + NAC, $P = 0.0002$ (vi) Mitochondrial mass by MitoTracker™ assay of REH cells in co-culture with HS27a MSC after no treatment, AraC treatment or AraC plus NAC 5mM. All statistically significant comparisons (by unpaired t-test) are as depicted: no treatment vs AraC treatment, $P < 0.0001$, AraC treatment vs AraC + NAC, $P < 0.0001$. (vii) Mitochondrial transfer by MitoTracker™ assay (MFI, Y axis) of SEM cells in co-culture with HS27a MSC after no treatment, AraC treatment or AraC plus DEX. All statistically significant comparisons (by unpaired t-test) are as depicted: AraC treatment vs AraC plus DEX, $P = 0.0111$.

Therefore in summary, I had confirmed that MSC can transfer mitochondria to B-ALL *cells in vitro* via a contact dependent mechanism, relative to the intrinsic ROS level of the B-ALL cell. The transfer is enhanced by ROS inducing chemotherapy such as AraC and DNR and abrogated by NAC and DEX.

Next, to completely exclude the possibility of passive transfer of dye rather than actual mitochondria, I used the murine stromal line MS5 as an alternative mitochondria donor. If mitochondrial transfer was truly occurring from murine MSC (MS5) to human ALL cell (SEM) I anticipated that murine mitochondrial DNA but not murine nuclear DNA would be present when SEM ALL cells were flow-sorted from the co-culture. I therefore co-cultured MS5 with SEM cells, with and without AraC for 72 hours, and then sorted the human CD19+ population (SEM). In ***figure 6-7***, murine mitochondrial, but not nuclear, DNA is clearly seen in flow-sorted SEM cells after co-culture, occurring at baseline and with a clear increase after AraC treatment. Taken together, these data confirm mitochondrial transfer is occurring *in vitro* from MSC to ALL cell.

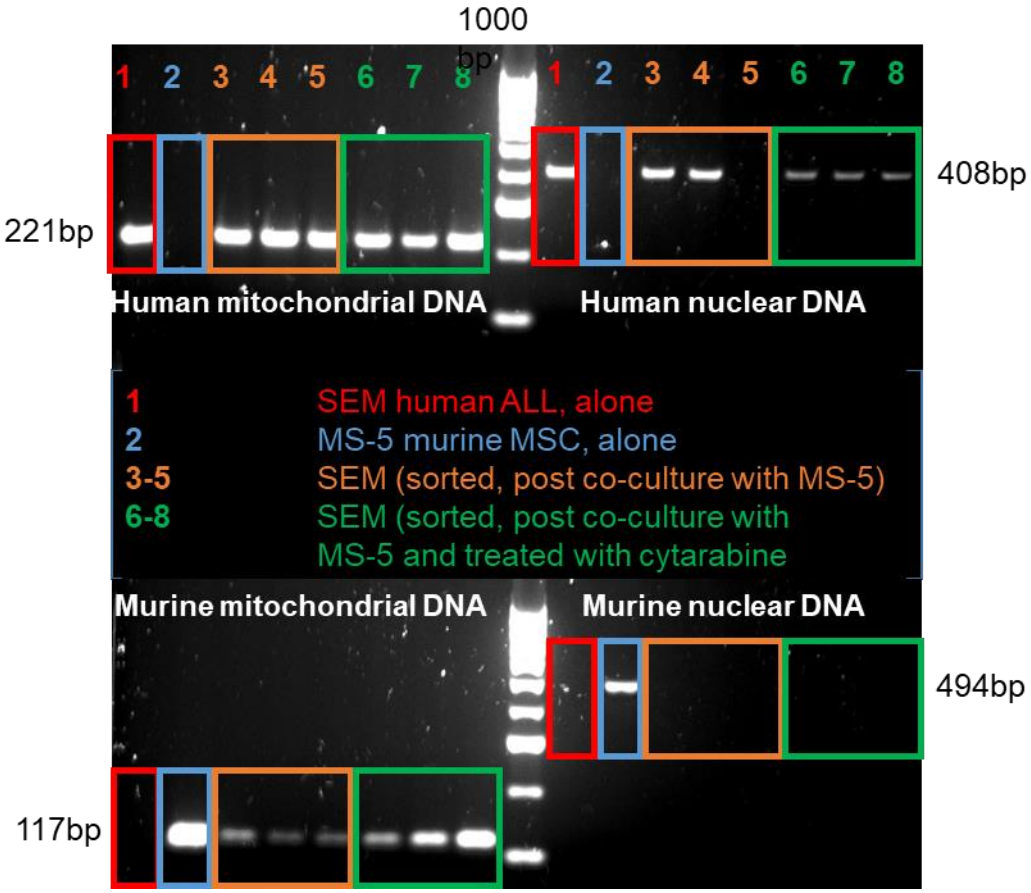

Figure 6-7: Murine mitochondrial DNA present in human ALL cells following co-culture with murine MSC. Agarose gel images showing PCR products from human nuclear and mitochondrial DNA and murine nuclear and mitochondrial DNA, as indicated in each quadrant. Lane 1, MS-5 murine MSC, Lane 2 SEM cells, Lanes 3-5 SEM cells sorted after co-culture with MS-5, Lanes 6-8 SEM cells sorted after cytarabine-treated co-culture with MS-5. Human nuclear DNA PCR in lane 5 failed.

6.3.3 Mitochondria are Transferred via Tunnelling Nanotubes from Mesenchymal Stromal Cell to Acute Lymphoblastic Leukaemia Cell

Next, I sought to determine the mechanism of mitochondrial transfer using confocal time lapse imaging of HS27a in co-culture with SEM ALL cells. Given my findings that the mitochondrial transfer occurred via a contact dependent mechanism and the previously discussed literature on mitochondrial transfer, I predicted that transfer occurred via tunnelling nanotubes (TNT). I used time lapse confocal imaging as this technique is widely described in the literature for identification of TNT[97,102,108] and given the dynamic state of the cellular connections and relative frailty of TNT I suspected they would be damaged with fixing of the cells.

Figure 6-8 shows direct images of the transfer of mitochondria along tunnelling nanotubes. In the images, HS27a cells are initially stained with a deep red MitoTracker™ dye and SEM ALL cells are stained with DiO, a green membrane dye. Immediately prior to imaging, the SEM ALL cells were added with AraC to the HS27a. The arrows in ***figure 6-8*** indicate the progress of two individual mitochondria over 24 minutes, travelling along the TNT from the MSC at the bottom of each image to the ALL cell. I observed ongoing mitochondrial transfer from MSC to ALL cell throughout the entire period of imaging (up to 8 hours). TNT were visualised projecting from both HS27a and ALL cell, although as in the images displayed, they were more frequent from the ALL cell. Therefore I had confirmed that mitochondrial transferring was occurring from MSC to ALL cell via TNT.

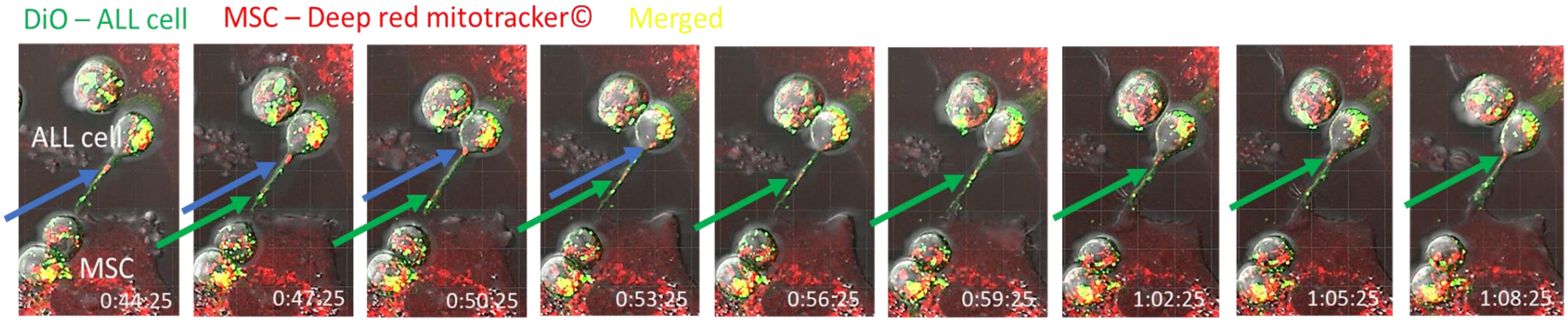

Figure 6-8: Confocal time lapse imaging of mitochondrial transfer from MSC to ALL cell. Live cell confocal imaging of HS27a, stained with deep red MitoTracker™ cells in co-culture with SEM ALL cells stained with DiO. Images were taken at the time points indicated (3 minutes apart). The blue and green arrows each indicate the progression of two individual mitochondria along a tunneling nanotube

6.3.4 Inhibition of Mitochondrial Transfer Overcomes Mesenchymal Stromal Cell Mediated Resistance

I then sought to confirm the functional relevance of mitochondrial transfer by studying the extent to which inhibition of mitochondrial transfer could impact the ability of MSC/ALL-CAF to protect ALL cells. First, I generated HS27a cells deficient in mitochondria following prolonged culture with low dose ethidium bromide, uridine and sodium pyruvate, a technique which selectively depletes mitochondrial DNA[166]. Mitochondrial depletion was confirmed as shown in ***Figure 6-9*** panels ***(i)*** and ***(ii)***, by PCR for mitochondrial DNA and MitoTracker™ deep red imaging in depleted cells and non-depleted controls. The mitochondria-depleted HS27a retained viability as measured by both trypan blue counting and cell death/apoptosis assay (not shown), became activated and retained capability to interact with SEM cells as imaged in ***figure 6-9 (iii)***. However, the mitochondria-depleted HS27a cells were clearly defective in their ability to rescue SEM ALL cells from AraC-induced apoptosis and cell death (***figure 6-9 iv – vi***). Thus confirming the essential role of mitochondria in the MSC rescue of ALL cells.

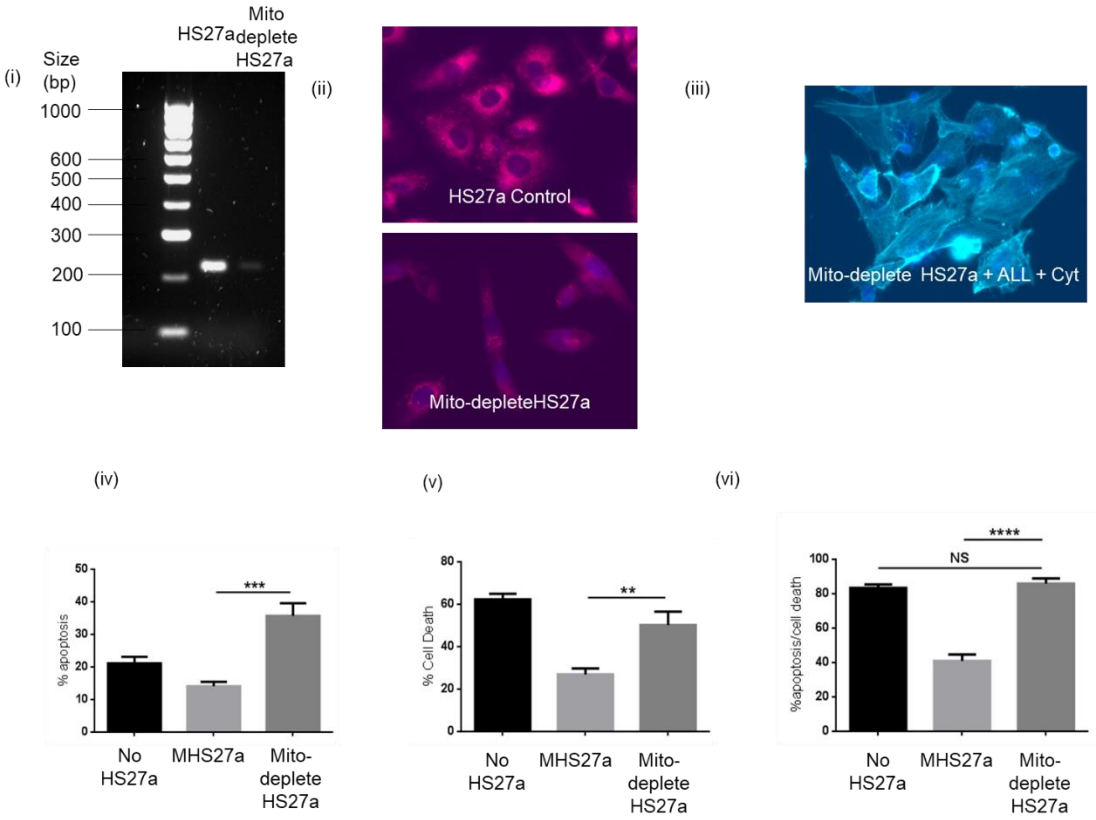

Figure 6-9: HS27a deficient in mitochondria unable to rescue ALL cells. (i) Agarose gel with PCR products from amplification of HS27a mitochondrial DNA, +/- mitochondrial depletion. (ii) Fluorescent microscopy imaging after MitoTracker™ dye in HS27a +/- mitochondrial depletion. (iii) 40X imaging of mitochondrially-depleted HS27a cells in culture with SEM cells after phalloidin and DAPI staining. (iv) % apoptosis (annexinV+, DAPI-, Y axis) of SEM cells treated with AraC, SEM cells co-cultured with HS27a treated with AraC or SEM co-cultured with HS27a mito-depleted cells treated with AraC, (X axis). All statistically significant comparisons (by unpaired t-test) are as depicted: HS27a versus Mito-deplete HS27a, P = 0.0008. (v) Percentage cell death (DAPI+, Y axis) of SEM cells treated with AraC, SEM cells co-cultured with HS27a treated with AraC, or SEM co-cultured with HS27a mito-depleted cells treated with AraC (X axis). All statistically significant comparisons (by unpaired t-test) are as depicted: MH27a versus Mito-deplete HS27a, P = 0.0043. (vi) Percentage cell death or apoptosis (DAPI+ or annexinV+/DAPI- Y axis) of SEM cells + AraC, SEM cells co-cultured with HS27a + AraC or SEM co-cultured with mito-depleted HS27a + AraC, (X axis). All data are mean +/- SE from 3 independent experiments. All statistically significant comparisons (by unpaired t-test) are as depicted: MH27a versus Mito-deplete HS27a, P < 0.0001.

Next, I explored if various microtubule damaging agents and an actin polymerisation inhibitor could inhibit TNT formation and therefore block mitochondrial transfer. Several authors have previously demonstrated that TNT are composed of actin and or microtubule[102,106], with Wang et al[102] demonstrating that microtubule is essential in TNT that transfer mitochondria. Furthermore, microtubule containing TNT were noted to be broader, more stable and last longer. Hence, I predominantly focused on microtubule damaging agents.

VCR is a known microtubule inhibitor. I also selected the microtubule inhibitors colchicine (COL) and nocodazole (NOC), which are not used as chemotherapeutic agents and I therefore predicted would be less likely to be directly toxic to MSC or B-ALL cells, enabling direct inhibition of TNT without compromising the viability of either cell population.

I first confirmed in ***Figure 6-10i + ii***, that as predicted at the doses used, neither COL (1.6nM) nor NOC (10nM) had any impact on HS27a or SEM ALL cell viability. VCR (1.6nM) as expected and previously demonstrated in chapter 5, reduced the viability of SEM ALL cells but had no impact on HS27a viability.

I had previously demonstrated in chapter 5 that MSC exposed to VCR underwent distinct morphological changes, which included rounding up of the cells and a reduction in membrane projections. I sought to confirm that the other microtubule

damaging drugs NOC and COL would induce the same morphological changes in HS27a as VCR. ***Figure 6-10 (iii)*** confirms that NOC and COL induce the same morphological changes as VCR including a clear diminution of visible connections between cells despite the previously demonstrated lack of impact on HS27a viability. This supported the notion that these microtubule damaging drugs, as demonstrated by other authors, would be able to inhibit TNT formation and therefore prevent mitochondrial transfer.

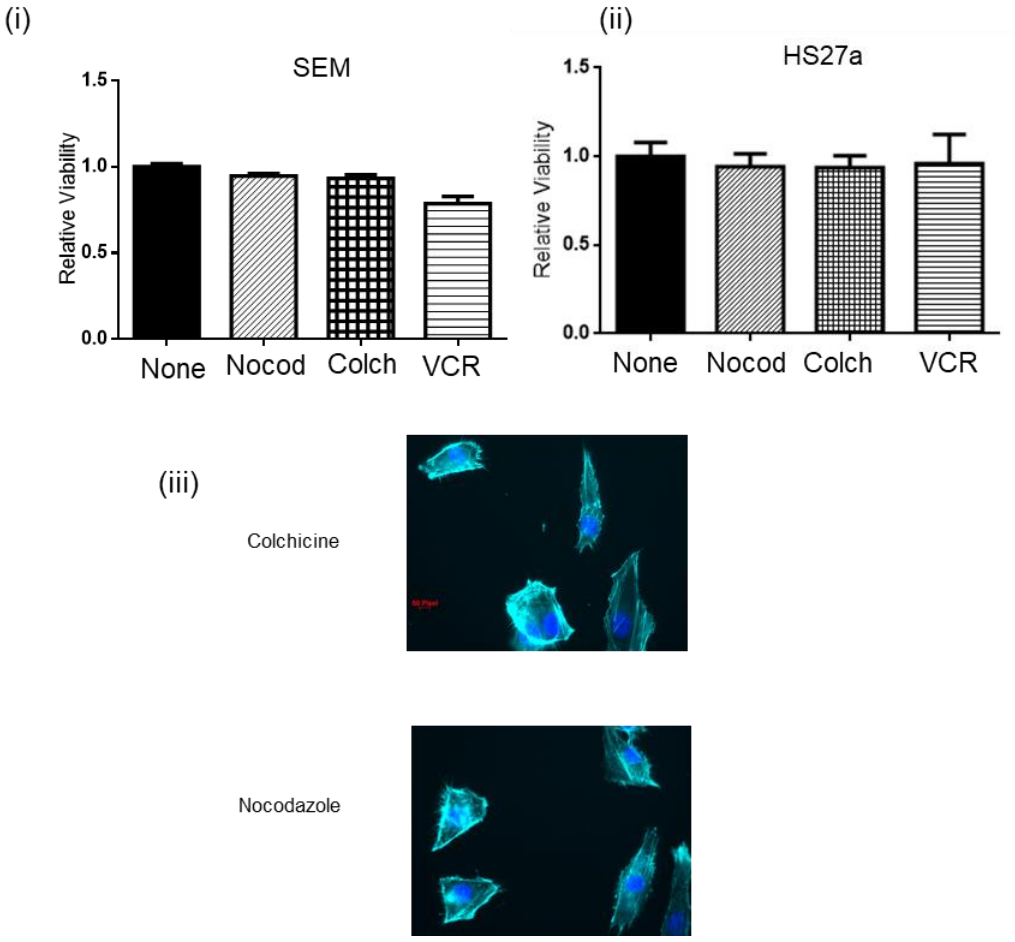

Figure 6-10: Microtubule damaging drugs induce similar changes in HS27a. (i) % viability (Y axis) after treatment of SEM ALL cells with the agents indicated (X axis). (ii) Relative viability (Y axis) after treatment of HS27a cells with the agents indicated (X axis). (iii) Phalloidin and DAPI staining of HS27a (40X) after exposure to nocodazole or colchicine.

I then sought to confirm that microtubule damaging drugs were able to both prevent induction of the ALL-CAF phenotype in HS27a following ROS-inducing chemotherapy and also reduce visible connections between the cells. This, I hypothesised, may prevent or overcome ALL-CAF mediated protection of B-ALL cells by preventing TNT formation and thus mitochondrial transfer from MSC to ALL cell.

As predicted, in ***figure 6-11***, I show that indeed microtubule damaging drugs such as VCR were able to inhibit AraC induced HS27a transformation to ALL-CAF. Firstly in ***figure 6-11 (i)***, the imaging shows that the addition of VCR to AraC prevented the characteristic appearance of ALL-CAF and furthermore induced rounding up of the cells in a similar way to VCR as a single agent. There was also a notable reduction in visible connections between the cells. Secondly, the addition of VCR led to a reduction in AraC induced cytokine secretion as demonstrated in ***figure 6-11 (ii),*** with IL8 reaching statistical significance. This provides support for the notion that VCR and other microtubule damaging agents may be able to prevent TNT formation between MSC and ALL cells and potentially rescue AraC mediated cytotoxicity of B-ALL cells in the presence of MSC.

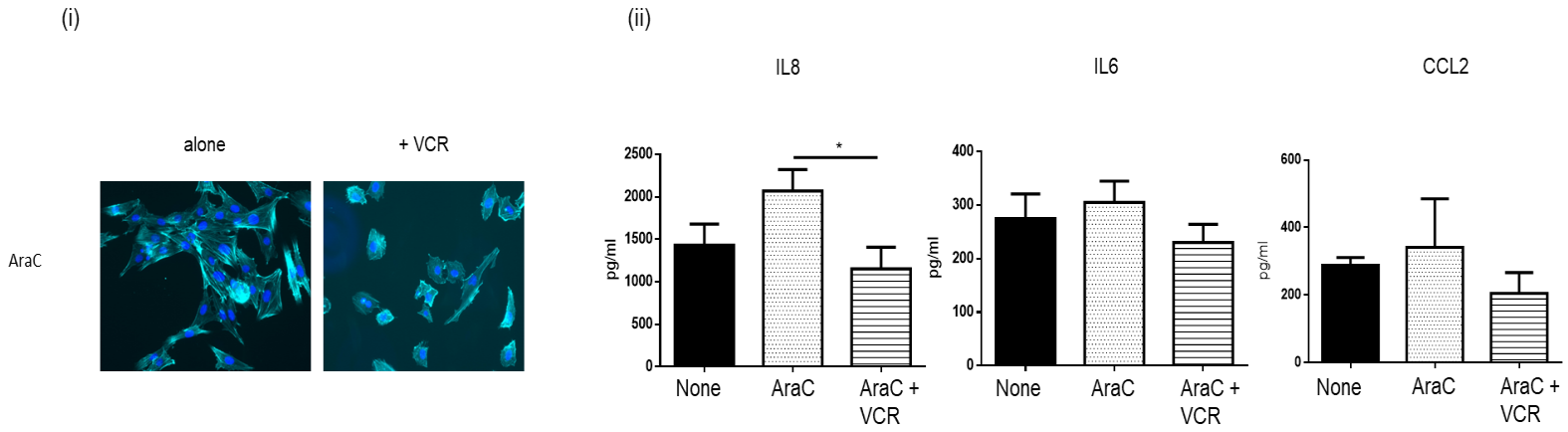

Figure 6-11: Vincristine prevents ALL-CAF induction by cytarabine. (i) Phalloidin/DAPI staining of AraC-treated HS27a cells either alone or with VCR (20X) (ii) Cytokines and chemokines (pg/ml, Y axis) secreted by HS27a after AraC treatment alone or with VCR. All statistically significant comparisons (by unpaired t-test) are as depicted: IL8 AraC vs AraC + VCR, P = 0.0112.

I next sought to determine if inhibition of TNT, via both an actin polymerisation inhibitor and a microtubule damaging drug, could abrogate AraC induced mitochondrial transfer from MSC to ALL cells. I selected Latrunculin-B and NOC, as these agents have been demonstrated by other authors to inhibit TNT. Furthermore at the doses used and previously demonstrated in ***figure 6-10***, NOC had no significant impact on the viability of either cell population. I once again used the MitoTracker™ flow cytometry based assay previously discussed. As shown in ***figure 6-12(i)***, both the actin polymerisation inhibitor latrunculin-B and the microtubule inhibitor, NOC, significantly blocked AraC-stimulated mitochondrial transfer from HS27a to ALL cells. NOC led to a greater reduction in mitochondrial transfer and this is in keeping with the previous discussed findings in the literature that microtubules are essential in TNT that transfer mitochondria[102].

Having demonstrated that microtubule damaging drugs were able to both inhibit AraC induced induction of ALL-CAF and mitochondrial transfer from MSC to ALL cells, I then sought to determine that these effects had functional relevance in ALL cell killing. In order to connect the inhibition of ALL-CAF and mitochondrial transfer to the functional impact of MSC on ALL, I quantified the impact of the addition of microtubule damaging drugs and Latrunculin-B on AraC-mediated SEM cell killing using the HS27a/SEM co-culture system. In ***figure 6-12(ii)*** I show that in the HS27a/SEM co-culture, latrunculin-B, NOC and COL all partially, but significantly, ablated HS27a MSC-mediated protection from AraC. VCR entirely ablated the protection, completely restoring AraC toxicity with superadded SEM cell killing, due to its own cytotoxic properties. These data confirm

that prevention of mitochondrial transfer via inhibition of TNT with actin polymerise inhibitors or microtubule damaging drugs prevent HS27a MSC rescue of B-ALL cells *in vitro*. Thus suggesting a central, functional role for mitochondrial transfer in chemotherapy resistance.

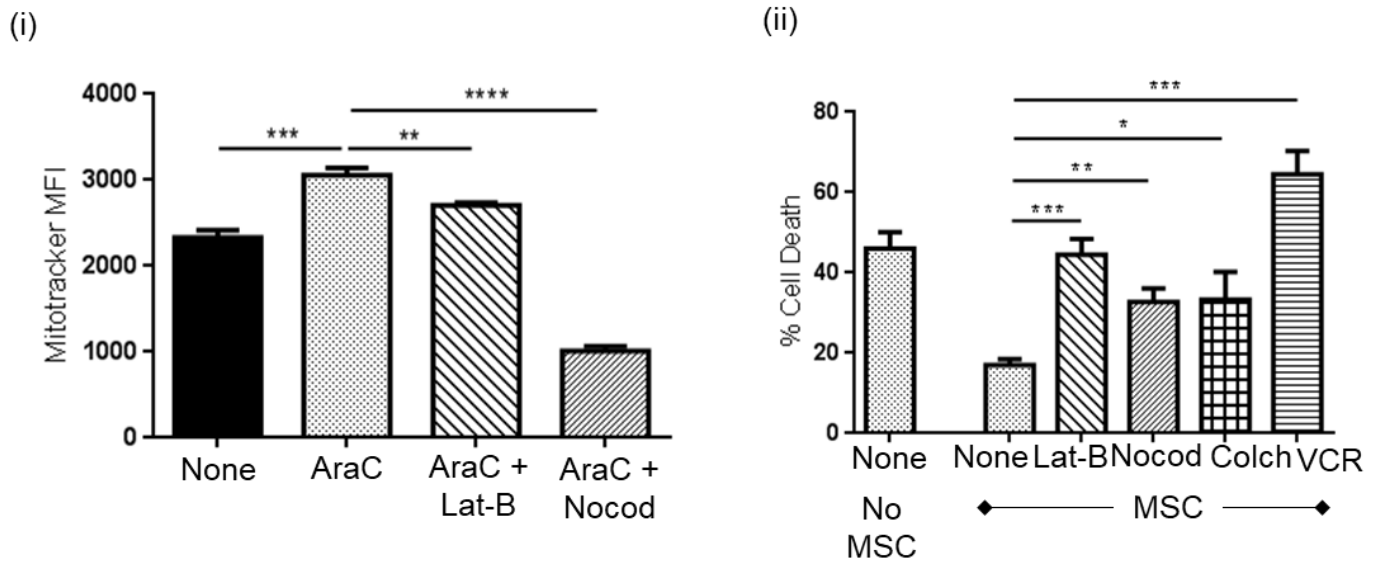

Figure 6-12: Microtubule inhibition of mitochondrial transfer overcomes MSC mediated protection (i) Mitochondrial transfer from HS27a to SEM cells following microtubule damaging blockade. (MitoTracker™ MFI, Y axis). Baseline condition is co-culture with no added agents, all other conditions are AraC-treated either alone or with latrunculin-B (lat-B), and nocodazole (Nocod) (X axis). All statistically significant comparisons (by unpaired t-test) are as depicted: none versus AraC, P = 0.0005, AraC versus AraC + latrunculin-b, P = 0.0028, AraC vs AraC + nocodazole, P < 0.0001. (ii) % cell death (Y axis) after AraC-treatment of SEM either in monoculture or co-culture with HS27a with nil, lat-B nocod, colchicine or VCR added (X axis). All data are mean +/- SE of 3 independent experiments. All statistically significant comparisons (by unpaired t-test) are as depicted: MSC none versus lat-B, P = 0.0004, MSC none versus nocod, P = 0.0018, MSC none versus colchicine, P = 0.0167, MSC none versus VCR, P = 0.0002.

6.3.5 Cytarabine Induces Activation of Stromal Cells and Mitochondrial Transfer *in vivo*

Finally, I sought to determine the relevance of our in vitro findings in a disseminated xenograft model of B-ALL. I aimed to demonstrate, using a murine model of ALL that AraC but not VCR or NOC could generate an ALL-CAF phenotype in stromal cells *in vivo*. I also sought to determine whether AraC would lead to the same ROS perturbation in ALL cells and mitochondrial transfer from murine stromal cells *in vivo*. Finally, I aimed to demonstrate that AraC but not VCR or NOC would generate a 'treatment resistant niche' composed of nestin positive stromal cells and residual B-ALL cells similar to that described by Duan et al[12].

To achieve this I developed an SEM cell line expressing blue fluorescent protein(BFP)/luciferase by retroviral vector transfer of (state plasmid) and flow sorting of the cells to 99% purity (***figure 6-13***) in order to facilitate serial imaging in live mice.

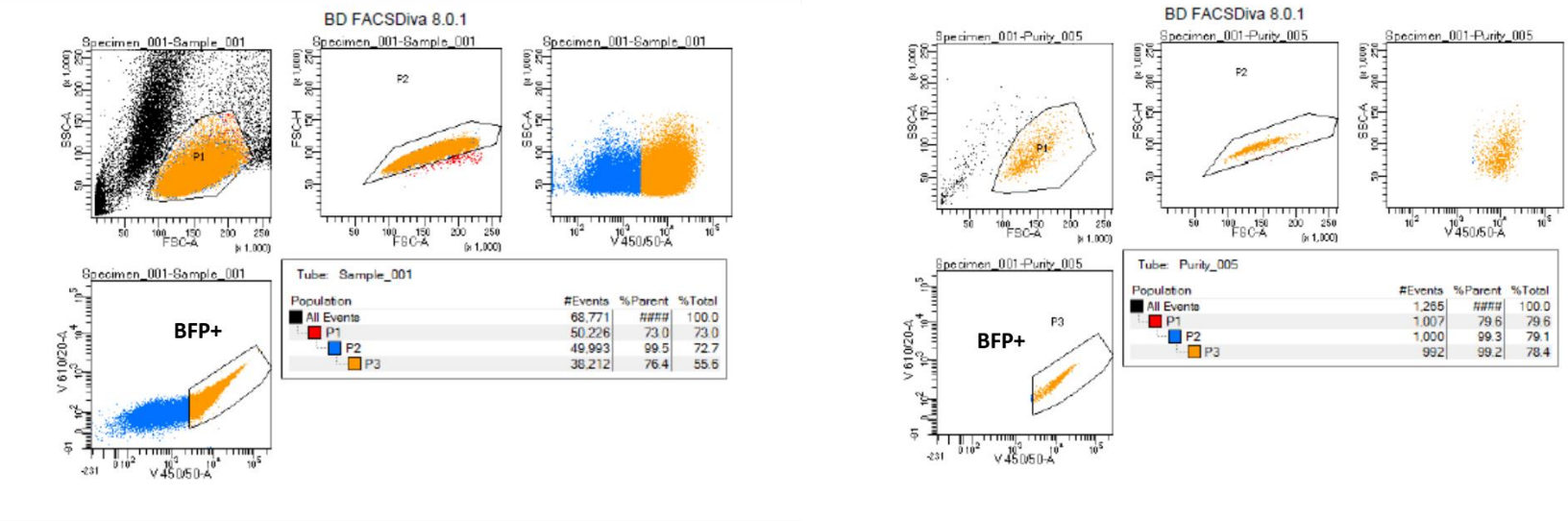

Figure 6-13: FACS sorting SEM cells with BFP expression. FACS sorting strategy to isolate SEM cells transduced with BFP expression. The dot plots on the right confirm the purity of the sorted BFP+ SEM cells.

The overall experimental design in shown in ***figure 6-14***. Two million BFP/luciferase-labelled SEM cells SEM B-ALLs were injected by the tail vein into NSG mice. As shown in ***figure 6-15***, engraftment was confirmed a week after injection of SEM cells. Three days later, mice were treated with either PBS control, AraC, VCR or NOC for two days and were then re-imaged and sacrificed two days after treatment.

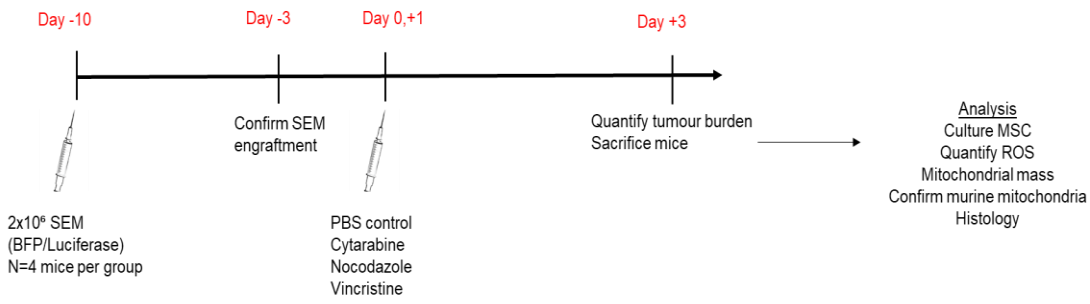

Figure 6-14: Design of *in vivo* experiment. Schema of in vivo experiments indicating timelines and experimental outputs from two independent experiments

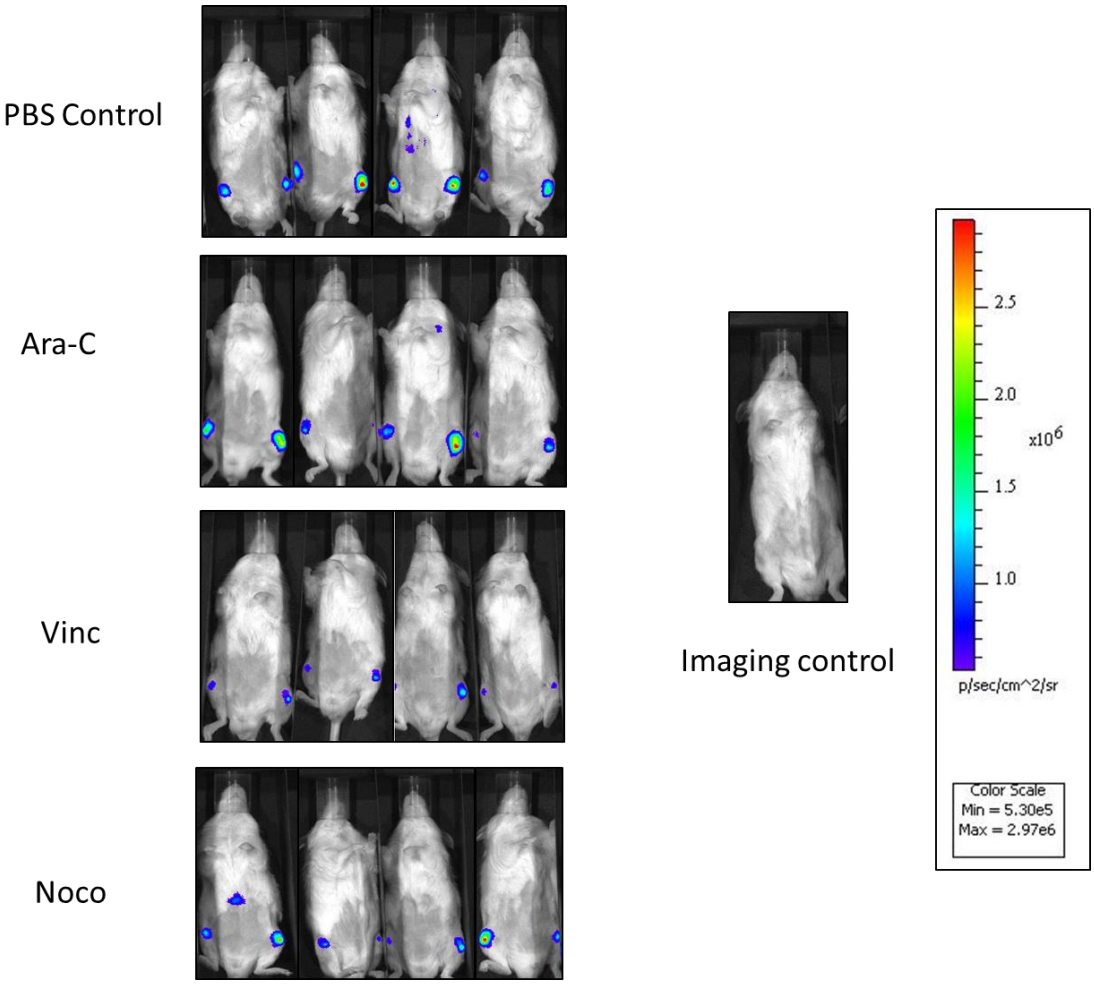

Figure 6-15: *In vivo* bioluminescent imaging confirms SEM engraftment. Live imaging of tumour burden at day -3 with respect to the treatments given. Images with colour scale bar and control mouse are shown.

Figure 6-16 shows non-invasive bioluminescence imaging two days after treatment. All agents except PBS control rapidly and significantly reduced the leukaemia burden, including NOC, which is not used as a chemotherapeutic agent and has not previously been shown to have anti-leukaemic activity.

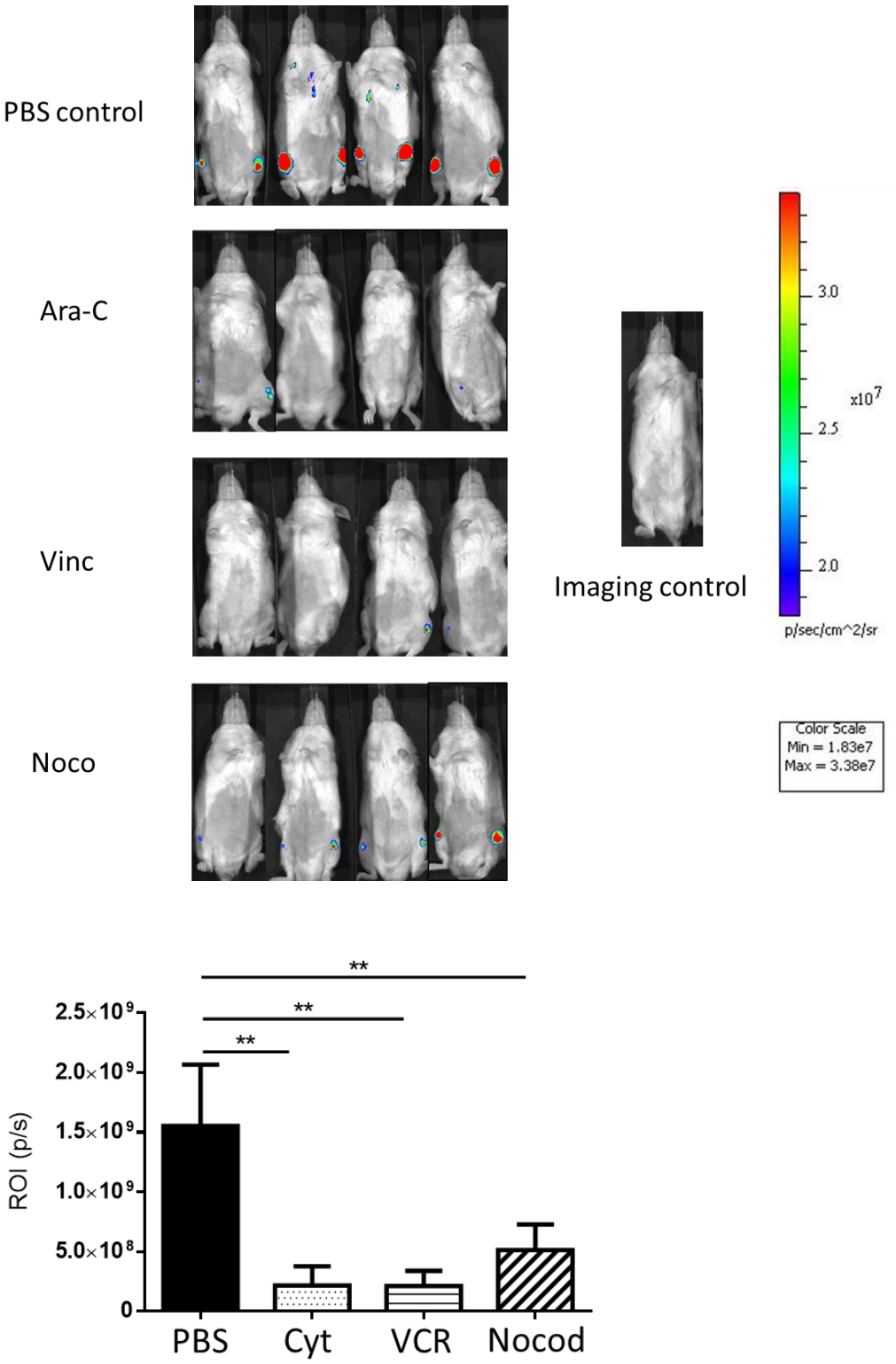

Figure 6-16: In vivo bioluminescent imaging following chemotherapy. Live imaging of tumour burden at day +3 with respect to the treatments given. Images with colour scale bar and control mouse are shown. (ii) Quantification of the luciferase expression with region of intensity units on the Y axis and experimental conditions on the X axis. P values are 0.0026 for PBS vs AraC, 0.0023 for PBS vs VCR and 0.0098 for PBS vs nocodazole.

Immediately following imaging the mice were sacrificed and MSC were isolated and cultured from the murine bone marrow. The MSC were then stained with phalloidin, DAPI and αSMA and imaged with a fluorescent microscope. After AraC treatment, imaged MSC showed appearances typical of ALL-CAF with a broadened, flattened appearance and prominence of actin stress fibres and expressed αSMA. These changes were not evident in VCR, NOC or control-treated mice (***figure 6-17***). Thus confirming that AraC, but not VCR or NOC, was indeed capable of inducing the ALL-CAF phenotype I had observed most commonly in patient specimens treated with AraC and in my *in vitro* models.

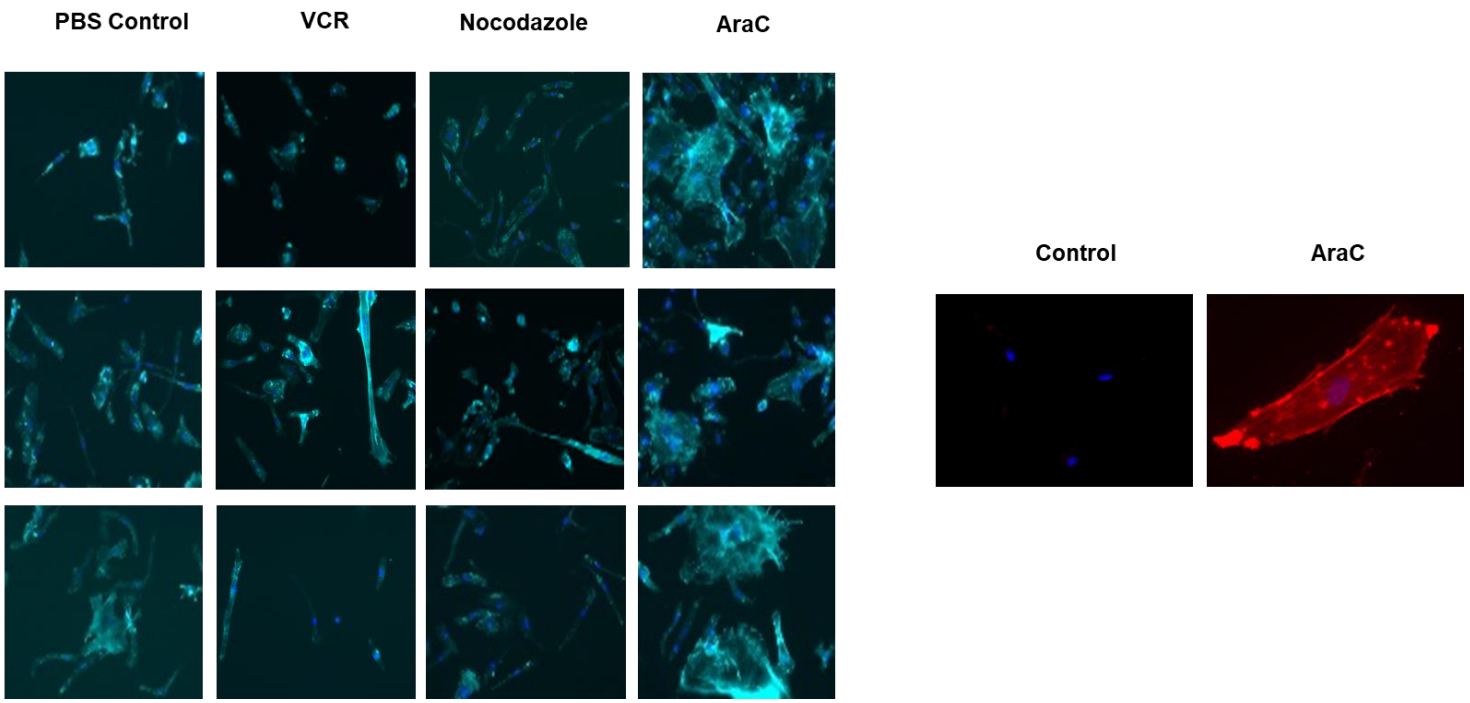

Figure 6-17: Cytarabine activates MSC *in vivo*. Phalloidin (Cyan)/DAPI (blue) staining of MSC isolated and expanded from 3 control, AraC, VCR or nocodazole-treated mice (20X). αSMA (red) staining of MSC isolated and expanded from one control and one AraC -treated mouse (40X)

I then explored whether AraC also induced ROS perturbation *in vivo* by measuring intracellular ROS in residual ALL cells immediately post sacrifice of the mice. Intracellular ROS was measured using CellROX green by flow cytometry. As shown in ***figure 6-18*** intracellular ROS levels measured by flow cytometry of the BFP positive population, were significantly elevated in SEM cells after AraC, but not VCR or NOC-treatment of the mice as compared to the PBS treated control. This is in keeping with other findings in the literature and my findings in chapter 5 where *in vitro* AraC and DNR induced increased ROS but not VCR.

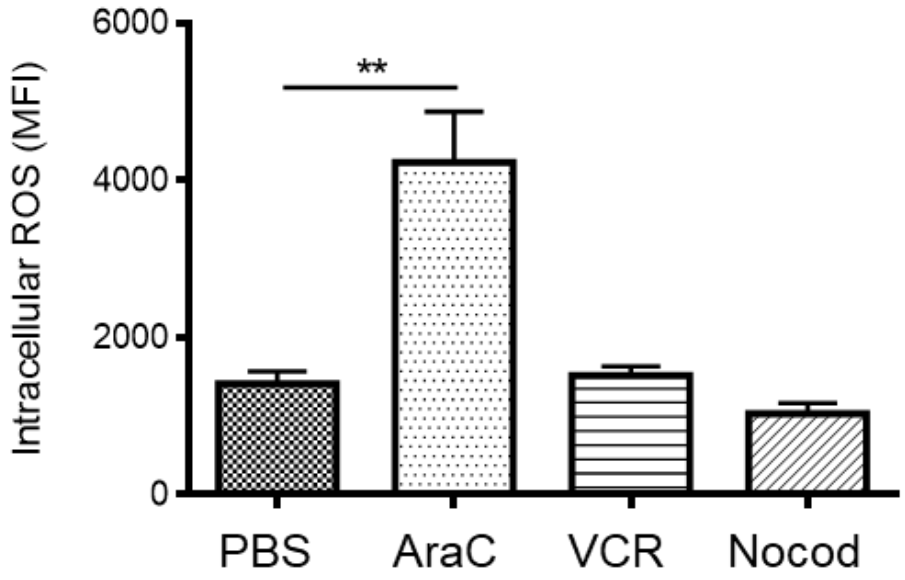

Figure 6-18: Cytarabine increases ROS in SEM cells. ROS (MFI, Y axis) after treatment of mice bearing SEM xenografts with the agents indicated (X axis). Cells were harvested from mice at day +3 after treatment with control, AraC, VCR or Nocod. All statistically significant comparisons (by unpaired t-test) are as depicted: PBS vs Ara-C, P = 0.053,

Figure 6-18: Cytarabine increases ROS in SEM cells

Given the increase in intracellular ROS in ALL cells following AraC but not VCR or NOC, I then sought to determine if mitochondrial transfer was also occurring *in vivo*. To determine if transfer was occurring, I first measured the mitochondrial mass of the ALL cells *ex vivo* using a green MitoTracker™ dye. ***Figure 6-19*** shows an increase in mitochondrial mass following treatment with AraC but not VCR or NOC as compared to the untreated control. Thus suggesting that mitochondrial transfer from stromal cells may be occurring following treatment with AraC.

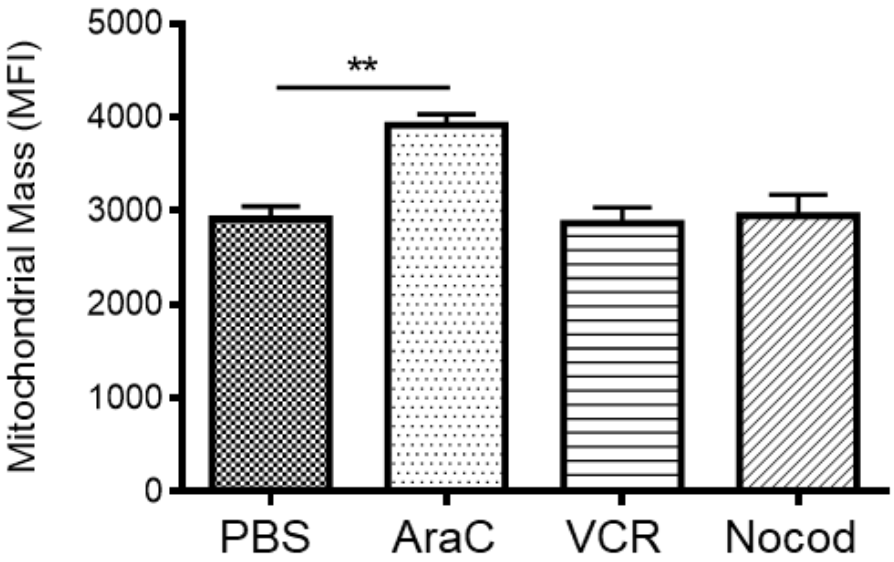

Figure 6-19: Cytarabine increases mitochondrial mass in residual ALL cells.
Mitochondrial mass (green MitoTracker™ MFI, Y axis) after treatment of mice bearing SEM xenografts with the agents indicated (X axis). Cells were harvested from mice at day +3 after treatment with control, AraC, VCR or nocodazole. All statistically significant comparisons (by unpaired t-test) are as depicted: PBS vs AraC, P = 0.0014.

To confirm that the increase in mitochondrial mass following AraC was at least in part due to mitochondrial transfer I then sought to determine the presence of mitochondrial DNA in sorted human SEM (ALL) cells. I used the same method as described earlier in this chapter of the co-culture between MS5 and SEM cells *in vitro.* ***Figure 6-20*** demonstrates the presence of murine mitochondrial but not nuclear DNA in AraC-treated, sorted SEM cells. Faint bands were also present in the PBS treated control murine mitochondrial DNA position suggesting a small amount of mitochondrial transfer may be occurring before AraC treatment. Murine mitochondrial DNA was not present in sorted SEM cells from the VCR or NOC treated mice (not shown).

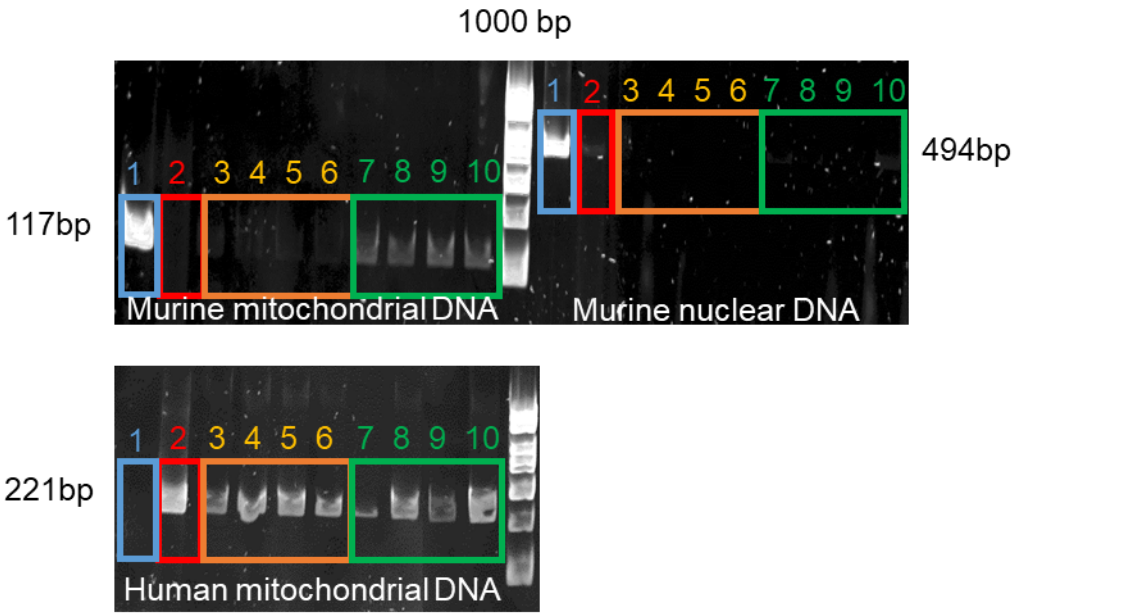

Figure 6-20: Mitochondrial transfer to ALL cells occurs *in vivo*. Agarose gel images showing PCR products from DNA extracted from human SEM cells xenografted into NSG mice. Murine nuclear and mitochondrial DNA and human mitochondrial DNA, is present as labelled. Lane 1, murine control bone marrow cells, Lane 2 Human SEM cell control, Lanes 3-6 SEM xenograft cells sorted on BFP after control treatment Lanes 7-10 SEM xenograft cells sorted on BFP after AraC treatment.

Finally I sought to determine that AraC, but not VCR or NOC, was capable of inducing the niche described by Duan[12], composed of nestin positive and αSMA positive stromal cells and residual ALL cells. To demonstrate this, following sacrifice of the mice, sections of murine femur were sectioned and stained with a mouse nestin antibody to identify nestin positive stromal cells and human CD19 to identify ALL cells. I also attempted staining with αSMA but as this led to staining of many other irrelevant components of the bone marrow interpretation was very difficult. I therefore used nestin to identify the relevant stromal cells.

Figure 6-21 shows CD19 (brown) and nestin (brown or pink as labelled) staining of sections of femur. This includes both single stained sections and double stained sections. Firstly, best demonstrated in the single stained nestin (brown) images, there is a notable increase in nestin positive stromal cells in the AraC treated mice as compared to the PBS control, VCR or NOC treated mice. This contrasts with the much more marked reduction in the overall cellularity of the bone marrow of the AraC treated mice as compared to the other conditions. This is in keeping with what is observed clinically, where AraC induces more myelosuppression than VCR. Therefore although AraC is leading to a marked reduction in overall cellularity due to its DNA damaging properties, it appears to induce both a relative and absolute increase in nestin positive stromal cells within the bone marrow.

I then used double staining (CD19 – brown, nestin – pink) to determine if residual CD19-positive ALL cells bore any spatial relationship to nestin-stained stromal cells in the different conditions. In the AraC treated mice, as shown in the representative images, residual ALL cells clustered closely to nestin positive stromal cells, in keeping with the niche identified by Duan et al[12]. Notably, as demonstrated in the images, in the VCR and NOC treated mice the nestin positive stromal cells bore no spatial relationship to the residual ALL cells. This is in keeping with the findings of Hawkins et al[78] in their T-ALL intravital murine model, treated with either VCR or DEX, where no niche formation was noted. Thus suggesting that niche formation may be ROS dependent and induced by DNA damaging chemotherapy whereas non-ROS inducing chemotherapy or drugs, such as VCR or NOC, did not induce niche formation and may even inhibit this process.

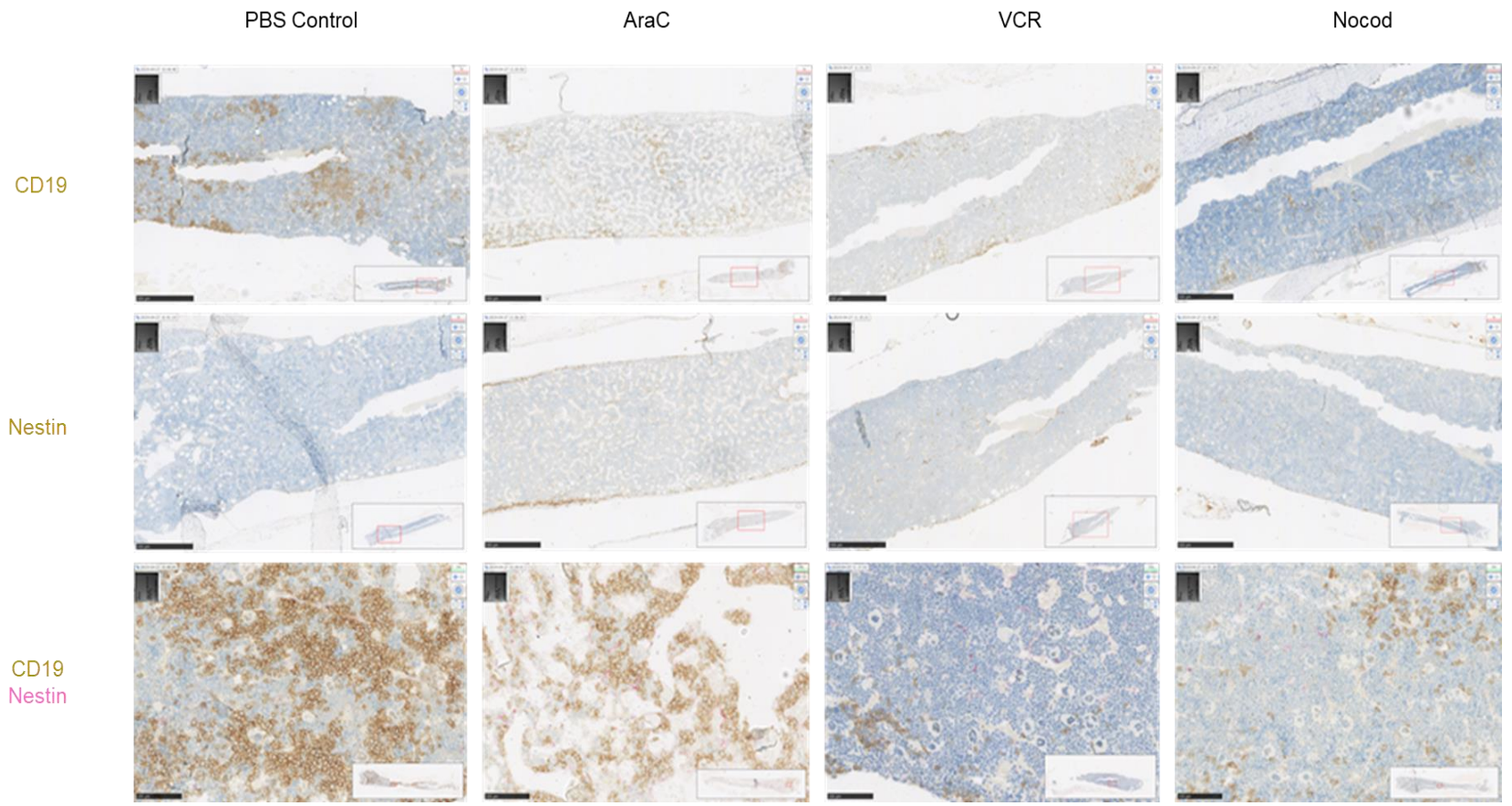

Figure 6-21: Immunohistochemistry of murine femur with nestin and CD19 staining. Immunohistochemistry of sections of representative whole femora from each treatment group. Femora are single stained for human CD19 (brown) and murine nestin (brown) plus dual-stained for human CD19 (brown) and murine nestin (pink). In the AraC but not the other conditions. CD19+ cells are seen closely associating with a nestin+ niche.

6.4 Discussion

I have demonstrated that MSC in co-culture with B-ALL cells following chemotherapy induced oxidative stress undergo transformation to an ALL-CAF phenotype and prevent AraC induced ROS increase in ALL cells. Importantly, this corresponds to a reduction in AraC-mediated ALL cell death, which is lost if the cells are not in contact. This corresponds closely with what is observed in the healthy haematopoietic stem cell (HSC) niche with MSC tightly controlling ROS to maintain HSC in a steady state[71].

I then demonstrated via a mitochondrial specific dye, time lapse imaging and species-specific mitochondrial DNA PCR that MSC transfer mitochondria to B-ALL cells. This occurs relative to the baseline ROS level of the B-ALL cell, can be increased by ROS-inducing chemotherapy (AraC, DNR) and decreased by the ROS scavenger, NAC and corticosteroid, DEX. Furthermore, we were able to confirm in a disseminated ALL murine model that this was also occurring *in vivo*. This is entirely in keeping with Marlein et al[108] where they also demonstrated that ROS species or ROS inducing agents increased mitochondrial transfer from MSC to AML cell and anti-oxidants reduced transfer.

This is likely a conserved MSC property, as other widely diverse disease models in different organ systems, have demonstrated the ability of MSC to transfer mitochondria to cells under oxidative stress. I did not explore whether or not other cells within the bone marrow microenvironment are capable of transferring

mitochondria given the focus of my work was on MSC, the extensive literature on MSC as mitochondrial donors and relative paucity of data with other cell types. However, it is possible that other cells, especially endothelial cells, may also be capable of transferring mitochondria and this would be a useful focus of additional work.

I was able to confirm that mitochondria were transferred via a contact dependent mechanism and directly imaged mitochondria travelling via TNT. This is in keeping with findings by groups in other disease models[108,112,173] including in acute myeloid leukaemia[108], which is also primarily a bone marrow based malignancy. While it is possible that mitochondrial transfer also occurs via different mechanisms, such as gap junctions and exosomes, we were able to demonstrate that actin polymerisation inhibition and microtubule damaging agents were able to significantly reduce transfer which had functional significance. Overall, TNT appear at the very least, to be an important if not the sole mechanism of mitochondrial transfer.

I demonstrated that mitochondrial transfer is essential in the protective effect MSC provided to ALL cells, by showing loss of protection firstly through depleting mitochondria in the MSC and secondly by inhibiting TNT with microtubule damaging drugs or an actin polymerisation inhibitor. It remains unclear how exactly the mitochondrial transfer 'rescues' the B-ALL cell. Again, this will be a critical focus for future work. It appears highly likely that the mitochondrial transfer is necessary for the ALL cell to overcome oxidative stress induced by DNA damaging chemotherapy on

the basis of this work and the findings of others in the literature. Foran et al[110] and Moschoi et al.[107] have noted enhanced energy potential of the leukaemic cells following AraC induced mitochondrial transfer. Moschoi et al observed that AML cells co-cultured for 72 hours with MSC increased their oxidative phosphorylation (OXPHOS)-derived ATP production after 72 hours of co-culture with MS-5 leading to a 4.5-fold increase in total adenosine triphosphate. Importantly this was not observed if mitochondrial deficient MSC were used or when the two cell populations were not in contact, confirming the essential role of the transferred mitochondria in the enhanced ATP production.

Another possibility is that MSC are replacing damaged or 'faulty' mitochondria in the ALL cells. Wang et al[114] in T-ALL and Golan et al[74] in the healthy haematopoietic stem cell niche demonstrated mitochondrial transfer in the opposite direction ie back to the MSC. Wang demonstrated that mitochondria travelling from the T-ALL cell to the MSC mediated chemotherapy resistance by reducing ROS in the T-ALL cell. Marlein et al[108] showed that as a result of ROS exposure from AML cells, peroxisome proliferator-activated receptor gamma coactivator 1-alpha (PGC1α), the master regulator of mitochondrial biogenesis, is upregulated in MSC in co-culture with AML cells. The MSC in co-culture with AML cells had an increased mitochondrial mass and increased mitochondrial respiration, suggesting the MSC are producing new and undamaged mitochondria as a pre-requisite to transfer. I also have preliminary data supportive of the notion that mitochondria travel from ALL cell to MSC and therefore an exchange occurs rather than mitochondria travelling in one direction. In work continuing from

this thesis, I am currently exploring whether the mitochondria transferred from the ALL cell are indeed damaged or dysfunctional mitochondria.

I was able to confirm my *in vitro* findings in a disseminated ALL murine model. AraC was observed to induce a niche, consistent with Duan et al. findings[12], composed of nestin positive stromal cells and residual ALL cells. Importantly, this was not observed in the control, VCR or NOC treated mice. I suspect niche formation with nestin positive cells may therefore occur due to oxidative stress induced either by the intrinsic ROS level of the ALL cell or ROS-inducing chemotherapy.

I deliberately selected SEM cells for our murine model, due to their low ROS level and inability to activate the MSC, so we could explore the differing effects of the chemotherapy drugs. I would predict, that SD1 cells with higher intrinsic ROS and ability to induce ALL-CAF, would lead to niche formation and relative increase in nestin positive stromal cells before any chemotherapy treatment. Ongoing work is exploring this hypothesis. Importantly, microtubule damaging drugs *in vitro*, were able to prevent AraC induced ALL-CAF formation, reduce mitochondrial transfer and overcome MSC mediated AraC resistance of ALL cells. They also did not induce niche formation *in vivo*. This raises the possibility that microtubule damaging drugs may be an effective agent to prevent niche formation in B-ALL. I am currently exploring the effects of the combination of VCR and AraC in niche formation *in vivo*.

Finally, the transfer of mitochondria in direct relationship to chemo-protection from ROS-inducing therapy is of particular and immediate relevance to the therapy of ALL. DNR, AraC, VCR and DEX are the mainstays of ALL treatment. Hyper CVAD, one of the most common therapeutic protocols used internationally for the treatment of ALL includes repeating blocks of relatively dose intensive AraC given without VCR or DEX. Our data suggests that outcomes of such therapeutic combinations used in ALL might benefit from adjustment to ensure that microtubule damaging agents such as VCR or anti-inflammatory agents such as DEX are always given with ROS-inducing agents. Our work demonstrates that when VCR or DEX are combined with AraC or DNR, HS27a MSC do not develop the cytopathological hallmarks of activated MSC and furthermore niche formation didn't occur in our disseminated mouse model following treatment with microtubule damaging agents such as VCR.

It is likely that these findings are also applicable to other cancers, especially haematological malignancies involving the bone marrow. I note the recent findings of Bertoli et al[172] of the benefit of the addition of DEX to DNR and AraC in AML induction chemotherapy in a subset of AML patients. Their subsequent *in vitro* experiments suggested that dexamethasone enhanced AML cell killing only when MSC were included in their model, suggesting an effect on MSC mediated protection of AML cells rather than a directly toxic effect on the AML cells. Furthermore, Gerby et al[171] demonstrated the effectiveness of several microtubule damaging drugs across a number of AML primary specimens in their niche model with MSC. Thus suggesting

that both DEX and VCR may also be effective at inhibiting MSC mediated protection of AML cells.

Chapter 7: General Discussion

ALL remains a challenging disease to treat. Although significant improvements have been made in outcomes especially in childhood ALL, treatment toxicity remains a significant issue and the relapse risk in adults remains unacceptably high despite excellent initial response rates[2,5]. Although our understanding of the biology of the disease has improved, several, long recognised clinical observations and unique to ALL lead to important questions which remain unanswered. These include:

- Why does a small fraction of the initial ALL cell population prove so challenging to eradicate in contrast with the treatment sensitive 'bulk population' of ALL cells?
- Why are certain genetic sub-types of ALL more resistant to treatment than others, especially genetic sub-types more common in adults as compared to children?
- Why and how does maintenance chemotherapy work to clear away the residual leukaemic cells?

Recently the microenvironment has emerged as playing a crucial role in treatment resistance in B-ALL with several authors describing the presence of a protective microenvironmental niche[12,13]. The recognition and improved understanding of this protective niche, especially following treatment, is arguably beginning to show promise in providing answers to the questions above.

In this thesis I have explored the role of MSC within this protective niche. I initially isolated MSC with an ALL-CAF phenotype from patient bone marrow specimens and then demonstrated this 'MSC phenotype' occurs in response to ROS induced either by the intrinsic genetic lesion within ALL cells or ROS inducing chemotherapy drugs. AraC, a ROS inducing chemotherapy agent, also induced the ALL-CAF phenotype in MSC in a disseminated mouse model of B-ALL in chapter 6. These findings are consistent with murine models of B-ALL by other authors including Duan et al[12] and Ebinger et al[13] where the presence of a niche of residual, treatment resistant, B-ALL cells was demonstrated following ROS inducing chemotherapy.

As previously discussed, I propose ALL-CAF induction following ROS exposure is an intrinsic physiological property of MSC, especially nestin positive MSC, to protect cells in the vicinity from oxidative stress rather than an ALL or cancer specific phenomenon. Evidence for this hypothesis includes the observation that MSC and fibroblasts are known to adopt a similar phenotype not just in a range of cancers but also in wound healing and a range of inflammatory conditions including bleomycin or chemotherapy induced pulmonary fibrosis[174].

Further evidence for this hypothesis is provided in my murine model where cytarabine, a ROS inducing chemotherapy agent, but not non-ROS inducing chemotherapy induced an increase in nestin positive MSC and the presence of MSC with an ALL-CAF appearance within the bone marrow. The previously discussed work by Mendez-

Ferrer[68] and Ludin[71] suggests that an important role of nestin positive MSC within the healthy haematopoietic niche may be to tightly control ROS levels within haematopoietic stem cells to maintain quiescence and ensure their survival following oxidative stress. I would postulate based on my thesis that leukaemic cells, residing within the niche with nestin positive MSC 'take advantage' of this protective effect and are therefore protected from ROS-inducing chemotherapy. Leukaemic cells within the niche may also take on features of the healthy HSC population including low ROS levels, increased mitochondrial mass and quiescence giving them the appearance of a 'leukaemic stem cell'. Importantly, however, as demonstrated by Ebinger et al, once the treatment resistant ALL cells are removed from their protective niche and tested ex vivo they are no longer quiescent, chemo-resistant and are indistinguishable from the bulk population. Thus, in ALL it appears there are no distinct leukaemic stem cells, rather the few surviving cells at least initially and possibly at relapse, are resistant as a function of the microenvironment rather than due to any unique intrinsic property of the ALL cell.

The findings in my thesis also suggest that niche formation may be dependent on the genetic subtype of B-ALL. My data shows that B-ALL cells with higher ROS more readily induce activation of the stroma and the ALL-CAF phenotype in MSC. Genetic lesions such as *BCR-ABL1* in ALL are known to induce increased ROS production within the cell[164] and this may explain why my data suggests they induce the ALL-CAF phenotype and possibly niche formation more readily than other genetic sub-types of ALL such as *MLL-AF4* with low ROS levels. In keeping with this is the clinical observation that *BCR-*

ABL1 positive ALL responds relatively poorly to conventional intensive chemotherapy regimens including ROS inducing chemotherapy as compared to other genetic subtypes of ALL[2].

Niche formation may even be a necessary adaption for high ROS producing *BCR-ABL1* cells to survive and proliferate within the bone marrow in a similar way to B-ALL cells within the niche after ROS inducing chemotherapy. Interestingly, in induction therapy in *BCR-ABL1* positive ALL, VCR and/or DEX are increasingly used as the sole chemotherapeutic agents in combination with a tyrosine kinase inhibitor and have been demonstrated to have similar efficacy to more intensive regimens. These drugs, as demonstrated in this thesis, appear to disrupt formation of the ALL-CAF phenotype and therefore disrupt formation and effectiveness of the protective niche to ALL cells. Thus, the efficacy of VCR and DEX in this setting may not solely relate to direct cytotoxicity to ALL cells but also be due to their effect on the protective niche.

In contrast, low ROS producing ALL genetic sub-types such as *MLL-AF4* may be less dependent on niche formation. This is supported by the observation of minimal nestin positive stromal cells in my SEM disseminated mouse model without any chemotherapy treatment. This could also potentially explain why *MLL-AF4* ALL typically presents with a higher number of leukaemic cells in the peripheral blood than other equally aggressive genetic subtypes of ALL. I am currently exploring this hypothesis in disseminated murine models.

My data also suggests mitochondrial transfer plays a central role in the protection ALL-CAF or MSC provide to ALL cells within the niche. This is in keeping with findings by other groups in AML including Marlein et al[108], Moschoi et al[107] and Mendez Ferrer group[110]. Similarly, to Marlein et al[108] and in keeping with the model proposed by Rustom[106], I found that ROS inducing agents enhanced mitochondrial transfer, whereas the ROS scavenger NAC and anti-inflammatory corticosteroid DEX reduced transfer. Furthermore, transfer of mitochondria was relative to the intrinsic ROS level of the receiving ALL cell. Therefore, as suggested by other groups in a range of different diseases[108,111,112], it appears highly likely that the mitochondrial transfer occurs to 'rescue' the receiving cell from oxidative stress. Work by the Rushworth group suggests that NOX2 expression in the leukaemic cells leads to enhanced ROS production[108], which is detected by the MSC leading to upregulation of the master regulator of mitochondrial biogenesis – PGC1α[109]. Suggesting that MSC may produce more mitochondria in preparation of transfer, when they sense cells in the vicinity are under oxidative stress.

However, it is not yet established exactly what the role of the transferred mitochondria is or how exactly the cell under oxidative stress is 'rescued' by the transfer. Perhaps the most logical explanation is that the transfer occurs to replace damaged or faulty mitochondria within the cell, which are damaged partly because of increasing levels of ROS. However, this has never been definitively demonstrated. Wang et al[114] and Golan et al[74] have demonstrated that mitochondria transfer does

occur in the other direction, that is from the leukaemic cell under oxidative stress or HSC to MSC and there is evidence to suggest that mitochondria travelling in this direction are indeed damaged[114].

I also have preliminary data supporting transfer of mitochondria from ALL to MSC *in vitro* via a ROS dependent but TNT independent mechanism. I am currently exploring whether the mitochondria transferred from ALL cell to MSC are damaged mitochondria via assessment of mitochondrial DNA damage following ROS inducing chemotherapy.

There are of course potential alternative explanations as to why the transfer of mitochondria occurs. This could include to enhance the oxidative phosphorylation or energy potential of the leukaemic cell as demonstrated by Moschoi[107] and Forte[110]. However, it is not immediately obvious the enhanced energetics would protect the leukaemic cell from cytotoxics although it may potentially enhance leukaemic cell proliferation.

A further explanation could be that the transferred mitochondria may alter the balance of pro-apoptotic versus anti-apoptotic factors associated with the mitochondria and therefore favour leukaemic cell survival. The anti-apoptotic factors include B-cell lymphoma-2 (BCL2), which Duan et al demonstrated was up-regulated in the surviving B-ALL cells in the niche in patient bone marrow specimens after treatment[12]. There is also evidence to support that mitochondria transferred from MSC

may have enhanced anti-oxidant properties and therefore may be more resistant to oxidative stress[175].

Interestingly, the recently developed BCL2 inhibitor Venetoclax is showing promise in the treatment of both relapsed and refractory AML[176] and pre-clinical models of ALL[177,178] and appears likely to be effective at targeting the leukaemic stem cell population in AML[179]. Thus, raising the possibility that the balance of pro versus anti-apoptotic factors may be important within the protective niche. Clearly, further work is required to gain a better understanding of why mitochondria transfer occurs and how this impacts survival of ALL cells.

As discussed in chapter 6 the transfer of mitochondria from MSC to ALL cells occurs via tunnelling nanotubes, consistent with findings from other studies in different disease models[108,112]. Importantly, the TNT capable of transferring mitochondria are composed of microtubule[102]. I was able to demonstrate that AraC-induced mitochondrial transfer is reduced when given in combination with a microtubule damaging drug, including non-chemotherapy drugs NOC and COL. This also had functional significance, as demonstrated by restoration of AraC mediated cytotoxicity when microtubule damaging drugs are added to in an *in vitro* niche model. This is keeping with findings of Moschoi et al[107] that all chemotherapy drugs tested except for VCR enhanced mitochondrial transfer.

The finding that VCR can restore AraC mediated ALL cell cytotoxicity and as a single agent can efficiently kill ALL cells within the niche as demonstrated by my work and others[171], has potentially important clinical relevance for several reasons. Firstly, my findings suggest that ROS inducing drugs, such as AraC or DNR, would be more appropriately be given together with a microtubule damaging such as VCR or a corticosteroid DEX to inhibit ALL-CAF and the transfer of mitochondria. In the most commonly used treatment regimen for ALL worldwide – HyperCVAD, AraC is given without VCR or DEX and similarly in phase 2 of the UKALL14 trial AraC is also given unopposed. Notably, in chapter 3 we isolated macrophages and ALL-CAF from a significantly greater percentage of patient specimens' following UKALL14 phase 2 than phase 1 (where DNR is given with DEX and VCR) and at diagnosis. Based on my work I would propose a clinical trial of rescheduling current drugs such that VCR or DEX would always be given prior to AraC. The UKALL15 trial investigators, in part due to my findings, will randomised current standard of care against a "microenvironment-adjusted regimen" as part of the planned NCRI UK wide B-ALL trial UKALL15. This will also enable us to prospectively isolate MSC from patients' samples and compare the induction of ALL-CAF with AraC with and without VCR and DEX.

Secondly, my findings also propose a testable hypothesis for the yet unexplained success of maintenance chemotherapy in ALL. As discussed earlier in this thesis, maintenance chemotherapy involves low dose chemotherapy given over several years and includes pulses of VCR and corticosteroids. A recent Japanese study showed the risk of relapse increases if the duration of maintenance therapy is reduced[44]. However,

the biological mechanism to explain how maintenance chemotherapy eradicates the few remaining ALL cells has remained elusive. Based on this work I would propose that pulses of DEX and VCR may inhibit niche mediated protection of the few surviving ALL cells eventually leading to eradication of the disease.

Thirdly, my work begins to provide a rationale for altering chemotherapy regimens according to the genetic sub-type of ALL. My data suggests that genetic subtypes which induce increased levels of ROS, such as *BCR-ABL1*, are relatively resistant to ROS inducing drugs such as AraC. As discussed earlier this is consistent with what is observed clinically. However, they may be more dependent on niche mediated protection for survival, providing a strong rationale for combining targeted agents such as tyrosine kinase inhibitors with VCR and DEX. This approach could potentially improve both treatment efficacy and reduce toxicity from intensive chemotherapy that may not be providing any therapeutic benefit despite increasing toxicity. Whereas in genetic subtypes with low intracellular ROS, such as *MLL-AF4,* the ALL cells themselves are sensitive to AraC but are protected by ALL-CAF following exposure to AraC negating the effectiveness of the drug. Hence, there is a rationale to combine AraC with VCR and DEX to overcome ALL-CAF mediated protection, which will be explored in the UKALL15 trial as discussed above.

Finally, as discussed in the introduction, toxicity is a significant problem in ALL treatment both in adults and children. Current treatment is intensive, prolonged and

leads to significant morbidity and mortality. ALL regimens were initially designed with drugs identified to kill ALL cells in vitro but relatively little thought was put into how the drugs should be combined, perhaps largely due to the limited understanding of both the biology of the disease and how chemotherapeutics worked *in vivo*. The relative importance of each individual drug in a cycle of treatment is also largely unknown. For these reasons it is highly likely a proportion of patients are given more intensive treatment than needed including drugs that may be ineffectual against their leukaemia, whilst having significant toxicity.

I strongly believe to improve outcomes in ALL, we need to invest more time gaining a better understanding of the biology of the disease, especially why minimal residual disease proves so challenging to eradicate. Increasing evidence suggests the microenvironment may be crucial in treatment resistance and my data supports this. I would argue that much energy and time is invested in identifying novel, druggable targets in ALL cells without really identifying the biological reasons for the very variable resistance to standard chemotherapy. In support of this is the fact that newer, novel targeted agents of ALL cells such as monoclonal antibodies[45], antibody drug conjugates[180] and bi-specific antibodies[181] although effective at inducing remission, appear to have limited ability to sustain long-term remissions.

Therefore, I believe further effort is required to investigate microenvironment-mediated protection of ALL cells, especially the metabolic properties of the residual

cells with the overall objective of further developing therapeutic combinations that target both microenvironment mediated protection and the ALL cells themselves.

Reference List

1. Terwilliger T, Abdul-Hay M. Acute lymphoblastic leukemia: a comprehensive review and 2017 update. Blood Cancer J 2017;7:e577.
2. Rowe JM, Buck G, Burnett AK, et al. Induction therapy for adults with acute lymphoblastic leukemia: results of more than 1500 patients from the international ALL trial: MRC UKALL XII/ECOG E2993. Blood 2005;106:3760-7.
3. Vora A, Goulden N, Wade R, et al. Treatment reduction for children and young adults with low-risk acute lymphoblastic leukaemia defined by minimal residual disease (UKALL 2003): a randomised controlled trial. Lancet Oncol 2013;14:199-209.
4. Hough R, Rowntree C, Goulden N, et al. Efficacy and toxicity of a paediatric protocol in teenagers and young adults with Philadelphia chromosome negative acute lymphoblastic leukaemia: results from UKALL 2003. Br J Haematol 2016;172:439-51.
5. Fielding AK. Current therapeutic strategies in adult acute lymphoblastic leukemia. Hematol Oncol Clin North Am 2011;25:1255-79, viii.
6. Aldoss IT, Marcucci G, Pullarkat V. Treatment of Acute Lymphoblastic Leukemia in Adults: Applying Lessons Learned in Children. Oncology (Williston Park) 2016;30:1080-91.
7. Moorman AV. The clinical relevance of chromosomal and genomic abnormalities in B-cell precursor acute lymphoblastic leukaemia. Blood Rev 2012;26:123-35.
8. Berry DA, Zhou S, Higley H, et al. Association of Minimal Residual Disease With Clinical Outcome in Pediatric and Adult Acute Lymphoblastic Leukemia: A Meta-analysis. JAMA Oncol 2017;3:e170580.
9. Rehe K, Wilson K, Bomken S, et al. Acute B lymphoblastic leukaemia-propagating cells are present at high frequency in diverse lymphoblast populations. EMBO Mol Med 2013;5:38-51.
10. le Viseur C, Hotfilder M, Bomken S, et al. In childhood acute lymphoblastic leukemia, blasts at different stages of immunophenotypic maturation have stem cell properties. Cancer Cell 2008;14:47-58.
11. van Delft FW, Horsley S, Colman S, et al. Clonal origins of relapse in ETV6-RUNX1 acute lymphoblastic leukemia. Blood 2011;117:6247-54.
12. Duan CW, Shi J, Chen J, et al. Leukemia propagating cells rebuild an evolving niche in response to therapy. Cancer Cell 2014;25:778-93.
13. Ebinger S, Ozdemir EZ, Ziegenhain C, et al. Characterization of Rare, Dormant, and Therapy-Resistant Cells in Acute Lymphoblastic Leukemia. Cancer Cell 2016;30:849-62.
14. Geethakumari PR, Hoffmann MS, Pemmaraju N, et al. Extramedullary B lymphoblastic leukemia/lymphoma (B-ALL/B-LBL): a diagnostic challenge. Clin Lymphoma Myeloma Leuk 2014;14:e115-8.
15. Faderl S, Kantarjian HM, Talpaz M, Estrov Z. Clinical significance of cytogenetic abnormalities in adult acute lymphoblastic leukemia. Blood 1998;91:3995-4019.
16. Pui CH, Robison LL, Look AT. Acute lymphoblastic leukaemia. Lancet 2008;371:1030-43.
17. Arber DA, Orazi A, Hasserjian R, et al. The 2016 revision to the World Health Organization classification of myeloid neoplasms and acute leukemia. Blood 2016;127:2391-405.
18. Dworzak MN, Buldini B, Gaipa G, et al. AIEOP-BFM consensus guidelines 2016 for flow cytometric immunophenotyping of Pediatric acute lymphoblastic leukemia. Cytometry B Clin Cytom 2018;94:82-93.
19. Pui CH, Relling MV, Downing JR. Acute lymphoblastic leukemia. N Engl J Med 2004;350:1535-48.
20. Pui CH, Nichols KE, Yang JJ. Somatic and germline genomics in paediatric acute lymphoblastic leukaemia. Nat Rev Clin Oncol 2019;16:227-40.

21. Lafage-Pochitaloff M, Baranger L, Hunault M, et al. Impact of cytogenetic abnormalities in adults with Ph-negative B-cell precursor acute lymphoblastic leukemia. Blood 2017;130:1832-44.
22. Den Boer ML, van Slegtenhorst M, De Menezes RX, et al. A subtype of childhood acute lymphoblastic leukaemia with poor treatment outcome: a genome-wide classification study. Lancet Oncol 2009;10:125-34.
23. Harrison CJ, Moorman AV, Schwab C, et al. An international study of intrachromosomal amplification of chromosome 21 (iAMP21): cytogenetic characterization and outcome. Leukemia 2014;28:1015-21.
24. Hirabayashi S, Ohki K, Nakabayashi K, et al. ZNF384-related fusion genes define a subgroup of childhood B-cell precursor acute lymphoblastic leukemia with a characteristic immunotype. Haematologica 2017;102:118-29.
25. Moorman AV, Harrison CJ, Buck GA, et al. Karyotype is an independent prognostic factor in adult acute lymphoblastic leukemia (ALL): analysis of cytogenetic data from patients treated on the Medical Research Council (MRC) UKALLXII/Eastern Cooperative Oncology Group (ECOG) 2993 trial. Blood 2007;109:3189-97.
26. Westbrook CA, Hooberman AL, Spino C, et al. Clinical significance of the BCR-ABL fusion gene in adult acute lymphoblastic leukemia: a Cancer and Leukemia Group B Study (8762). Blood 1992;80:2983-90.
27. Fielding AK, Rowe JM, Buck G, et al. UKALLXII/ECOG2993: addition of imatinib to a standard treatment regimen enhances long-term outcomes in Philadelphia positive acute lymphoblastic leukemia. Blood 2014;123:843-50.
28. Bassan R, Rossi G, Pogliani EM, et al. Chemotherapy-phased imatinib pulses improve long-term outcome of adult patients with Philadelphia chromosome-positive acute lymphoblastic leukemia: Northern Italy Leukemia Group protocol 09/00. J Clin Oncol 2010;28:3644-52.
29. Wassmann B, Gokbuget N, Scheuring UJ, et al. A randomized multicenter open label phase II study to determine the safety and efficacy of induction therapy with imatinib (Glivec, formerly STI571) in comparison with standard induction chemotherapy in elderly (>55 years) patients with Philadelphia chromosome-positive (Ph+/BCR-ABL+) acute lymphoblastic leukemia (ALL) (CSTI571ADE 10). Ann Hematol 2003;82:716-20.
30. Chalandon Y, Thomas X, Hayette S, et al. Randomized study of reduced-intensity chemotherapy combined with imatinib in adults with Ph-positive acute lymphoblastic leukemia. Blood 2015;125:3711-9.
31. Sanjuan-Pla A, Bueno C, Prieto C, et al. Revisiting the biology of infant t(4;11)/MLL-AF4+ B-cell acute lymphoblastic leukemia. Blood 2015;126:2676-85.
32. Hilden JM, Dinndorf PA, Meerbaum SO, et al. Analysis of prognostic factors of acute lymphoblastic leukemia in infants: report on CCG 1953 from the Children's Oncology Group. Blood 2006;108:441-51.
33. Winters AC, Bernt KM. MLL-Rearranged Leukemias-An Update on Science and Clinical Approaches. Front Pediatr 2017;5:4.
34. Ramakers-van Woerden NL, Beverloo HB, Veerman AJ, et al. In vitro drug-resistance profile in infant acute lymphoblastic leukemia in relation to age, MLL rearrangements and immunophenotype. Leukemia 2004;18:521-9.
35. Stam RW, den Boer ML, Meijerink JP, et al. Differential mRNA expression of Ara-C-metabolizing enzymes explains Ara-C sensitivity in MLL gene-rearranged infant acute lymphoblastic leukemia. Blood 2003;101:1270-6.
36. Wiemels J, Kang M, Greaves M. Backtracking of leukemic clones to birth. Methods Mol Biol 2009;538:7-27.
37. Wiemels JL, Cazzaniga G, Daniotti M, et al. Prenatal origin of acute lymphoblastic leukaemia in children. Lancet 1999;354:1499-503.

38. Papaemmanuil E, Rapado I, Li Y, et al. RAG-mediated recombination is the predominant driver of oncogenic rearrangement in ETV6-RUNX1 acute lymphoblastic leukemia. Nat Genet 2014;46:116-25.
39. O'Connor D, Moorman AV, Wade R, et al. Use of Minimal Residual Disease Assessment to Redefine Induction Failure in Pediatric Acute Lymphoblastic Leukemia. J Clin Oncol 2017;35:660-7.
40. Kager L, Lion T, Attarbaschi A, et al. Incidence and outcome of TCF3-PBX1-positive acute lymphoblastic leukemia in Austrian children. Haematologica 2007;92:1561-4.
41. Burmeister T, Gokbuget N, Schwartz S, et al. Clinical features and prognostic implications of TCF3-PBX1 and ETV6-RUNX1 in adult acute lymphoblastic leukemia. Haematologica 2010;95:241-6.
42. Farber S, Diamond LK. Temporary remissions in acute leukemia in children produced by folic acid antagonist, 4-aminopteroyl-glutamic acid. N Engl J Med 1948;238:787-93.
43. Frei E, 3rd, Karon M, Levin RH, et al. The effectiveness of combinations of antileukemic agents in inducing and maintaining remission in children with acute leukemia. Blood 1965;26:642-56.
44. Kato M, Ishimaru S, Seki M, et al. Long-term outcome of 6-month maintenance chemotherapy for acute lymphoblastic leukemia in children. Leukemia 2017;31:580-4.
45. Maury S, Chevret S, Thomas X, et al. Rituximab in B-Lineage Adult Acute Lymphoblastic Leukemia. N Engl J Med 2016;375:1044-53.
46. Maude SL, Laetsch TW, Buechner J, et al. Tisagenlecleucel in Children and Young Adults with B-Cell Lymphoblastic Leukemia. N Engl J Med 2018;378:439-48.
47. Lazarus HM, Richards SM, Chopra R, et al. Central nervous system involvement in adult acute lymphoblastic leukemia at diagnosis: results from the international ALL trial MRC UKALL XII/ECOG E2993. Blood 2006;108:465-72.
48. Cortes J, O'Brien SM, Pierce S, Keating MJ, Freireich EJ, Kantarjian HM. The value of high-dose systemic chemotherapy and intrathecal therapy for central nervous system prophylaxis in different risk groups of adult acute lymphoblastic leukemia. Blood 1995;86:2091-7.
49. Kantarjian HM, O'Brien S, Smith TL, et al. Results of treatment with hyper-CVAD, a dose-intensive regimen, in adult acute lymphocytic leukemia. J Clin Oncol 2000;18:547-61.
50. Terwey TH, Le Duc TM, Hemmati PG, et al. NIH-defined graft-versus-host disease and evidence for a potent graft-versus-leukemia effect in patients with acute lymphoblastic leukemia. Ann Oncol 2013;24:1363-70.
51. Goldstone AH, Richards SM, Lazarus HM, et al. In adults with standard-risk acute lymphoblastic leukemia, the greatest benefit is achieved from a matched sibling allogeneic transplantation in first complete remission, and an autologous transplantation is less effective than conventional consolidation/maintenance chemotherapy in all patients: final results of the International ALL Trial (MRC UKALL XII/ECOG E2993). Blood 2008;111:1827-33.
52. Patel B, Rai L, Buck G, et al. Minimal residual disease is a significant predictor of treatment failure in non T-lineage adult acute lymphoblastic leukaemia: final results of the international trial UKALL XII/ECOG2993. Br J Haematol 2010;148:80-9.
53. Bruggemann M, Gokbuget N, Kneba M. Acute lymphoblastic leukemia: monitoring minimal residual disease as a therapeutic principle. Semin Oncol 2012;39:47-57.
54. Schofield R. The relationship between the spleen colony-forming cell and the haemopoietic stem cell. Blood Cells 1978;4:7-25.
55. Anthony BA, Link DC. Regulation of hematopoietic stem cells by bone marrow stromal cells. Trends Immunol 2014;35:32-7.
56. Wang H, Leng Y, Gong Y. Bone Marrow Fat and Hematopoiesis. Front Endocrinol (Lausanne) 2018;9:694.

57. Guerra DAP, Paiva AE, Sena IFG, et al. Adipocytes role in the bone marrow niche. Cytometry A 2018;93:167-71.
58. Devlin MJ. Why does starvation make bones fat? Am J Hum Biol 2011;23:577-85.
59. Cawthorn WP, Scheller EL, Learman BS, et al. Bone marrow adipose tissue is an endocrine organ that contributes to increased circulating adiponectin during caloric restriction. Cell Metab 2014;20:368-75.
60. van der Eerden B, van Wijnen A. Meeting report of the 2016 bone marrow adiposity meeting. Adipocyte 2017;6:304-13.
61. Shafat MS, Oellerich T, Mohr S, et al. Leukemic blasts program bone marrow adipocytes to generate a protumoral microenvironment. Blood 2017;129:1320-32.
62. Friedenstein AJ, Chailakhjan RK, Lalykina KS. The development of fibroblast colonies in monolayer cultures of guinea-pig bone marrow and spleen cells. Cell Tissue Kinet 1970;3:393-403.
63. Malgieri A, Kantzari E, Patrizi MP, Gambardella S. Bone marrow and umbilical cord blood human mesenchymal stem cells: state of the art. Int J Clin Exp Med 2010;3:248-69.
64. Glenn JD, Whartenby KA. Mesenchymal stem cells: Emerging mechanisms of immunomodulation and therapy. World J Stem Cells 2014;6:526-39.
65. Dominici M, Le Blanc K, Mueller I, et al. Minimal criteria for defining multipotent mesenchymal stromal cells. The International Society for Cellular Therapy position statement. Cytotherapy 2006;8:315-7.
66. Roson-Burgo B, Sanchez-Guijo F, Del Canizo C, De Las Rivas J. Insights into the human mesenchymal stromal/stem cell identity through integrative transcriptomic profiling. BMC Genomics 2016;17:944.
67. Niehage C, Steenblock C, Pursche T, Bornhauser M, Corbeil D, Hoflack B. The cell surface proteome of human mesenchymal stromal cells. PLoS One 2011;6:e20399.
68. Mendez-Ferrer S, Michurina TV, Ferraro F, et al. Mesenchymal and haematopoietic stem cells form a unique bone marrow niche. Nature 2010;466:829-34.
69. Pinho S, Lacombe J, Hanoun M, et al. PDGFRalpha and CD51 mark human nestin+ sphere-forming mesenchymal stem cells capable of hematopoietic progenitor cell expansion. J Exp Med 2013;210:1351-67.
70. Isern J, Garcia-Garcia A, Martin AM, et al. The neural crest is a source of mesenchymal stem cells with specialized hematopoietic stem cell niche function. Elife 2014;3:e03696.
71. Ludin A, Gur-Cohen S, Golan K, et al. Reactive oxygen species regulate hematopoietic stem cell self-renewal, migration and development, as well as their bone marrow microenvironment. Antioxid Redox Signal 2014;21:1605-19.
72. Taniguchi Ishikawa E, Gonzalez-Nieto D, Ghiaur G, et al. Connexin-43 prevents hematopoietic stem cell senescence through transfer of reactive oxygen species to bone marrow stromal cells. Proc Natl Acad Sci U S A 2012;109:9071-6.
73. Ludin A, Itkin T, Gur-Cohen S, et al. Monocytes-macrophages that express alpha-smooth muscle actin preserve primitive hematopoietic cells in the bone marrow. Nat Immunol 2012;13:1072-82.
74. Karin Golan AW, Yuji Takihara, Anju Kumari, Eman Khatib-Massalha, Orit Kollet, Hui Cheng, Tao Cheng, Mark J. Althoff, Shiri Gur-Cohen, Tomer Itkin, Marie-Dominique Fillipi, Jose A Cancelas, Toshio Suda and Tsvee Lapidot. Mitochondria Transfer from Hematopoietic Stem and Progenitor Cells to Pdgfrα+/Sca-1-/CD48dim BM Stromal Cells Via CX43 Gap Junctions and AMPK Signaling Inversely Regulate ROS Generation in Both Cell Populations. Blood 2016;128:5.
75. Roecklein BA, Torok-Storb B. Functionally distinct human marrow stromal cell lines immortalized by transduction with the human papilloma virus E6/E7 genes. Blood 1995;85:997-1005.
76. Iwata M, Sandstrom RS, Delrow JJ, Stamatoyannopoulos JA, Torok-Storb B. Functionally and phenotypically distinct subpopulations of marrow stromal cells are fibroblast

in origin and induce different fates in peripheral blood monocytes. Stem Cells Dev 2014;23:729-40.
77. Kumagai M, Manabe A, Pui CH, et al. Stroma-supported culture in childhood B-lineage acute lymphoblastic leukemia cells predicts treatment outcome. J Clin Invest 1996;97:755-60.
78. Hawkins ED, Duarte D, Akinduro O, et al. T-cell acute leukaemia exhibits dynamic interactions with bone marrow microenvironments. Nature 2016;538:518-22.
79. Civini S, Jin P, Ren J, et al. Leukemia cells induce changes in human bone marrow stromal cells. J Transl Med 2013;11:298.
80. Polak R, de Rooij B, Pieters R, den Boer ML. B-cell precursor acute lymphoblastic leukemia cells use tunneling nanotubes to orchestrate their microenvironment. Blood 2015;126:2404-14.
81. de Vasconcellos JF, Laranjeira AB, Zanchin NI, et al. Increased CCL2 and IL-8 in the bone marrow microenvironment in acute lymphoblastic leukemia. Pediatr Blood Cancer 2011;56:568-77.
82. Burger JA, Kipps TJ. CXCR4: a key receptor in the crosstalk between tumor cells and their microenvironment. Blood 2006;107:1761-7.
83. van den Berk LC, van der Veer A, Willemse ME, et al. Disturbed CXCR4/CXCL12 axis in paediatric precursor B-cell acute lymphoblastic leukaemia. Br J Haematol 2014;166:240-9.
84. Koga K, Matsumoto K, Akiyoshi T, et al. Purification, characterization and biological significance of tumor-derived exosomes. Anticancer Res 2005;25:3703-7.
85. Pan L, Liang W, Fu M, et al. Exosomes-mediated transfer of long noncoding RNA ZFAS1 promotes gastric cancer progression. J Cancer Res Clin Oncol 2017;143:991-1004.
86. Zhang X, Yuan X, Shi H, Wu L, Qian H, Xu W. Exosomes in cancer: small particle, big player. J Hematol Oncol 2015;8:83.
87. Johnson SM, Dempsey C, Chadwick A, et al. Metabolic reprogramming of bone marrow stromal cells by leukemic extracellular vesicles in acute lymphoblastic leukemia. Blood 2016;128:453-6.
88. Paggetti J, Haderk F, Seiffert M, et al. Exosomes released by chronic lymphocytic leukemia cells induce the transition of stromal cells into cancer-associated fibroblasts. Blood 2015;126:1106-17.
89. Richards NG, Kilberg MS. Asparagine synthetase chemotherapy. Annu Rev Biochem 2006;75:629-54.
90. Iwamoto S, Mihara K, Downing JR, Pui CH, Campana D. Mesenchymal cells regulate the response of acute lymphoblastic leukemia cells to asparaginase. J Clin Invest 2007;117:1049-57.
91. Yang Y, Mallampati S, Sun B, et al. Wnt pathway contributes to the protection by bone marrow stromal cells of acute lymphoblastic leukemia cells and is a potential therapeutic target. Cancer Lett 2013;333:9-17.
92. Nwabo Kamdje AH, Krampera M. Notch signaling in acute lymphoblastic leukemia: any role for stromal microenvironment? Blood 2011;118:6506-14.
93. Jacamo R, Chen Y, Wang Z, et al. Reciprocal leukemia-stroma VCAM-1/VLA-4-dependent activation of NF-kappaB mediates chemoresistance. Blood 2014;123:2691-702.
94. Matsunaga T, Takemoto N, Sato T, et al. Interaction between leukemic-cell VLA-4 and stromal fibronectin is a decisive factor for minimal residual disease of acute myelogenous leukemia. Nat Med 2003;9:1158-65.
95. Sison EA, Brown P. The bone marrow microenvironment and leukemia: biology and therapeutic targeting. Expert Rev Hematol 2011;4:271-83.
96. Pillozzi S, Masselli M, De Lorenzo E, et al. Chemotherapy resistance in acute lymphoblastic leukemia requires hERG1 channels and is overcome by hERG1 blockers. Blood 2011;117:902-14.

97. Rustom A, Saffrich R, Markovic I, Walther P, Gerdes HH. Nanotubular highways for intercellular organelle transport. Science 2004;303:1007-10.
98. Ahmad T, Mukherjee S, Pattnaik B, et al. Miro1 regulates intercellular mitochondrial transport & enhances mesenchymal stem cell rescue efficacy. EMBO J 2014;33:994-1010.
99. Inaba M, Buszczak M, Yamashita YM. Nanotubes mediate niche-stem-cell signalling in the Drosophila testis. Nature 2015;523:329-32.
100. Sowinski S, Jolly C, Berninghausen O, et al. Membrane nanotubes physically connect T cells over long distances presenting a novel route for HIV-1 transmission. Nat Cell Biol 2008;10:211-9.
101. Wang X, Gerdes HH. Long-distance electrical coupling via tunneling nanotubes. Biochim Biophys Acta 2012;1818:2082-6.
102. Wang X, Gerdes HH. Transfer of mitochondria via tunneling nanotubes rescues apoptotic PC12 cells. Cell Death Differ 2015;22:1181-91.
103. Wang X, Veruki ML, Bukoreshtliev NV, Hartveit E, Gerdes HH. Animal cells connected by nanotubes can be electrically coupled through interposed gap-junction channels. Proc Natl Acad Sci U S A 2010;107:17194-9.
104. de Rooij B, Polak R, Stalpers F, Pieters R, den Boer ML. Tunneling nanotubes facilitate autophagosome transfer in the leukemic niche. Leukemia 2017;31:1651-4.
105. Zhu S, Victoria GS, Marzo L, Ghosh R, Zurzolo C. Prion aggregates transfer through tunneling nanotubes in endocytic vesicles. Prion 2015;9:125-35.
106. Rustom A. The missing link: does tunnelling nanotube-based supercellularity provide a new understanding of chronic and lifestyle diseases? Open Biol 2016;6.
107. Moschoi R, Imbert V, Nebout M, et al. Protective mitochondrial transfer from bone marrow stromal cells to acute myeloid leukemic cells during chemotherapy. Blood 2016;128:253-64.
108. Marlein CR, Zaitseva L, Piddock RE, et al. NADPH oxidase-2 derived superoxide drives mitochondrial transfer from bone marrow stromal cells to leukemic blasts. Blood 2017;130:1649-60.
109. Marlein CR, Zaitseva L, Piddock RE, et al. PGC-1alpha driven mitochondrial biogenesis in stromal cells underpins mitochondrial trafficking to leukemic blasts. Leukemia 2018;32:2073-7.
110. Dorian Forte MG-F, Abel Sánchez-Aguilera, Vaya Stavropoulou, Claire Fielding, Daniel Martín-Pérez, Alexandar Tzankov, Juerg Schwaller and Simón Méndez-Ferrer. Leukemic Stem Cells Co-Opt Normal Bone Marrow Niches As a Source of Energy and Antioxidant Defence. Blood 2017;130:94.
111. Jiang D, Gao F, Zhang Y, et al. Mitochondrial transfer of mesenchymal stem cells effectively protects corneal epithelial cells from mitochondrial damage. Cell Death Dis 2016;7:e2467.
112. Islam MN, Das SR, Emin MT, et al. Mitochondrial transfer from bone-marrow-derived stromal cells to pulmonary alveoli protects against acute lung injury. Nat Med 2012;18:759-65.
113. Han H, Hu J, Yan Q, et al. Bone marrow-derived mesenchymal stem cells rescue injured H9c2 cells via transferring intact mitochondria through tunneling nanotubes in an in vitro simulated ischemia/reperfusion model. Mol Med Rep 2016;13:1517-24.
114. Wang J, Liu X, Qiu Y, et al. Cell adhesion-mediated mitochondria transfer contributes to mesenchymal stem cell-induced chemoresistance on T cell acute lymphoblastic leukemia cells. J Hematol Oncol 2018;11:11.
115. Entrena A, Varas A, Vazquez M, et al. Mesenchymal stem cells derived from low risk acute lymphoblastic leukemia patients promote NK cell antitumor activity. Cancer Lett 2015;363:156-65.
116. Denu RA, Nemcek S, Bloom DD, et al. Fibroblasts and Mesenchymal Stromal/Stem Cells Are Phenotypically Indistinguishable. Acta Haematol 2016;136:85-97.

117. Kalluri R. The biology and function of fibroblasts in cancer. Nat Rev Cancer 2016;16:582-98.
118. Benyahia Z, Dussault N, Cayol M, et al. Stromal fibroblasts present in breast carcinomas promote tumor growth and angiogenesis through adrenomedullin secretion. Oncotarget 2017;8:15744-62.
119. Ni WD, Yang ZT, Cui CA, Cui Y, Fang LY, Xuan YH. Tenascin-C is a potential cancer-associated fibroblasts marker and predicts poor prognosis in prostate cancer. Biochem Biophys Res Commun 2017;486:607-12.
120. von Ahrens D, Bhagat TD, Nagrath D, Maitra A, Verma A. The role of stromal cancer-associated fibroblasts in pancreatic cancer. J Hematol Oncol 2017;10:76.
121. Zhai Y, Zhang J, Wang H, et al. Growth differentiation factor 15 contributes to cancer-associated fibroblasts-mediated chemo-protection of AML cells. J Exp Clin Cancer Res 2016;35:147.
122. Dorsam B, Bosl T, Reiners KS, et al. Hodgkin Lymphoma-Derived Extracellular Vesicles Change the Secretome of Fibroblasts Toward a CAF Phenotype. Front Immunol 2018;9:1358.
123. Dvorak HF. Tumors: wounds that do not heal-redux. Cancer Immunol Res 2015;3:1-11.
124. Shiga K, Hara M, Nagasaki T, Sato T, Takahashi H, Takeyama H. Cancer-Associated Fibroblasts: Their Characteristics and Their Roles in Tumor Growth. Cancers (Basel) 2015;7:2443-58.
125. Tommelein J, Verset L, Boterberg T, Demetter P, Bracke M, De Wever O. Cancer-associated fibroblasts connect metastasis-promoting communication in colorectal cancer. Front Oncol 2015;5:63.
126. Arcucci A, Ruocco MR, Granato G, Sacco AM, Montagnani S. Cancer: An Oxidative Crosstalk between Solid Tumor Cells and Cancer Associated Fibroblasts. Biomed Res Int 2016;2016:4502846.
127. Cirri P, Chiarugi P. Cancer associated fibroblasts: the dark side of the coin. Am J Cancer Res 2011;1:482-97.
128. Pavlides S, Vera I, Gandara R, et al. Warburg meets autophagy: cancer-associated fibroblasts accelerate tumor growth and metastasis via oxidative stress, mitophagy, and aerobic glycolysis. Antioxid Redox Signal 2012;16:1264-84.
129. Erez N, Truitt M, Olson P, Arron ST, Hanahan D. Cancer-Associated Fibroblasts Are Activated in Incipient Neoplasia to Orchestrate Tumor-Promoting Inflammation in an NF-kappaB-Dependent Manner. Cancer Cell 2010;17:135-47.
130. Hashimoto O, Yoshida M, Koma Y, et al. Collaboration of cancer-associated fibroblasts and tumour-associated macrophages for neuroblastoma development. J Pathol 2016;240:211-23.
131. Quail DF, Joyce JA. Microenvironmental regulation of tumor progression and metastasis. Nat Med 2013;19:1423-37.
132. Pavlides S, Whitaker-Menezes D, Castello-Cros R, et al. The reverse Warburg effect: aerobic glycolysis in cancer associated fibroblasts and the tumor stroma. Cell Cycle 2009;8:3984-4001.
133. Yoshida GJ. Metabolic reprogramming: the emerging concept and associated therapeutic strategies. J Exp Clin Cancer Res 2015;34:111.
134. Fu Y, Liu S, Yin S, et al. The reverse Warburg effect is likely to be an Achilles' heel of cancer that can be exploited for cancer therapy. Oncotarget 2017;8:57813-25.
135. Gentric G, Mieulet V, Mechta-Grigoriou F. Heterogeneity in Cancer Metabolism: New Concepts in an Old Field. Antioxid Redox Signal 2017;26:462-85.
136. Avagliano A, Granato G, Ruocco MR, et al. Metabolic Reprogramming of Cancer Associated Fibroblasts: The Slavery of Stromal Fibroblasts. Biomed Res Int 2018;2018:6075403.

137. Martinez-Outschoorn UE, Lisanti MP, Sotgia F. Catabolic cancer-associated fibroblasts transfer energy and biomass to anabolic cancer cells, fueling tumor growth. Semin Cancer Biol 2014;25:47-60.
138. Capparelli C, Guido C, Whitaker-Menezes D, et al. Autophagy and senescence in cancer-associated fibroblasts metabolically supports tumor growth and metastasis via glycolysis and ketone production. Cell Cycle 2012;11:2285-302.
139. Ippolito L, Morandi A, Taddei ML, et al. Cancer-associated fibroblasts promote prostate cancer malignancy via metabolic rewiring and mitochondrial transfer. Oncogene 2019;38:5339-55.
140. Martinez-Outschoorn UE, Goldberg A, Lin Z, et al. Anti-estrogen resistance in breast cancer is induced by the tumor microenvironment and can be overcome by inhibiting mitochondrial function in epithelial cancer cells. Cancer Biol Ther 2011;12:924-38.
141. Martinez-Outschoorn UE, Lisanti MP. Tumor microenvironment: introduction. Semin Oncol 2014;41:145.
142. Farge T, Saland E, de Toni F, et al. Chemotherapy-Resistant Human Acute Myeloid Leukemia Cells Are Not Enriched for Leukemic Stem Cells but Require Oxidative Metabolism. Cancer Discov 2017;7:716-35.
143. Kim HK, Noh YH, Nilius B, et al. Current and upcoming mitochondrial targets for cancer therapy. Semin Cancer Biol 2017;47:154-67.
144. Fielding AK, Richards SM, Chopra R, et al. Outcome of 609 adults after relapse of acute lymphoblastic leukemia (ALL); an MRC UKALL12/ECOG 2993 study. Blood 2007;109:944-50.
145. Martinez-Outschoorn UE, Pavlides S, Whitaker-Menezes D, et al. Tumor cells induce the cancer associated fibroblast phenotype via caveolin-1 degradation: implications for breast cancer and DCIS therapy with autophagy inhibitors. Cell Cycle 2010;9:2423-33.
146. Peiris-Pages M, Sotgia F, Lisanti MP. Chemotherapy induces the cancer-associated fibroblast phenotype, activating paracrine Hedgehog-GLI signalling in breast cancer cells. Oncotarget 2015;6:10728-45.
147. Sun Y, Campisi J, Higano C, et al. Treatment-induced damage to the tumor microenvironment promotes prostate cancer therapy resistance through WNT16B. Nat Med 2012;18:1359-68.
148. Chan TS, Hsu CC, Pai VC, et al. Metronomic chemotherapy prevents therapy-induced stromal activation and induction of tumor-initiating cells. J Exp Med 2016;213:2967-88.
149. Safavi S, Paulsson K. Near-haploid and low-hypodiploid acute lymphoblastic leukemia: two distinct subtypes with consistently poor prognosis. Blood 2017;129:420-3.
150. Hu JM, Liu K, Liu JH, et al. The increased number of tumor-associated macrophage is associated with overexpression of VEGF-C, plays an important role in Kazakh ESCC invasion and metastasis. Exp Mol Pathol 2017;102:15-21.
151. Madsen CD, Pedersen JT, Venning FA, et al. Hypoxia and loss of PHD2 inactivate stromal fibroblasts to decrease tumour stiffness and metastasis. EMBO Rep 2015;16:1394-408.
152. Silzle T, Kreutz M, Dobler MA, Brockhoff G, Knuechel R, Kunz-Schughart LA. Tumor-associated fibroblasts recruit blood monocytes into tumor tissue. Eur J Immunol 2003;33:1311-20.
153. Zhang R, Qi F, Zhao F, et al. Cancer-associated fibroblasts enhance tumor-associated macrophages enrichment and suppress NK cells function in colorectal cancer. Cell Death Dis 2019;10:273.
154. Takahashi H, Sakakura K, Kudo T, et al. Cancer-associated fibroblasts promote an immunosuppressive microenvironment through the induction and accumulation of protumoral macrophages. Oncotarget 2017;8:8633-47.
155. Guilloton F, Caron G, Menard C, et al. Mesenchymal stromal cells orchestrate follicular lymphoma cell niche through the CCL2-dependent recruitment and polarization of monocytes. Blood 2012;119:2556-67.

156. Herranz N, Gil J. Mechanisms and functions of cellular senescence. J Clin Invest 2018;128:1238-46.
157. Apollonio B NNS, Sutton L, Salisbury J, Patten P, Kassam S, Devereux S, Amini R M, Rosenquist R, Ramsay A G. Diffuse Large B-Cell Lymphoma (DLBCL) Tumor Cells Reprogram Lymphatic Fibroblasts into Cancer-Associated Fibroblasts (CAFs) That Contribute to Tumor Microenvironment (TME)-Driven Immune Privilege. Blood 2015;126.
158. Raz Y, Cohen N, Shani O, et al. Bone marrow-derived fibroblasts are a functionally distinct stromal cell population in breast cancer. J Exp Med 2018;215:3075-93.
159. Greil J, Gramatzki M, Burger R, et al. The acute lymphoblastic leukaemia cell line SEM with t(4;11) chromosomal rearrangement is biphenotypic and responsive to interleukin-7. Br J Haematol 1994;86:275-83.
160. Uphoff CC, MacLeod RA, Denkmann SA, et al. Occurrence of TEL-AML1 fusion resulting from (12;21) translocation in human early B-lineage leukemia cell lines. Leukemia 1997;11:441-7.
161. Okabe M, Matsushima S, Morioka M, et al. Establishment and characterization of a cell line, TOM-1, derived from a patient with Philadelphia chromosome-positive acute lymphocytic leukemia. Blood 1987;69:990-8.
162. Gora-Tybor J, Deininger MW, Goldman JM, Melo JV. The susceptibility of Philadelphia chromosome positive cells to FAS-mediated apoptosis is not linked to the tyrosine kinase activity of BCR-ABL. Br J Haematol 1998;103:716-20.
163. Kamps MP, Look AT, Baltimore D. The human t(1;19) translocation in pre-B ALL produces multiple nuclear E2A-Pbx1 fusion proteins with differing transforming potentials. Genes Dev 1991;5:358-68.
164. Sattler M, Verma S, Shrikhande G, et al. The BCR/ABL tyrosine kinase induces production of reactive oxygen species in hematopoietic cells. J Biol Chem 2000;275:24273-8.
165. McBee ME, Chionh YH, Sharaf ML, Ho P, Cai MW, Dedon PC. Production of Superoxide in Bacteria Is Stress- and Cell State-Dependent: A Gating-Optimized Flow Cytometry Method that Minimizes ROS Measurement Artifacts with Fluorescent Dyes. Front Microbiol 2017;8:459.
166. King MP, Attardi G. Human cells lacking mtDNA: repopulation with exogenous mitochondria by complementation. Science 1989;246:500-3.
167. Heasman SA, Zaitseva L, Bowles KM, Rushworth SA, Macewan DJ. Protection of acute myeloid leukaemia cells from apoptosis induced by front-line chemotherapeutics is mediated by haem oxygenase-1. Oncotarget 2011;2:658-68.
168. Burk M, Heyll A, Arning M, Volmer M, Fartash K, Schneider W. Pharmacokinetics of high-dose cytarabine and its deamination product--a reappraisal. Leuk Lymphoma 1997;27:321-7.
169. Eunice S. Wang GJS, Leonard T. Heffner, Wendy Stock, Arati V. Rao, Gail J. Roboz, Peter Westervelt, Matthew J. Wieduwilt, Jay Yang, Lucy Prasad, Karen Segarini and Stuart L. Goldberg. Plasma Vincristine Levels Are 100-Fold Higher with Marqibo® (Vincristine Sulfate LIPOSOME Injection) in Place of Standard Vincristine in Combination Chemotherapy of Patients ≥ 60 Years Old with Newly Diagnosed Acute Lymphoblastic Leukemia (ALL). Blood 2015;126:2491.
170. Corcione A, Arduino N, Ferretti E, et al. Chemokine receptor expression and function in childhood acute lymphoblastic leukemia of B-lineage. Leuk Res 2006;30:365-72.
171. Gerby B, Veiga DF, Krosl J, et al. High-throughput screening in niche-based assay identifies compounds to target preleukemic stem cells. J Clin Invest 2016;126:4569-84.
172. Bertoli S, Picard M, Berard E, et al. Dexamethasone in hyperleukocytic acute myeloid leukemia. Haematologica 2018;103:988-98.
173. Marlein CR, Piddock RE, Mistry JJ, et al. CD38-Driven Mitochondrial Trafficking Promotes Bioenergetic Plasticity in Multiple Myeloma. Cancer Res 2019;79:2285-97.

174. Huang C, Xiao X, Yang Y, et al. MicroRNA-101 attenuates pulmonary fibrosis by inhibiting fibroblast proliferation and activation. J Biol Chem 2017;292:16420-39.
175. Paliwal S, Chaudhuri R, Agrawal A, Mohanty S. Regenerative abilities of mesenchymal stem cells through mitochondrial transfer. J Biomed Sci 2018;25:31.
176. DiNardo CD, Pratz K, Pullarkat V, et al. Venetoclax combined with decitabine or azacitidine in treatment-naive, elderly patients with acute myeloid leukemia. Blood 2019;133:7-17.
177. Frismantas V, Dobay MP, Rinaldi A, et al. Ex vivo drug response profiling detects recurrent sensitivity patterns in drug-resistant acute lymphoblastic leukemia. Blood 2017;129:e26-e37.
178. Khaw SL, Suryani S, Evans K, et al. Venetoclax responses of pediatric ALL xenografts reveal sensitivity of MLL-rearranged leukemia. Blood 2016;128:1382-95.
179. Andreeff M, Jiang S, Zhang X, et al. Expression of Bcl-2-related genes in normal and AML progenitors: changes induced by chemotherapy and retinoic acid. Leukemia 1999;13:1881-92.
180. Kantarjian HM, Su Y, Jabbour EJ, et al. Patient-reported outcomes from a phase 3 randomized controlled trial of inotuzumab ozogamicin versus standard therapy for relapsed/refractory acute lymphoblastic leukemia. Cancer 2018;124:2151-60.
181. Kantarjian H, Stein A, Gokbuget N, et al. Blinatumomab versus Chemotherapy for Advanced Acute Lymphoblastic Leukemia. N Engl J Med 2017;376:836-47.